AD NUMBER

AD825633

LIMITATION CHANGES

TO:

Approved for public release; distribution is unlimited.

FROM:

**Distribution authorized to U.S. Gov't. agencies and their contractors;
Administrative/Operational Use; 15 DEC 1967.
Other requests shall be referred to Office of Naval Research, Arlington, VA 22203.**

AUTHORITY

ONR ltr 27 Jul 1971

HOLOGRAPHIC HEAD-UP DISPLAY
PHASE I

T. J. Harris
M. A. Habegger
G. T. Sincerbox
D. W. Hanna

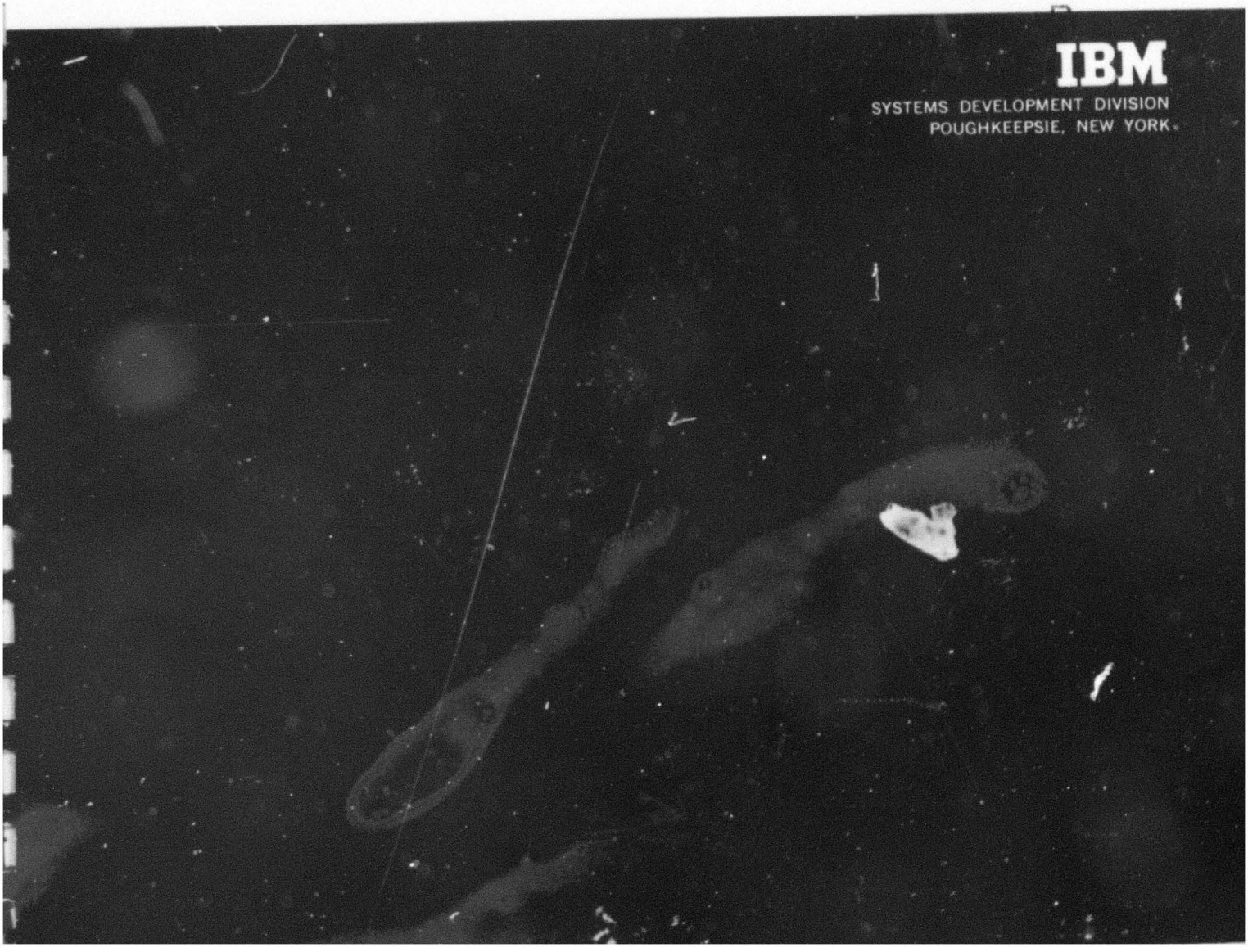

IBM
SYSTEMS DEVELOPMENT DIVISION
POUGHKEEPSIE, NEW YORK

Holographic Head-Up Display
Phase I

by

T. J. Harris, M. A. Habegger, G. T. Sincerbox, D. W. Hanna

December 15, 1967

This research was sponsored by the Office of Naval Research, Naval Applications and Analysis Group, Air Programs, Code 461, Washington, D. C. under Contract N00014-67-C0453, NR 215-030.

IBM

International Business Machines Corporation
Systems Development Division, Poughkeepsie, New York

ABSTRACT

Numerous applications of display systems require the presentation of visual information that can be continuously altered with time. In particular, a head-up display system as used by an aircraft commander must provide a simulation of the real-world exterior to his vehicle, and, at the same time, represent any change in his attitude with respect to a predetermined segment of this real world.

In the particular case of an aircraft landing approach, one can characterize the pilot's view of the aircraft carrier and its subsequent variations into six degrees of freedom. The display must provide the view corresponding to the instantaneous values of these parameters and change as any one or more of the parameters change.

This report describes the development work on displays of this type using sideband or carrier-frequency Fresnel holographic recorded images. An important feature of the holographic approach is that a true 3-D image of an object can be recorded. It is, therefore, possible with a single hologram to present an infinite number of different views of an object to an observer. Continuous control of the pertinent parameters is required to make a dynamic real-time display.

High quality holograms of aircraft carrier models have been made in sizes up to 8 by 10 inches. Techniques and systems for manipulating the holographic real and virtual images from these holograms have been tested and are described.

This work was performed by the IBM Systems Development Division, Product Development Laboratory, at Poughkeepsie, N. Y. with assistance from IBM's Federal Systems Division, Electronics Systems Center, at Owego, N. Y.

CONTENTS

ILLUSTRATIONS

SYMBOLS

λ	wavelength of radiation	4
U_s	complex amplitude of plane-wave object wavefront	4
a	real part of complex amplitude of object wavefront	4
φ	angle between object wavefront and recording plane normal	4
ν_s	spatial frequency of object wavefront; $\nu_s = (\sin \varphi)/\lambda$	4
ξ	spatial frequency of object wavefront in radians; $\xi = 2\pi\nu_s$	4
U_r	complex amplitude of plane-wave reference wavefront	4
b	real part of complex amplitude of reference wavefront	4
θ	angle between reference wavefront and recording plane normal	4
ν_r	spatial frequency of reference wavefront; $\nu_r = (\sin \theta)/\lambda$	4
η	spatial frequency of reference wavefront in radians; $\eta = 2\pi\nu_r$	4
U	complex amplitude distribution of interference pattern	6
I(x)	intensity distribution of interference pattern; $I(x) = UU^*$	8
V	visibility function	8
t	exposure time	8
E(x)	exposure (product of intensity and exposure time, t)	8
$T_a(x)$	amplitude transmittance of hologram	8
k	constant of proportionality relating amplitude transmittance to exposure	8

$U'(x)$	reconstructed complex amplitude	9
A	constant given by $k t b (a^2 + b^2)$	9
B	constant given by $k t b^2$	9
$A(x, y)$	complex amplitude of generalized object wavefront	14
ω	maximum spatial frequency of generalized object wavefront	18
n	refractive index of recording media	22
t_e	thickness of recording media	22
d	separation of planes in Lippmann photography	22
N	number of planes in Lippmann photography	22
$\Delta\lambda$	bandwidth of optical radiation	23
θ_i	angle between readout illumination and hologram normal	28
φ_i	angular direction of reconstructed wavefront	28
H_R	wavefront forming the holographic real image	35
H_V	wavefront forming the holographic virtual image	35
R, φ_r	amplitude and phase of reference wavefront	35
O, φ_o	amplitude and phase of the wavefront originating from the object being holographically recorded	35
C, φ_c	amplitude and phase of reconstruction wave-wavefront	35
Φ_R	phase of wavefront forming the real image	36
Φ_V	phase of wavefront forming the virtual image	36
$P(x_o, y_o, z_o)$	point of origin of object wavefront	36
$P(x_r, y_r, z_r)$	point of origin of reference wavefront	38
$P(x_c, y_c, z_c)$	point of origin of reconstruction wavefront	38
$P(\alpha_V, \beta_V, \gamma_V)$	holographic virtual image point	40

$P(\alpha_R, \beta_R, \gamma_R)$	holographic real image point	40
M_{ang}	angular magnification	40
M_{lat}	lateral magnification of image	41
$M_{V\ lat}$	lateral magnification of virtual image	41
$M_{R\ lat}$	lateral magnification of real image	41
ρ	observation distance from hologram	41
M_{long}	longitudinal magnification	43
$\lvert\gamma_{11}(\tau)\rvert$	real part of the complex degree of coherence	44
τ	time interval between interfering light beams	44
$\Delta\nu$	frequency bandwidth of the light beam	44
c	vacuum speed of light	44
L	length of laser cavity	44
ℓ_c	coherence length	44
$\alpha_1, \alpha_2, \beta_1, \beta_2$	perception angles	63
γ	stereopsis angle	63
γ_t	minimum perceptible angle	65
s	spacing between eyes	65
S	observation distance	65
δ	difference in depth of two objects	65
(x_1, y_1, z_1) } (x_2, y_2, z_2)	coordinate systems whose relative orientation in an inertial frame is fixed. They translate with the center of gravity of the aircraft carrier and the aircraft, respectively.	68
$(\theta_1, \varphi_1, \psi_1)$	Euler angles describing the motion of axes A_1, B_1, C_1 with respect to axes x_1, y_1, z_1	68
$(\theta_2, \varphi_2, \psi_2)$	Euler angles describing the motion of axes A_2, B_2, C_2 with respect to axes x_2, y_2, z_2	68

R	distance of aircraft from center of gravity of carrier	70
ϵ	azimuth angle	110
κ	depression angle	110
μ	image pitch angle	110
χ	image yaw angle	110
ζ	roll angle	110
$\vec{k}$	propagation vector of wavefront; $\|k\| = 2\pi/\lambda$	119

1. INTRODUCTION

The first airborne head-up display was a simple optical gunsight consisting of an illuminated crosshair reticle, a collimating lens, and a beam splitter or "combining glass" mounted at 45 degrees to the pilot's line of sight. This simple system presented the pilot with a luminous image (the crosshairs) that appeared at virtual infinity directly in front of the aircraft. The potential advantages of such a system for information display were readily apparent:

(1) the pilot could receive visual information without diverting his attention from the outside world, and without even changing his eye focus;

(2) the information that was displayed held a fixed spatial relationship to the aircraft's principal axes, regardless of the pilot's head position.

This embryonic head-up display remained nothing more than a gunsight until flyable cathode ray tubes and computers appeared on the avionics scene. When a CRT screen was first substituted for the illuminated reticle, the old gunsight became a contact analog head-up display, which had an information presentation capability limited only by the capacity of the computer that fed it. Present day head-up displays are used to present a variety of information in several different modes of operation. In the navigation mode, attitude, command flight path, airspeed, and altitude might all be presented in one integrated format. Other modes of operation present weapons delivery information and landing approach information.

Despite continuing advances in display technology, present head-up displays are limited to providing highly symbolic presentations, which require a large degree of mental interpretation. Typical display formats consist of crude, computer-generated line images, which are sometimes augmented by alpha-numeric data. Some development work is being done on continuous-tone computer-generated imagery intended to simulate a real-

world scene during conditions of reduced visibility. Such imagery is two-dimensional, and its complexity and refresh rate are still ultimately limited by the capacity of the computer that generates it.

Recent developments in holography suggest a greatly accelerated evolution of display systems. Holographic images are three-dimensional images and exhibit all the depth and parallax of their real-world counterparts; their realism and detail are not limited by a computer's storage capacity. Because they are truly three-dimensional, holographic images may be manipulated in six degrees of freedom to simulate the relative motion of the scenes that they represent. This manipulation may be done directly, without going through a coordinate transform computation for each point in the image, as is required with contact analog imagery.

This report presents the findings of a study to adapt holography to a dynamic head-up display for carrier-deck landing approaches during restricted visibility.

2. THEORY OF HOLOGRAPHY

2.1 INTRODUCTION

The ability to use holographic images for a real-time display system depends upon the degree to which these images can be manipulated. To some extent an appreciation of the image itself, and its subsequent possibilities, can be gained in the laboratory. This observation, however, does not give an indication of the limits within which the hologram can be operated in order to simulate the required motions. In order to assess these constraints, and where possible exploit them, it is necessary to delve into the theory of this unique process. Only in this way can a comparison be made between the almost unlimited variations in this concept. It should be possible with holography to structure a system that allows the best simulation of a real-world/real-time event. Of course, theoretical predictions must be verified experimentally before they can be accepted.

It is the purpose of this section to present the basic concepts of the holographic process and establish a common base and terminology for further development. The more important properties and their impact on display applications are also included.

2.2 GENERAL THEORY

2.2.1 Introduction

In order to present a cohesive treatment of the theory of the holographic process, we will first consider the case of interference between two plane waves, the recording of this interference, and the subsequent reconstruction of one plane wave. The analysis will then be extended to treat the general case of recording and reconstructing the information contained in a three-dimensional object space. In all cases we will assume that the radiation is monochromatic and that scalar theory applies (i. e. , polarization effects can be ignored).

2.2.2 Plane Wave Holography

If we consider a point at infinity as a simple object, then in the region of space where the recording is to be made, the wavefronts of the radiation from the point are essentially plane waves. In any arbitrary plane this wavefront may be characterized by a constant amplitude and a sinusoidally varying phase factor. The rate at which the phase varies is proportional to the spatial frequency (ν) of the light incident on the plane. Spatial frequency may be thought of as the number of intersections per unit length that the plane makes with the antinodes comprising the plane wave. It is hence proportional to the wavelength of the light (λ) and the angle (φ) between the beam direction and the plane normal, $\vec{n}$.

$$\nu = (\sin \varphi)/\lambda \tag{1}$$

The plane waves from the object, hereafter called the signal beam, can be described by the function U_s where

$$U_s = a\, e^{i \xi x} \tag{2}$$

with $\xi = 2\pi \nu_s = (2\pi \sin\varphi)/\lambda$.

If we now introduce a second plane wave, called a reference beam, its amplitude and phase distribution with respect to the same arbitrary plane can be represented in a similar manner by

$$U_r = b\, e^{i \eta x} \tag{3}$$

where $\eta = 2\pi \nu_r = (2\pi \sin \theta)/\lambda$.

The relationship between the signal and reference beams and the sampling plane (P) is shown in Figure 1.

If the reference and signal beams are phase-coherent, i. e., with respect to an arbitrary reference point any phase difference between the two beams remains constant with time, then the beams can interact to produce

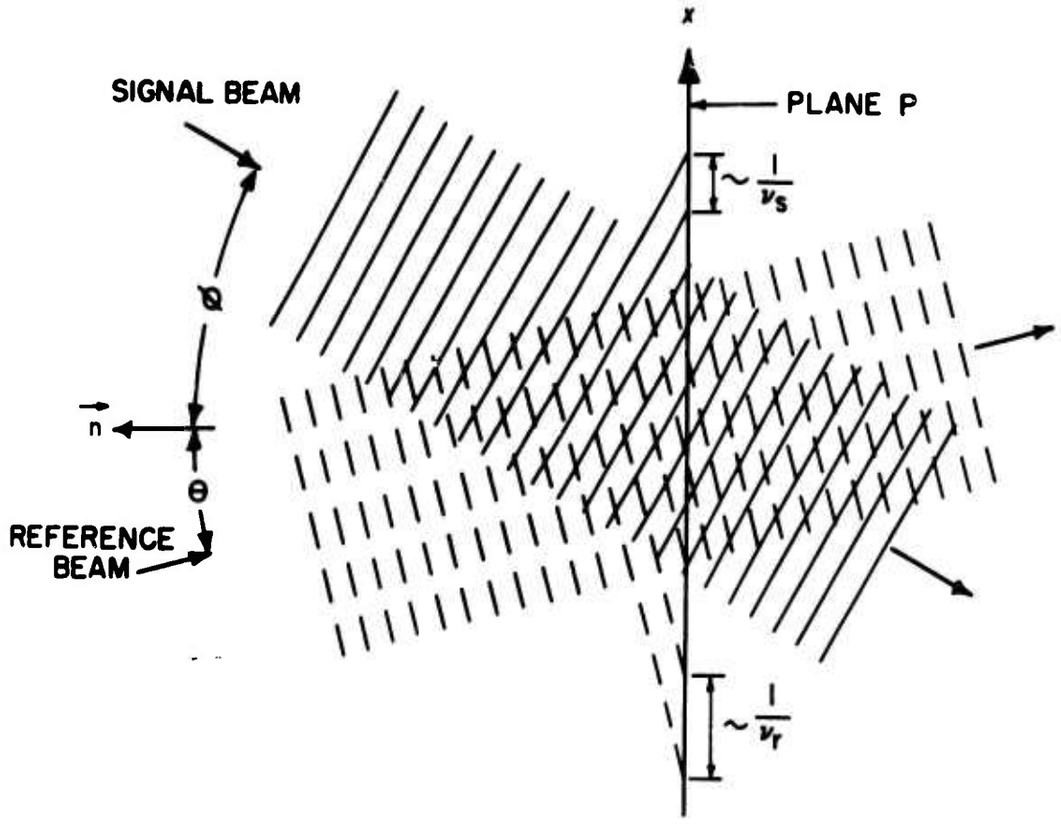

Figure 1. Plane Wave Holography.

an interference pattern that is time-independent and remains fixed in space. The amplitude distribution of the interference pattern on plane P is given by the sum of the individual amplitude distributions. Thus,

$$U = U_s + U_r = a\, e^{i\xi x} + b\, e^{i\eta x} \tag{4}$$

Since a photosensitive device such as a photodetector or a photographic plate is a square-law detector, it will respond only to the intensity of the light in plane P and not to the amplitude. The intensity of the light distribution is determined by multiplying the sum in Equation 4 by its complex conjugate.

$$UU^* = a^2 + b^2 + ab\left[e^{i(\eta-\xi)x} + e^{-i(\eta-\xi)x}\right] \tag{5}$$

where a and b are real numbers.

This can be better visualized by considering the case of two plane waves equal in amplitude (a = b). These waves make equal angles with the plane normal ($\eta = -\xi$). In this case Equation 5 reduces to:

$$UU^* = 4a^2 \cos^2 \eta x \tag{6}$$

This is then the intensity distribution of the interference pattern between the signal and reference beams that would be observed if plane P were scanned in the x direction with a detector having a linear response. Figure 2a is a plot of Equation 6 and shows that the beams interact to produce alternate regions of constructive and destructive interference (i. e. , a periodic pattern of light and dark fringes). The spacing between the fringes is determined by the angle between the beams and by the wavelength (spacing decreases as the angle is increased).

The more general case of Equation 5 ($a \neq b$) is shown in Figure 2b, which also shows a similar cosinusoidal intensity variation. This variation, however, has a bias level that prevents the minimums from going to zero. This lack of contrast is characterized by a quantity called

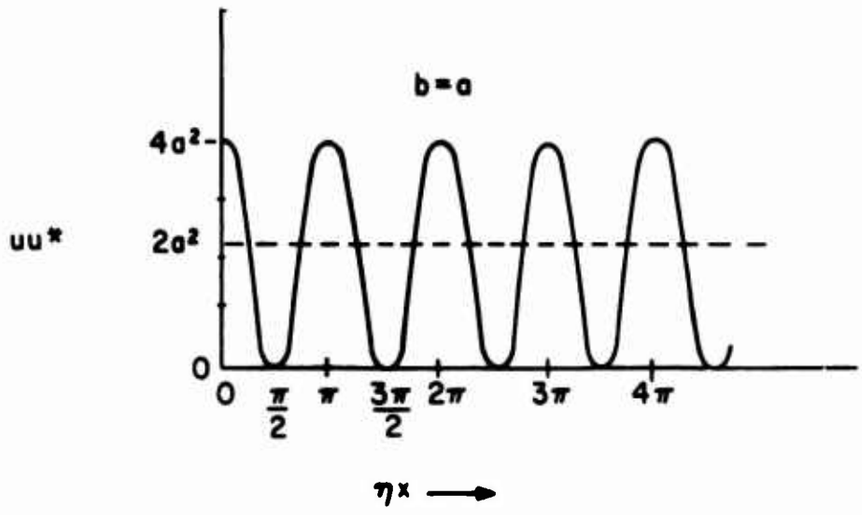

Figure 2a. Intensity Distribution in Interference Pattern between Two Plane Waves of Equal Amplitude.

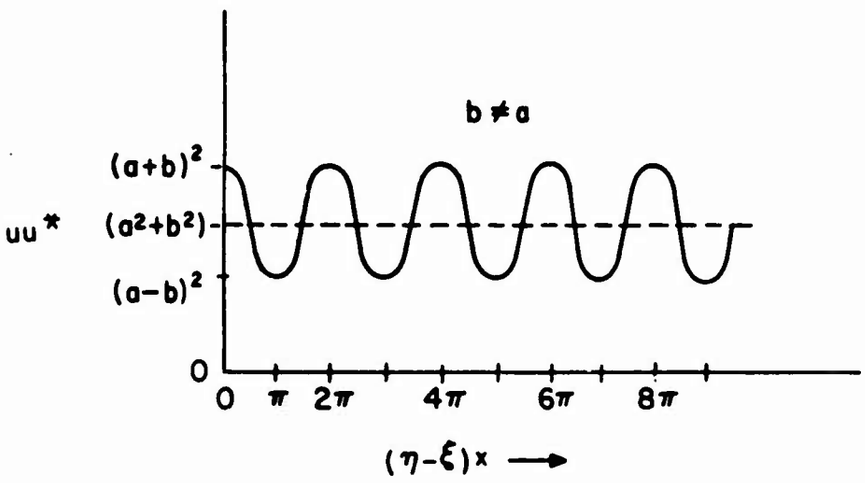

Figure 2b. Intensity Distribution in Interference Pattern between Two Plane Waves of Unequal Amplitude.

visibility, which can assume values between zero and one and is defined by:

$$V = \frac{I_{max} - I_{min}}{I_{max} + I_{min}} \tag{7}$$

In the example shown in Figure 2a, b = a and V = 1. In Figure 2b, b = 5a and $V \approx 0.4$.

If we assume that a photosensitive medium placed in the location of plane P has a linear response in that the resulting amplitude transmittance of the processed photograph is directly proportional to the exposure, then we may write:

$$T_a(x) = k\, E(x) = k\, I(x) t \tag{8}$$

where $T_a(x)$ is the amplitude transmittance,

I(x) is the intensity distribution of the exposing radiation,

t is the exposure time,

k is a constant of proportionality.

Amplitude transmittance is defined as $T_a = (I'/I'_o)^{1/2}$ where I'_o is the intensity of light incident on an attenuating medium and I' is the light intensity transmitted by the medium. We are assuming that the amplitude transmittance is a real function and, hence, is independent of the thickness variations of the recording medium.

The recording of the two-beam interference pattern given by Equation 5 produces a density variation that gives a subsequent amplitude transmittance of:

$$\begin{aligned} T_a(x) &= k t\, U U^* \\ &= k t\,(a^2 + b^2) + k t a b\,[e^{i(\eta-\xi)x} + e^{-i(\eta-\xi)x}] \end{aligned} \tag{9}$$

From Figure 2b we see that Equation 9 represents a hologram consisting of alternately light and dark regions or bars. It is, in fact, a photographically

generated diffraction grating and, as will be shown, exhibits many of the properties of a conventional grating.

If this hologram is then illuminated with only the reference beam as given by Equation 3, the amplitude distribution of the light coming out of the hologram will be given by:

$$U'(x) = U_r(x)\, T_a(x)$$

$$= [b\, e^{i\eta x}][kt(a^2 + b^2) + kta\,b(e^{i(\eta-\xi)x} + e^{-i(\eta-\xi)x}]$$

$$= A\, e^{i\eta x} + Ba\, e^{i(2\eta-\xi)x} + Ba\, e^{i\xi x} \qquad (10)$$

where $A = ktb(a^2 + b^2)$

$B = ktb^2$

Equation 10 shows that three beams of light are generated from the single, illuminating, beam. These are shown in Figure 3. The first term represents a beam travelling in the same direction as the illuminating beam and contains no useful information about the signal beam. This is called the zero-order beam and is analogous to the undiffracted beam from a diffraction grating. The third term in Equation 10 is identical (within a multiplicative constant) to the wavefront that had originally emanated from the object point (see Equation 2). Consequently, this reconstructed wavefront would appear to an observer to come from an image located in space in the exact position as the original object; the reconstructed image would appear to be a point located at infinity. Since the reconstructed wavefront is generated by the hologram and directed only into the space on the observer's side of the plate, no light exists in the region between the hologram and the apparent location of the image. Any obstruction placed in this region would not affect the observed image; hence it is called a virtual image. The reconstructed wavefront can be operated on with lenses, mirrors, screens, etc., just as if the light were coming from the original object.

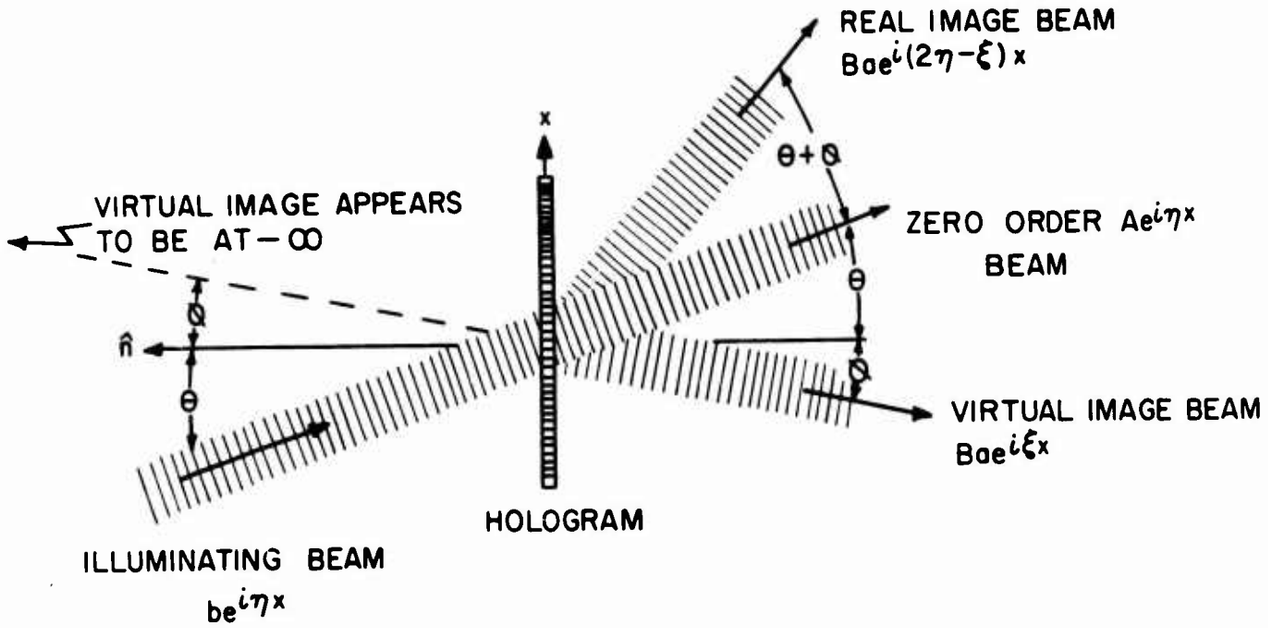

Figure 3. Reconstruction from a Hologram.

The second term in Equation 10 represents a third beam of light that is formed on the opposite side of the zero-order beam symmetric with the previously discussed virtual image beam (see Figure 3). This is also a reconstruction of the object wavefront except for its direction and, as will be shown later, is modified such that it forms a focused or real image of the object in the space on the observer's side of the hologram.

We have shown, therefore, that in the special case of plane waves the resulting hologram contains a grating-like structure, which upon subsequent illumination creates three beams of light analogous to the zero-order and two first-order beams from a conventional grating. The analysis must now be enlarged to encompass the more general case of a three-dimensional object and to show that the reconstructions are again a faithful reproduction of the object.

2.2.3 Three-Dimensional Holography

The concept of how a hologram records information about three-dimensional space can be built up by referring to the previous discussion on plane waves. In that treatment we demonstrated that the fringes recorded on the hologram plate have a spacing that is proportional to the angle between the signal and reference beams. The larger this angle becomes, the more the fringe spacing decreases, and conversely. We can also observe that the fringe spacing remains constant from one side of the hologram to the other. This indicates that the angle between signal and reference beam does not vary from one position in the signal beam to another. That is, all the rays comprising the beam are parallel and appear to come from a point at infinity. If, however, the origin of the signal beam were located at a point other than infinity, the rays would not be parallel at the hologram plane. Consequently, the angle between the reference beam and the signal beam would not be constant but would vary from point to point. The resulting fringes will then vary in spacing according to the variation of this angle. An example of this is shown in Figure 4 where light from a point

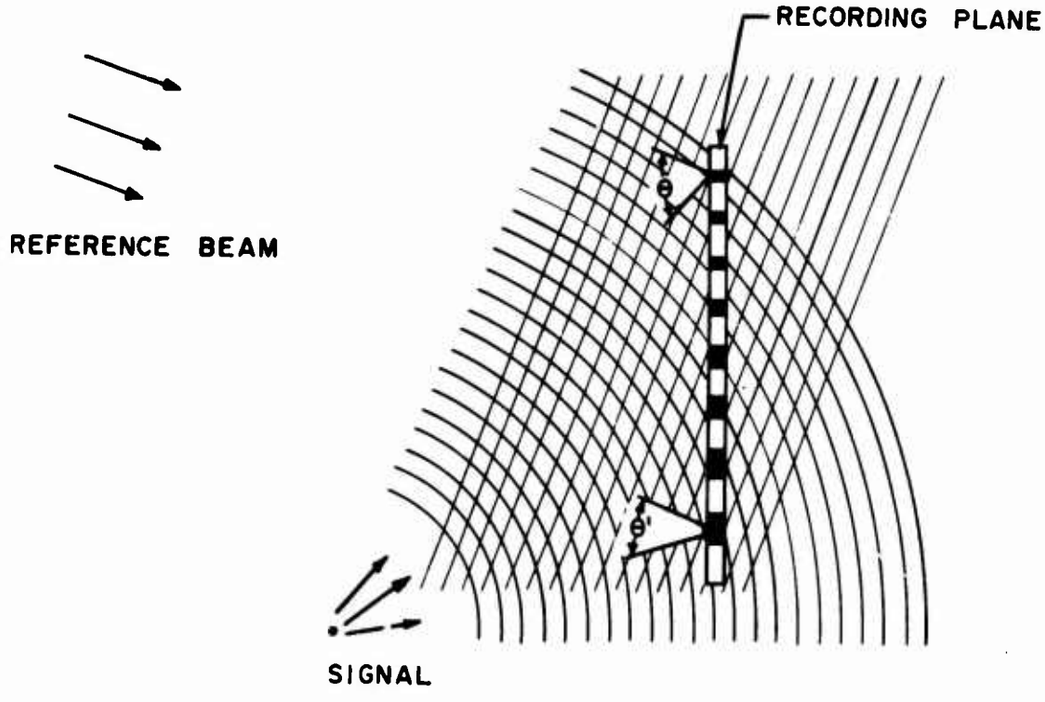

Figure 4. Interference Fringes Formed between Plane Wave and Cylindrical Wave Showing Variation in Fringe Spacing.

source interferes with a plane wave (shown in two dimensions). We can make a general statement and say that the average spacing (frequency) is indicative of the angular direction of the point source, and the range or variation in spacing is a measure of the distance of the point from the recording plane. Each point in the three-dimensional object space may be considered to be a point generator of light; they each create a characteristic fringe pattern representing their particular position. The resultant on the recording medium is a complicated superposition of all the fringe patterns. In general, the fringe pattern over a two-dimensional recording media is not a simple grating-like structure except for the cases cited above. A spherical wavefront from a point source interacts with a plane wave to create an interférence pattern. This pattern consists of concentric circles whose common center is at the foot of the perpendicular drawn from the point object to the recording plane (when the plane wave is incident along the normal to the recording plane). If the plane reference wave makes an angle with the normal, then the interference pattern recorded is the projection of the concentric circles--ellipses--onto the recording plane. For a reference beam that is not a plane wave, the pattern is even more complicated. In any event, the phase information regarding direction and distance of the object point from the recording plane is transformed, via interference, to a variation in spacing of intensity peaks or fringes. This is analogous to storing information via frequency modulation in communication theory. In a like manner, the intensity of a point is transformed into contrast or visibility of the fringes by virtue of its relative strength with respect to the reference beam. This, also, is analogous to communications theory as it represents amplitude modulation. This comparison can be extended even further as will be shown later.

We may now formalize the process of recording information about a three-dimensional object. If a three-dimensional object is illuminated with coherent radiation, as from a laser, then each object point will act as a spherical radiator. The total effect of all these radiators will be to

generate a complex wavefront that propagates through space. (It is this wavefront that is intercepted by the eye and creates an image on the retina.) With respect to an arbitrarily placed plane, the amplitude and phase of this wavefront can be described by the complex function A(x, y) where

$$A(x,y) = \sum_{n=1}^{N} a_n(x,y)\, e^{-i\varphi_n(x,y)} \tag{11}$$

In this expression, $a_n(x,y)$ represents the amplitude, and $\varphi_n(x,y)$ represents the phase of an individual object point as measured on the recording plane. (The quantities $a_n(x,y)$ and $\varphi_n(x,y)$ are related to the object through the Kirchhoff diffraction integral.) In this analysis we have defined the complex function A(x, y) to represent the wavefront emanating from the object. Hence, it will only be necessary to show that the holographic process recreates this identical wavefront in order to prove that an image of the original object will be observed.

For the purpose of analysis, let us position our recording plane as shown in Figure 5 and introduce a plane wave reference beam at an angle θ to the plane normal. In the same manner as Equation 4, we may write for the resulting amplitude distribution on the recording plane:

$$U(x,y) = A(x,y) + b\, e^{i\eta x} \tag{12}$$

where b is the amplitude of the plane wave (constant over x and y), and $\eta = (2\pi \sin\theta)/\lambda$ is the spatial frequency (in radians) of the reference beam. The intensity is given by

$$\begin{aligned} U U^* &= [A(x,y) + b\, e^{i\eta x}][A^*(x,y) + b\, e^{-i\eta x}] \\ &= |A(x,y)|^2 + b^2 + A(x,y)\, b\, e^{-i\eta x} + A^*(x,y)\, b\, e^{i\eta x} \end{aligned} \tag{13}$$

If we assume a linear recording medium, the resulting amplitude transmission becomes

$$T_a(x,y) = k t\, [|A(x,y)|^2 + b^2] + k t b\, [A(x,y)\, e^{-i\eta x} + A^*(x,y)\, e^{i\eta x}] \tag{14}$$

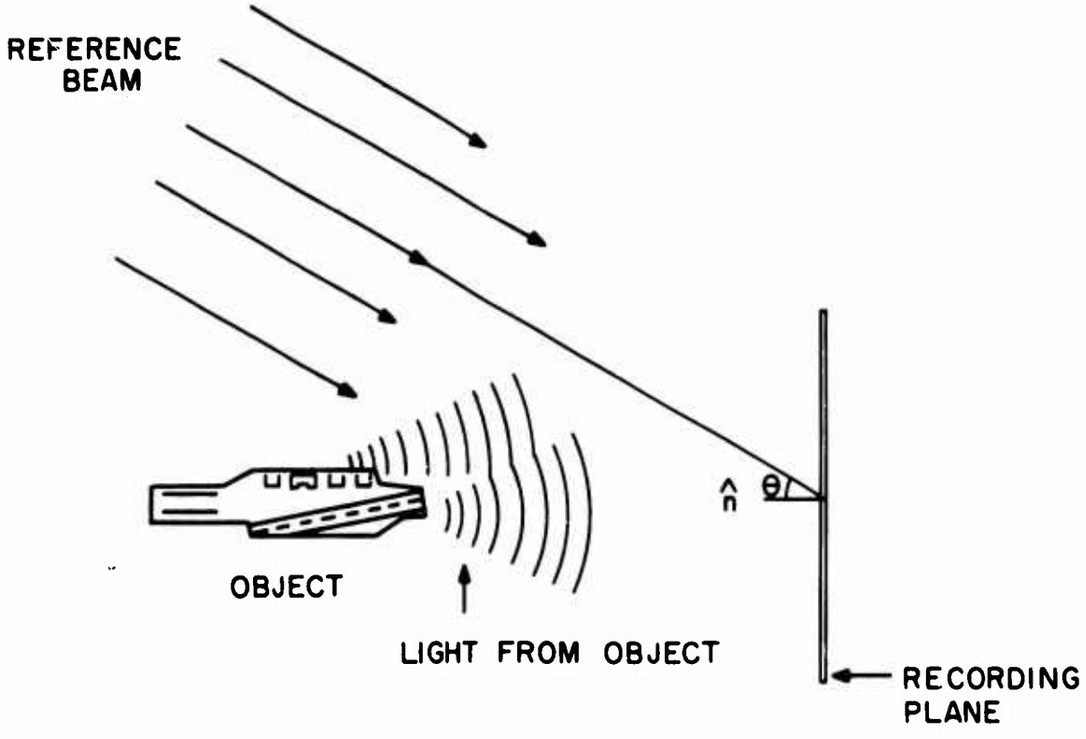

Figure 5. Recording a Three-Dimensional Object.

If the hologram is now illuminated with a beam identical to the reference beam, the resulting wavefront coming from the hologram will be:

$$U'(x,y) = T_a(x,y)\, b\, e^{i\eta x}$$

$$= ktb\,[|A(x,y)|^2 + b^2]\, e^{i\eta x} + ktb^2\, A(x,y)$$

$$+ ktb^2\, A^*(x,y)\, e^{i2\eta x} \qquad (15)$$

From this we see that the first term represents a beam travelling in the same direction as the illuminating beam and containing no phase information--the zero-order beam. The second term contains the function A(x, y), which is identical to the original wavefront that existed in the region of space where the recording was made. As far as an observer is concerned, the image formed by the reconstructed wavefront cannot be distinguished from the original object (except for the constant multiplier, which affects the reconstructed brightness, and other factors that will be considered later). As before, this is a virtual image, since the image appears to be in the original object position although there is no light in that region of space.

The effect of the third term is more difficult to interpret in view of the complex conjugate involved. It can be readily verified (see Section 9. Appendix) that the expression $A^*(x,y)$ represents a wavefront in which all curvatures have been reversed; i. e., diverging light becomes converging light and vice versa. Thus, a conjugate wavefront is generated that, instead of diverging from an object, will converge to form a real image of the object. This image exists in the space on the opposite side of the hologram from the original object and may be observed, in focus, on a viewing screen. The exponential factor in the third term causes the real image to be located in a symmetric position on the opposite side of the zero-order beam. The relationship between the various images is shown in Figure 6.

An important property of the hologram should be mentioned at this time. Since we can assume that each point of the object emits a spherical

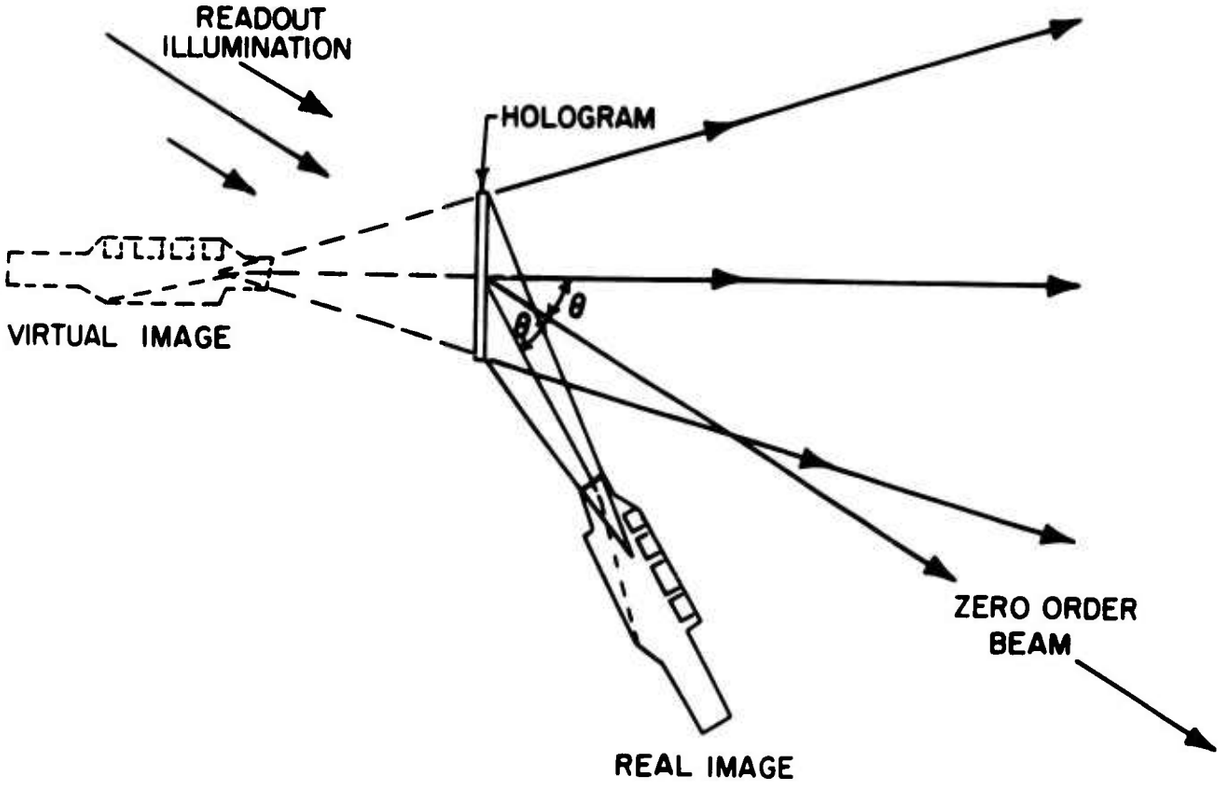

Figure 6. Reconstructed Images from a Hologram.

wave, it is easy to see (Figure 5) that the light from each point spreads out over the entire recording medium. That is, information about a particular object point is not localized as in conventional photography but rather is spread out and intermingled with the information about all other points. This provides a high degree of storage redundancy in that any defects in or on the photosensitive medium will not affect the quality of the reconstructed image. This also means that any small subarea of the hologram contains information about the entire image and can be used for the reconstruction by itself. An individual area, of course, acts like a window of the same size, thereby reducing the angular view and restricting the observer's head motion, so that change in perspective view is limited. Reduction of the size of the interrogated area also produces other image effects. These will be discussed as they become pertinent.

At this point we can draw another analogy between holography and communications theory. That is, the reference beam can be considered to represent a spatial carrier frequency, similar to an RF carrier wave. As in communications, the spatial bandwidth of the signal, $A(x, y)$, will determine the minimum carrier frequency that will permit undistorted recording and retrieval of the signal wavefront.

The spatial bandwidth of the signal is determined by the physical size of the object and its separation from the recording plane. These dimensions determine the extreme angles at which the signal wavefront arrives at the recording plane and, hence, the maximum and minimum angles between the signal wave and the reference wave. These angles, in turn, determine the maximum and minimum spatial frequencies that are created by the interference between the two wavefronts. As an example, in Figure 7, an object is located on the normal through the center of the recording plane so that the extreme rays from the object form angles of $\pm \varphi$ with respect to the normal. Since all angles between $\pm \varphi$ may exist, the spatial bandwidth of the signal is restricted to the range $\pm \omega$, where $\omega = (2 \pi \sin \varphi)/\lambda$.

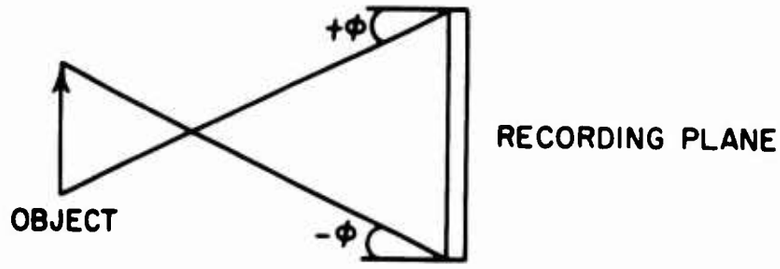

Figure 7. Angles Determining Spatial Bandwidth of the Object.

With reference to Equation 13, we can construct a spatial frequency spectrum representing the intensity distribution to be recorded. This is shown in Figure 8. The first expression $|A(x,y)|^2$ contains the intermodulation terms and extends between $\pm 2\omega$ in the spectrum. This, and the next term b^2, at zero frequency, give rise to the d-c term in readout. The third term is the complete signal wavefront $A(x,y)$ on a spatial carrier of frequency η and will form the virtual image. The last term is the conjugate wavefront $A^*(x,y)$ on a carrier of frequency $-\eta$ and will generate the real image. From this we see that, for the signal spectrums not to overlap the d-c terms, the carrier must have a frequency η such that $\eta \geq 3\omega$. This means that, for a distortionless reconstruction, the reference beam must make an angle θ with the recording plane normal such that $\theta \geq \sin^{-1}(3 \sin\phi)$. Therefore, the signal information stored in a hologram is carried in the sidebands in the same manner as for a modulated R.F carrier wave.

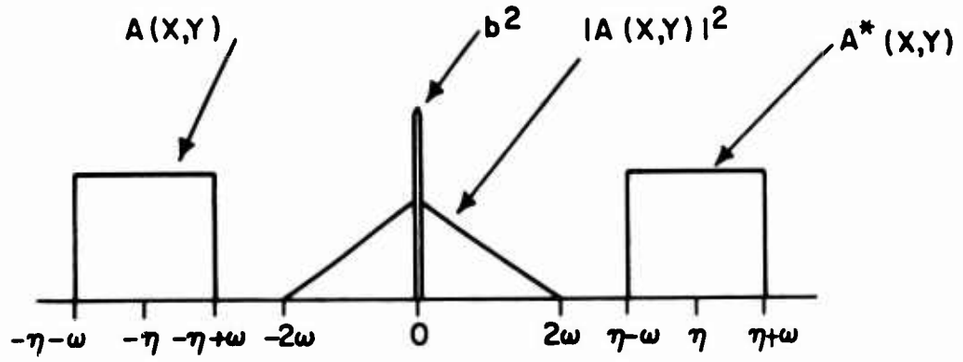

Figure 8. Spatial Frequency Spectrum of Hologram Showing Information Contained in Sidebands.

Thus far in the treatment of holography we have restricted our discussion to the particular case of a recording medium so oriented that the reference and signal beams impinge onto the same side of the emulsion. In general, however, the recording media can be located at any position within the region of space where the signal beam and reference beam overlap. This gives rise to an interesting application when the orientation is such that the two beams enter from opposite sides of the emulsion as shown in Figure 9a for a plane wave "object" and in Figure 9b for a general object. The arrangement in Figure 9a closely resembles a process known as Lippmann Photography, invented at the turn of the century.[1] The more general case in Figure 9b is termed Lippmann Holography.

Where both the signal and reference beams are plane waves, the resulting interference pattern is a standing wave consisting of alternate dark and light fringes--nodes and antinodes. These regions are oriented perpendicular to the collinear axis of the beams and hence are parallel to the emulsion surface. The photosensitive medium, therefore, becomes exposed throughout its depth or thickness in such a manner that, after

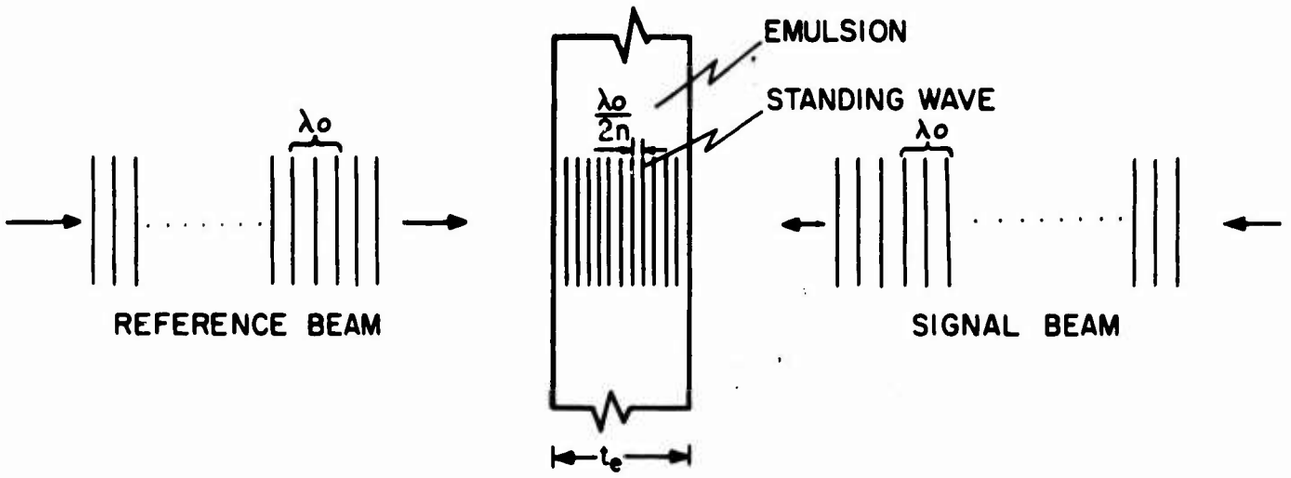

Figure 9a. Lippmann Photography: The Formation of Parallel Silver Planes throughout the Thickness of a Photosensitive Medium.

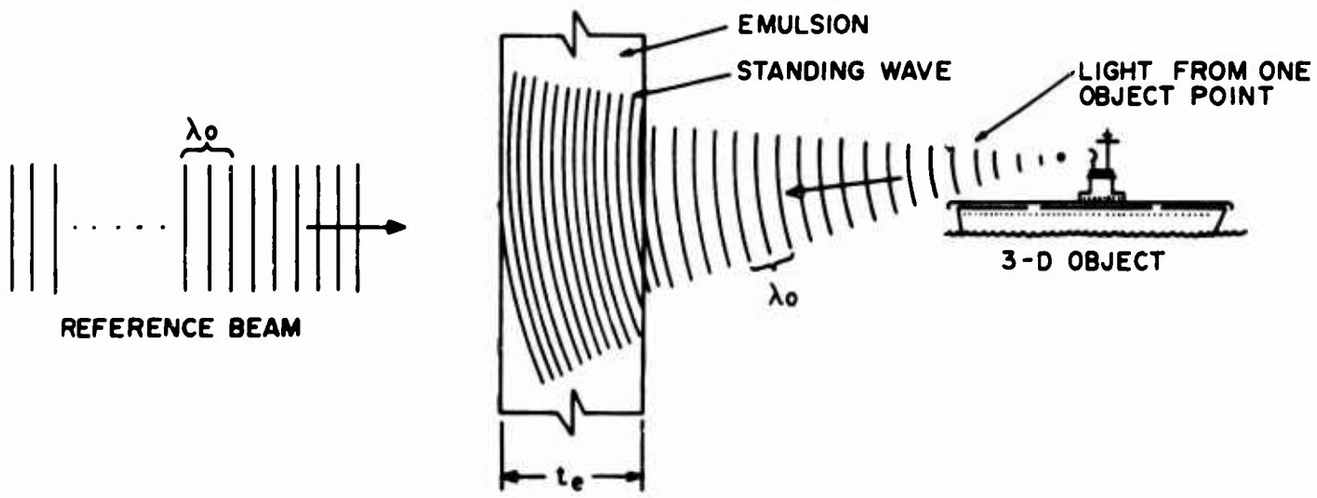

Figure 9b. Lippmann Holography: The Formation of a Multilayer Structure for Each Point of an Extended Object.

processing, the resultant is a multilayered structure consisting of partially transparent silver planes separated by clear gelatine. These planes are separated by a distance

$$d = \frac{\lambda_0}{2n} \tag{16}$$

where λ_0 is the wavelength of the light and n is the refractive index of the emulsion. The number of planes formed would be

$$N = \frac{2\,n\,t_e}{\lambda_0} \tag{17}$$

where t_e is the emulsion thickness. (For example, N = 95 when $t_e = 15\ \mu$, $\lambda = 5000$ Å and n = 1.5.) This "photograph" will now act much like a reflection interference filter if it is illuminated with incoherent white light. That is, as the white light passes through the structure, a small fraction of it will be reflected by each silver plane. All of the individual reflections will add together to form the reflected light. However, this addition will be coherent for only that wavelength component of the reflected light that satisfies Equation 16. It is only for this wavelength that the individual reflections will be in phase and allow a superposition of amplitudes. The resulting intensity of the reflection at this wavelength (neglecting absorption) is given by:

$$I = |A|^2 = \left|\sum_{n=1}^{N} a_n\right|^2 \approx |N\,a|^2 = N^2 I_0 \tag{18}$$

where $I_0 = |a|^2$ is the intensity reflected from an individual plane.

Since none of the other wavelengths can satisfy Equation 16, their resultant total intensity will result from incoherent superposition and, hence, will be the sum of the individual intensities, not the amplitudes.

$$I' = \sum_{n=1}^{N} I_m = N I_0 \tag{19}$$

From this we see that the reflection spectrum contains a peak at wavelength λ_0 that is N times stronger than the light at any other wavelength. This peak will have a finite bandwidth by virtue of the finite number of reflecting planes that are recorded. It has been shown[2] that this bandwidth is inversely proportional to the number of planes and is given approximately by:

$$\Delta\lambda \approx \frac{0.9\,\lambda_0}{N} \tag{20}$$

For λ_0 = 5000 Å and N = 95, the resulting bandwidth would be $\Delta\lambda$ = 45 Å.

If, therefore, this "photograph" is illuminated with a plane wave of white light, a reconstruction will be generated that is identical to the original object wavefront in both direction and wavelength.

It is interesting to note that if the illuminating radiation is incident on the emulsion at an angle different from the original reference beam, then the wavelength peak of the reconstructed beam will shift to shorter wavelengths. This is analogous to the Bragg effect in crystallography. The relationship between the reconstructed wavelength λ_r and the angular misalignment θ is given by:[3]

$$\lambda_r = \lambda_0 \cos \theta \tag{21}$$

This process can be extended even further by exposing the same volume of emulsion to a second standing wave of different wavelengths. The reconstruction will then contain two reflection peaks, one for each wavelength recorded. This technique can, and has been,[4] extended to the recording and simultaneous reconstruction of at least 12 different wavelengths.

This type of recording can be extended to a general, three-dimensional object as shown in Figure 9b. One can consider each point on the object to set up its own standing wave with the reference beam, independent of the other points. An individual multilayer structure will, in general, not be a set of parallel planes, but rather a set of equally spaced spherical surfaces with a common center of curvature. The resultant structure due

to the entire object will be a complicated superposition of all of these individual structures.

In readout, however, each structure will reconstruct an image point corresponding to the original object point in both location and wavelength. Consequently, this type of hologram is capable of being illuminated with white light and of producing a multicolor reconstructed image of a three-dimensional object.

2.2.4 Special Properties

In an attempt to present the concepts of holographic storage and retrieval, it was necessary to use a rather simple theoretical model. This is unfortunate, however, as many of the fine points of the process cannot be treated easily. It is the purpose of this section to elaborate on some of these subtleties and their interesting, and sometimes troublesome, properties.

The Linearity of the Photosensitive Medium. In determining the response of the photographic medium to the intensity distribution of the interference pattern, it was assumed that a linear transform existed (Equation 8). In reality, however, the relationship between the amplitude transmittance of the processed photograph (hologram) and the original exposure is linear only over a small portion of the dynamic range of the medium. A typical set of experimentally determined amplitude transmittance curves for 649F plates is shown in Figure 10 as a function of exposure energy density. From these curves we see that a reasonable approximation to linearity can be obtained only over a very short range. This means that the modulation or visibility of the interference pattern must be restricted so that the maximum and minimum exposures fall within this linear range. This is most easily obtained by adjusting the amplitudes of the signal and reference beams so that the bias intensity, I_B, represented by the first two terms in Equation 13, produces an exposure that is in the center of the range. At the same time, the extremes given by $I_{\pm} = I_B \pm |2A(x,y)B|$ are adjusted so as not to exceed the range.

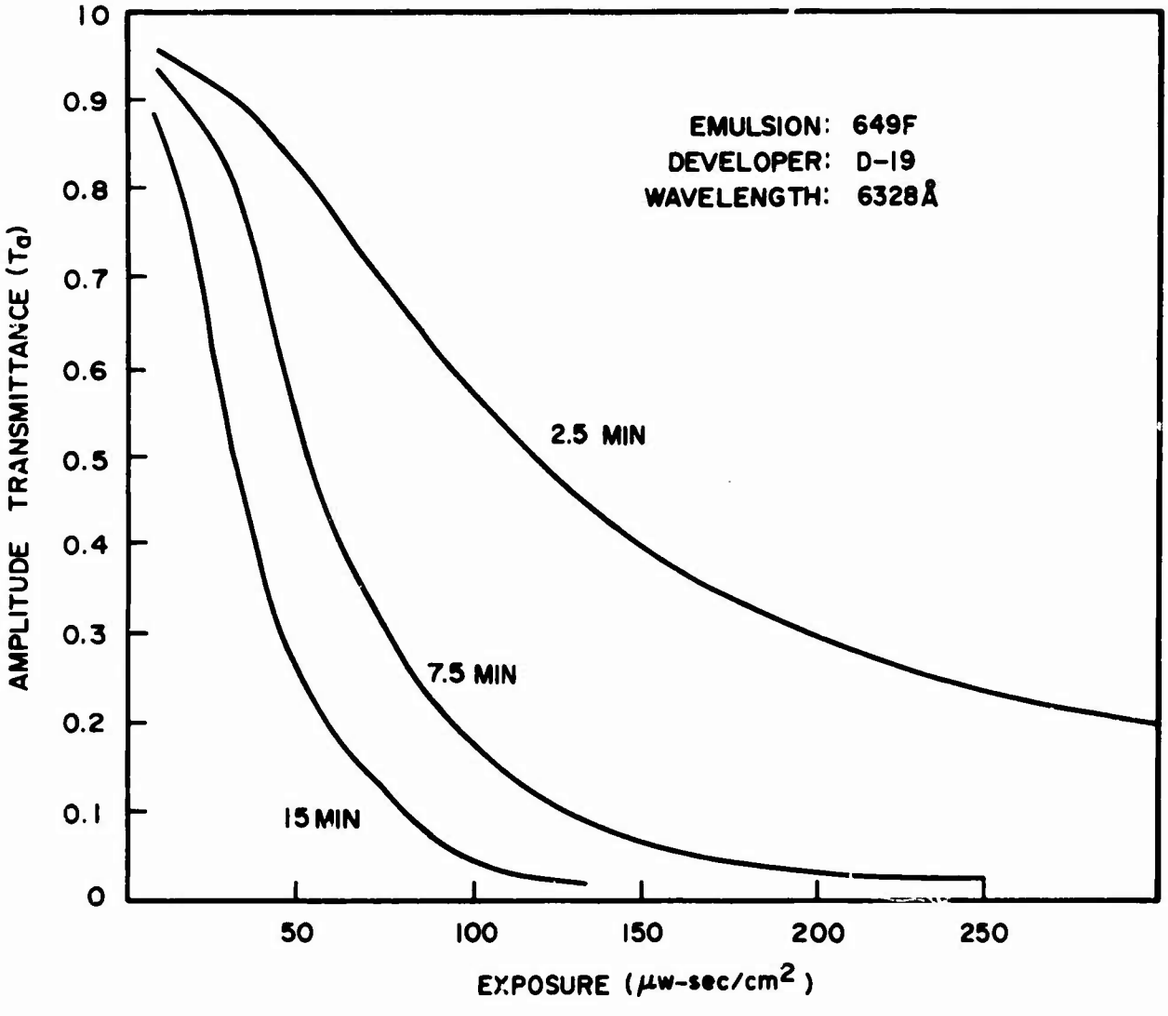

Figure 10. Experimentally Determined Amplitude Transmittance Curves of Kodak 649F Plates for Three Different Development Times.

This solution produces a hologram that will give almost distortion-free reconstructions. This, however, is done at the expense of efficiency, which is the fraction of the illuminating radiation diffracted into the reconstructed image. It has been determined[5] that the efficiency is linearly related to the modulation (or visibility) of the fringes for a fixed bias level. Consequently, a trade-off exists between reconstructed image brightness and possible degradations such as a decreased signal-to-noise ratio and false image generation. The particular application of holography will determine which factor can be sacrificed.

The MTF of the Photosensitive Medium. In addition, a photosensitive medium does not respond equally to all spatial frequencies. The response is measured by a function called the modulation transfer function (MTF), which is the ratio of the resulting image modulation (visibility) to the original object, or exposing, modulation. This is measured as a function of modulation (spatial) frequency and is generally found to be relatively constant up to a certain frequency, after which the response decreases to zero and no image modulation occurs. This cutoff is primarily caused by image diffusion due to scattering and is related to the mean grain size and the type of development process. For 649F film the response at 2200 lines/mm is down to 70% of its peak value. The cutoff for this film has not, as yet, been precisely determined; however our previous work[4] in Lippmann photography showed a response out to at least 6000 lines/mm.

Spatial frequency response limitations impose two restrictions on the holographic process. The first is that the maximum angle between signal and reference beam is limited by the maximum spatial frequency that can be recorded. By the communications theory analogy, this means that the upper limit of the information bearing sideband ($\eta + \omega$) is determined. For a particular carrier frequency, η, this then limits the angular size of the object that can be recorded. The second restriction is that the "zone lens" type of interference pattern due to a particular object point becomes washed out at a certain frequency (diameter). Since the resolution in the final image is

determined primarily by the aperture of this effective lens, any restriction in its diameter will, of course, limit the resolution. This is most serious for the carrier frequency type of hologram since the "lens" is biased on a carrier and hence will cut off faster.

The Thickness of the Photosensitive Medium. When the spatial frequency of the recorded fringe pattern produces a fringe separation comparable to the thickness of the photosensitive medium, the medium can no longer be considered to be two-dimensional. Just as in the special case of Lippmann photography, the fringes must now be considered to produce structure throughout the thickness of the emulsion, thereby forming a hologram that has the properties of a three-dimensional grating. The reconstruction process must now be analyzed on the basis of Bragg angle diffraction in a manner analogous to x-ray diffraction from crystals. This analysis has been carried out[6] and shows that the diffraction efficiency is a function of the angle at which the incident illumination strikes the hologram and of the wavelength of the illumination. The relationship is approximately a $((\sin x)/x)^2$ function, which oscillates such that each successive peak is weaker than the previous one. The argument of the above function not only contains factors relating to the previously mentioned readout parameters, but is also dependent on the exposing parameters (angles) as well as thickness.

This means that, for a particular set of exposure values, the efficiency of the reconstruction process will be a maximum when the hologram is illuminated from the same angle as the original reference beam. Any deviation from this angle will cause the image intensity to decrease to zero (in theory) and then to rise again to another peak value that is lower than the primary peak. As the angle is increased further the intensity again drops, and so forth. The effect of the exposing parameters is to regulate the rate at which this function oscillates. For example a low spatial frequency hologram (small angles) will allow a large angular misregistration of the reference beam before the reconstructed image is extinguished at the first minimum of the $((\sin x)/x)^2$ function. As the spatial frequency increases,

the angular tolerance on the readout beam direction becomes tighter. Actual data shows, for example, that for an angle of 15° between the signal and reference beams, the readout beam can vary ± 15° before the image is extinguished. At a 70° angle, however, the readout beam can vary only ± 4°.

This effect allows a means for storing multiple holograms within the same volume. This is accomplished by storing the first hologram with a large angle between signal and reference beam. The second hologram containing different information is then stored with a new reference beam angle. This angle is selected so that a subsequent illumination from this new direction would produce a minimum reconstruction from the first hologram. Hence, each hologram can be retrieved individually, with a minimum of signal cross talk from the other holograms. The number of holograms that can be stored in this manner is limited by the rapidity at which an individual hologram can be extinguished by an angular change of the readout beam. This is primarily a function of the thickness of the storage medium.

In addition to a change in the intensity of the reconstructed image, there is also a change in its angular position with respect to the hologram plate. This arises because the reconstruction process must obey the grating equation at all times. The grating equation may be written for the virtual image as

$$\sin \theta_i - \sin \varphi_i = - \sin \varphi + \sin \theta \qquad (22)$$

where θ_i is the angle of incidence of the readout illumination, φ_i is the angular direction of the reconstructed image, φ is the original angular direction of the object, and θ the original angle of incidence of the reference beam. If the readout angles shift from θ_i to $\theta_i + \Delta\theta_i$, then the reconstruction angle changes from φ_i to $\varphi_i + \Delta\varphi_i$ such that

$$\sin (\theta_i + \Delta\theta_i) - \sin (\varphi_i + \Delta\varphi_i) = - \sin \varphi + \sin \theta \qquad (23)$$

is satisfied. If, before rotation, the illumination exactly reproduced the

reference beam (i. e., optimum alignment), we could put $\varphi_i = \varphi$ and $\theta_i = \theta$ and write:

$$\sin(\theta + \Delta\theta_i) - \sin(\varphi + \Delta\varphi_i) = \sin\theta - \sin\varphi \qquad (24)$$

From this we see that for small angles we can write $\sin\alpha \approx \alpha$; hence, $\Delta\varphi_i = \Delta\theta_i$. Consequently, the reconstructed image can be repositioned angularly by changing the angle of illumination of the hologram. There is, of course, associated with this repositioning a corresponding fall off in intensity as previously discussed.

2.2.5 Other Properties and Their Applications

In addition to the holographic properties treated so far, many modifications and extensions of the process have been made in order to satisfy particular applications. Some of these will be briefly described here in an attempt to give an overall picture of the wide scope of applications possible with this concept.

Multicolor Holograms. A method for obtaining a multicolor hologram has been proposed by Leith and Upatnieks.[7] This method is essentially a superposition of three planar holograms and, as such, is a natural extension of the monochrome technique. Widely different angles for each spectral component of the reference beams are required to avoid the cross talk between colors. A method proposed by Pennington and Lin[8] obviates the need of multidirectional reference beams and has the advantages of less noise and more holograms that can be stored on the recording plate. Figure 11 shows an arrangement for making a two-color hologram.

Collimated beams from an argon laser (4880 Å) and a He-Ne laser (6328 Å) are mixed through a beam splitter. The two beams are recombined at the recording plane by two mirrors. A color transparency is placed in one of the beam paths as the object. The most important feature of this system is that all reference beams can be directed toward the plate at the same angle. The information fringes of each color build a set of planes

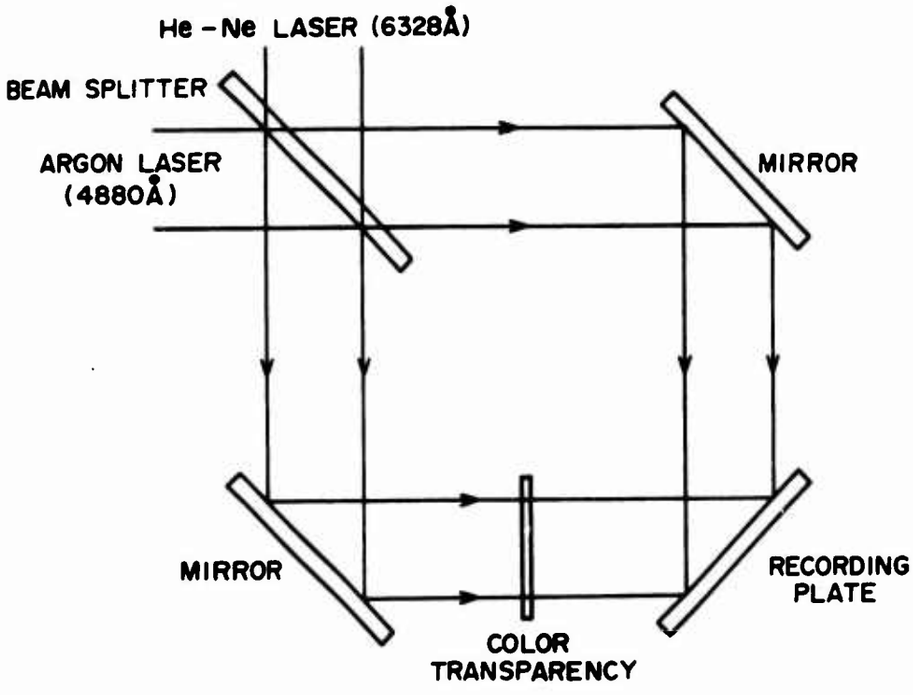

Figure 11. Method of Making a Two-Color Hologram.

within the emulsion. A particular color reconstruction is obtained by illuminating the hologram with that particular beam. If multicolor beams are used, a single multicolor image is produced.

Contour Generation. Ordinary holography presents a three-dimensional image of an object in a dramatic way. However, the measurement of an object's depth is no surer than the measurement by a viewer of any object seen at a distance. An observer cannot tell precisely from the holographic image how far away each point in the image is, just as in general he cannot judge distances with an accuracy of better than 5 to 10 percent. Contour holography brings precision to the technique.

To produce an image with contours, more than the usual amount of information must be put on the hologram. Two methods have been reported for producing contour mapping of certain objects.[9] The object is illuminated with coherent light sources located at two different positions with a small angle between them, and the hologram is placed at 90° relative to the illuminating beams. The depth of separation of the adjacent contours can be calculated by a mathematical formula. The object can also be illuminated with two different coherent frequencies. If the object lies at a distance such that the phase difference between two waves is a multiple of 2π or is an integral number of wavelengths, the two waves are in phase and a bright line results. Otherwise the dark lines would show. This sequence of bright and dark lines represents the contours of certain distances from the hologram recording plate. The depth separation between contours is $\lambda^2/\Delta\lambda$, where $\Delta\lambda$ is the difference of the two wavelengths and λ is the mean wavelength. The contour interval can be chosen by selecting the appropriate frequency separation.

Data Storage and Character Recognition. Data can be efficiently stored at high densities in photosensitive materials using interference techniques such as the Lippmann[10] process and holography. Data can be stored in holograms either by varying color or by varying exposure angles. Storage capabilities

of one million bits on a half-inch-square potassium bromide crystal have been reported.[11]

Character recognition[12] with many variants is another interesting application of holography. Let the reference beam be a character and the signal beam be a combination of point sources, forming a unique code word for each character. The unknown character can be read by a machine when the character illuminates the hologram. The coded signal word will be presented as a real image. N characters are discriminated, each with M variants; the product MN can be made on the order of a thousand or more.

Synthetic Holograms. The main feature of this type of hologram is that the object does not have to exist physically. Several methods[13, 14, 15] were reported to produce synthetic holograms. A computer program that represents a "mathematical object" guides a plotter that draws a binary pattern. The pattern consists of many short parallel lines at proper positions. When reduced in size and recorded on film, such a binary pattern acts essentially like an ordinary hologram. Another method is the multiple exposures of a photographic plate to a pattern of Newton's rings. This method is essentially the interpretation of holograms as a collection of zone plates.

Holograms with Incoherent Light. Holograms produced using incoherent light have been described in several articles.[16, 17] The methods are based on forming two images, which produce the interference pattern between them. In a system reported by G. W. Stoke,[18] the light from the object is split into two beams by a beam splitter. Each beam passes through a lens to a mirror and back again through a lens. The two images are formed at different positions. The image points within each image are incoherent with each other. However, each point of one image is coherent with the corresponding point of the other image. At a specific plane each such coherent pair of points produces an interference pattern, and the summation at all patterns forms a hologram.

Copying Holograms. In a typical hologram the fringe spacings are in the order of microns. These fringes have an intensity gradient that, in the viewing process, effectively eliminates images beyond the first order. Accordingly, it is necessary to have a resolution on the order of 1000 lines/mm to make a good copy. Experiments were carried out[19] for copying holograms from a Michigan plate hologram and a Westinghouse film hologram. The film used was Eastman Kodak 649-GH, which has a resolution better than 2500 lines/mm.[20] Conclusions of these experiments can be summarized as follows.

The distance between the hologram and copying emulsions is very critical. An estimated [illegible] separation was used. The copy from the Michigan plate hologram was observed to have some loss of resolution; the Westinghouse film hologram is nearly perfect. The illuminating light should come from a similar direction, with respect to the hologram, as the incident light in the original. Best results for the glass-plate hologram were obtained by having the printing source come from a direction midway between the viewing virtual image direction and the original reference light source direction. When the angular orientation of the source was reversed, no image could be seen in the copy. The film processing is not critical. Kodak D-19, D-8, and High Resolution Plate Developer have been used and were found satisfactory.

3-D Holographic Television and Motion Pictures. The possibility of holographic television was discussed in a paper by Leith and his colleagues.[21,22] The results show that such a system is feasible in principle, but wide bandwidth and high camera resolution limit the system. A hologram 10 inches square with 1000 lines/mm has 6×10^{10} picture elements, compared with 2.5×10^{5} for a conventional television picture. If the scan rates of present television systems were maintained, a 10^{5} increase in bandwidth would be necessary--a jump from 6 to 600,000 megahertz. Reasonable design compromise could reduce the problem to 100 MHz bandwidth, which is still in the microwave region. The best solution for this problem is to use a modulated

laser beam to obtain the required bandwidth of the holographic television system.

Some scenes of 3-D holographic movies were successively demonstrated at the Stanford University System Techniques Laboratory.[23] The holographic movies were a series of still holograms. A steady "shooting platform," which has a movement of less than 1/8 wavelength, is required to make the holographic movies.

Others. Holograms can be used as a unique type of interferometer, capable of detecting different motions of the order of 1/10 wavelength in a diffuse reflecting surface. Real time strain analysis and vibration analysis use hologram interferometry. Different techniques are describes in various articles.[24-29]

360° holograms were first made by two Japanese scientists.[30] A monochromatic coherent light illuminates the object through an unsilvered central portion of a convex spherical mirror. A Fresnel diffraction pattern of the object is formed at the recording plate. The recording plate is on a cylindrical surface with the object at its center. Light reflected from a mirror is the reference beam. These two beams form an interference pattern and a hologram is made.

The reconstruction process was carried out by winding the hologram around the same cylindrical surface and illuminating it with light from the mirror. The image of the object is produced at its original position suspended in space.

Undistorted reconstructed images have been obtained by placing an inhomogeneous medium between an object and the recording plane.[31,32] The same inhomogeneous medium that was used for making the hologram must be used in the reconstruction. This technique can be used for controlling wave transmission through inhomogeneous media for communication purposes or for measurement of the stresses of other disturbances in nonopaque media.

A Laser Fog Disdrometer was built by Technical Operations, Inc. This is a holographic camera for recording the size and distribution of particles suspended in the air.[33,34] A Q-switched laser emits highly intense light every two seconds, lasting 20 billionths of a second. During this instant, a recording film in another section of the instrument records a hologram of all particles illuminated by this camera. Later, a history of the growth and decay of the particles is analyzed in detail when the scenes are reconstructed.

A laboratory demonstration of x-ray holograms was given by El Sum[35] in 1955. The reconstructed images of simple objects, which only showed up to three fringes, were obtained. The poor image quality is mainly due to the lack of an intense coherent x-ray source. If this difficulty could be overcome, the rewards would be considerable, especially in the field of medical science. Several technical discussions on this subject have appeared in various articles.[36,37]

2.3 MAGNIFICATION[38]

Real and virtual images can be obtained in the reconstruction of a hologram according to Equation 15. The amplitude distribution of the light in the real image is

$$H_R = k t b^2 A^*(x,y)\, e^{i2\eta x}$$

and in the virtual image is

$$H_V = k t b^2 A(x,y)$$

These expressions were obtained by assuming a plane wave $b\, e^{i\eta x}$ as the reference beam and also as the reconstructing beam. The complex quantity used as the wavefront from the object is $A(x,y)$. In general, one could write the reference wavefront as $R e^{i\varphi_r}$, the wavefront from the object being recorded holographically as $O e^{i\varphi_o}$, and the reconstruction wavefront as $C e^{i\varphi_c}$. The amplitude distribution in the real image would then be given by

$$H_R = k\,t\,ROC\,e^{i(\varphi_c - \varphi_o + \varphi_r)} = k\,t\,ROC\,e^{i\Phi_R} \tag{25}$$

and in the virtual image by

$$H_V = k\,t\,ROC\,e^{i(\varphi_c + \varphi_o - \varphi_r)} = k\,t\,ROC\,e^{i\Phi_V} \tag{26}$$

The phase of the wavefront forming the real image is given by

$$\Phi_R = \varphi_c - \varphi_o \quad \varphi_r \tag{27}$$

and the virtual image by

$$\Phi_V = \varphi_c + \varphi_o - \varphi_r \tag{28}$$

Specific expressions in terms of space coordinates can be obtained for φ_c, φ_o, and φ_r. Consider an object point $P(x_o, y_o, z_o)$ in a coordinate system whose origin is in the center of the hologram with the x and y axes in the hologram plane (Figure 12). If the object is illuminated with monochromatic light of wavelength λ from the left, a spherical wave will emerge from P. Its phase within the hologram plane relative to the phase at the origin is given by

$$\begin{aligned}
\varphi_o(x,y) &= \frac{2\pi}{\lambda} \quad (PQ - PO) \\
&= \frac{2\pi}{\lambda} \quad \{ [(x - x_o)^2 + (y - y_o)^2 + z_o^2]^{1/2} \\
&\quad - [x_o^2 + y_o^2 + z_o^2]^{1/2} \} \\
&= \frac{2\pi}{\lambda} z_o \{ [1 + \frac{[(x - x_o)^2 + (y - y_o)^2]}{z_o^2}]^{1/2} \\
&\quad - [1 + \frac{x_o^2 + y_o^2}{z_o^2}]^{1/2} \}
\end{aligned} \tag{29}$$

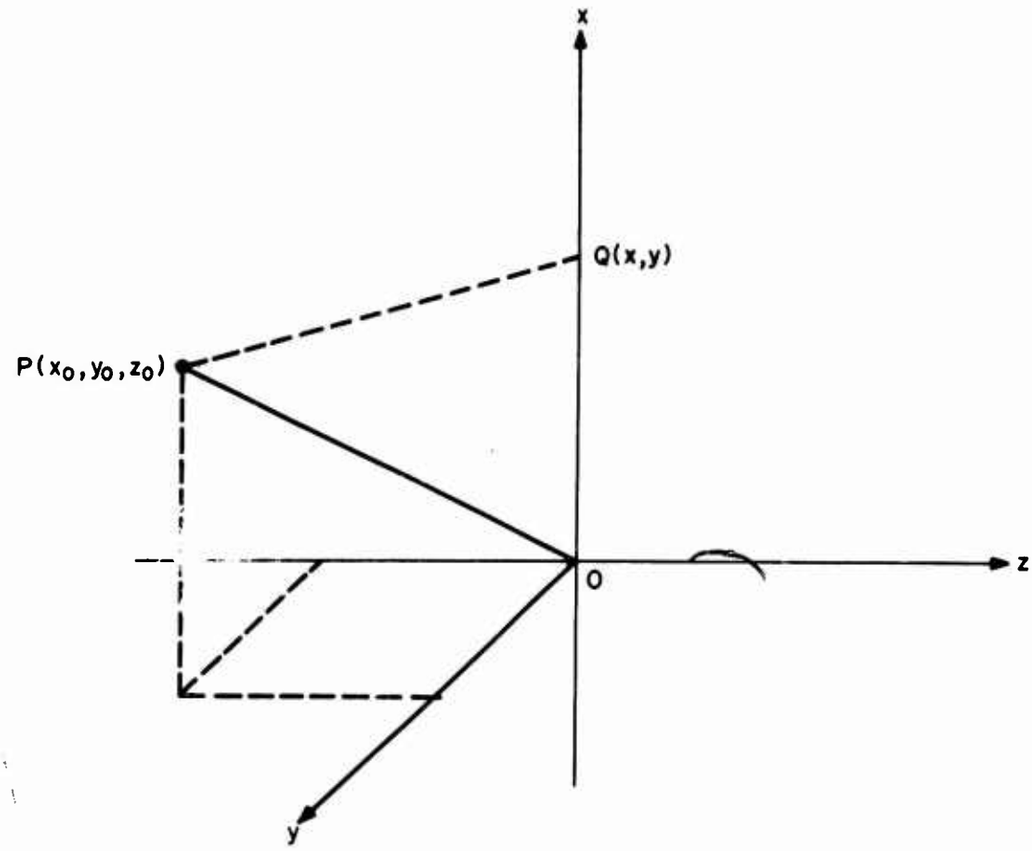

Figure 12. Coordinate System Used to Calculate the Relative Phase in the Hologram Plane (x-y Plane) of the Wavefront Originating from the Illuminated Object.

Expansion of the square roots in Equation 29 in the form of

$$(1 + a)^{1/2} = 1 + \frac{a}{2} - \frac{a^2}{8} + \text{(higher order terms)}$$

leads to the following expression for φ_o. (Terms of higher order than $1/z$ are neglected since they are only important when considering aberrations.)

$$\varphi_o(x, y) = \frac{2\pi}{\lambda} \left[\frac{x^2 + y^2 - 2xx_o - 2yy_o}{2z_o} \right] \tag{30}$$

The reference beam wavefront originates from a point $P(x_r, y_r, z_r)$, and the phase at some point (x, y) in the hologram plane relative to the origin is obtained exactly as φ_o was obtained. The result is

$$\varphi_r = \frac{2\pi}{\lambda} \left[\frac{x^2 + y^2 - 2xx_r - 2yy_r}{2z_r} \right] \tag{31}$$

The reconstruction beam of the same wavelength λ originates at a point $P(x_c, y_c, z_c)$, and the phase relative to the origin is

$$\varphi_c = \frac{2\pi}{\lambda} \left[\frac{x^2 + y^2 - 2xx_c - 2yy_c}{2z_c} \right] \tag{32}$$

The phase of the wavefront forming the virtual image (Equation 28) is

$$\Phi_V = \frac{2\pi}{\lambda} \left[\frac{x^2 + y^2 - 2xx_c - 2yy_c}{2z_c} \right] + \frac{2\pi}{\lambda} \left[\frac{x^2 + y^2 - 2xx_o - 2yy_o}{2z_o} \right]$$

$$- \frac{2\pi}{\lambda} \left[\frac{x^2 + y^2 - 2xx_r - 2yy_r}{2z_r} \right] \tag{33}$$

and the real image (Equation 27) is

$$\Phi_R = \frac{2\pi}{\lambda}\left[\frac{x^2 + y^2 - 2xx_c - 2yy_c}{2z_c}\right] - \frac{2\pi}{\lambda}\left[\frac{x^2 + y^2 - 2xx_o - 2yy_o}{2z_o}\right]$$

$$+ \frac{2\pi}{\lambda}\left[\frac{x^2 + y^2 - 2xx_r - 2yy_r}{2z_r}\right] \tag{34}$$

Equation 33 can be rewritten as

$$\Phi_V = \frac{2\pi}{\lambda}\left[\frac{x^2 + y^2 - 2x\alpha_V - 2y\beta_V}{2\gamma_V}\right] \tag{35}$$

where

$$\alpha_V = \frac{x_c z_o z_r + x_o z_c z_r - x_r z_c z_o}{z_o z_r + z_c z_r - z_c z_o} \tag{36}$$

$$\beta_V = \frac{y_c z_o z_r + y_o z_c z_r - y_r z_c z_o}{z_o z_r + z_c z_r - z_c z_o} \tag{37}$$

$$\gamma_V = \frac{z_c z_o z_r}{z_o z_r + z_c z_r - z_c z_o} \tag{38}$$

Equation 35 can be considered as representing the first-order term of a new sphere, the Gaussian reference sphere with α_V, β_V, and γ_V the off-axis coordinates of its center, the Gaussian image point.

The corresponding expressions for the real image are

$$\Phi_R = \frac{2\pi}{\lambda}\left[\frac{x^2 + y^2 - 2x\alpha_R - 2y\beta_R}{2\gamma_R}\right] \tag{39}$$

where

$$\alpha_R = \frac{x_c z_o z_r - x_o z_c z_r + x_r z_c z_o}{z_o z_r - z_c z_r + z_c z_o} \tag{40}$$

$$\beta_R = \frac{y_c z_o z_r - y_o z_c z_r + y_r z_c z_o}{z_o z_r - z_c z_r + z_c z_o} \tag{41}$$

$$\gamma_R = \frac{z_c z_o z_r}{z_o z_r - z_c z_r + z_c z_o} \tag{42}$$

The object, reconstruction, and reference wavefronts were all assumed to originate from points, and the calculation of the relative phase in the hologram plane gave rise to a particular type of expression with the coordinates of the point of origin as constants in the expression. The expressions for Φ_V and Φ_R (Equations 35 and 39) appear identical to the expressions obtained for φ_o, φ_c, and φ_r. Consequently, by analogy the constants in the expressions for Φ_V and Φ_R are interpreted as the coordinates of the images. The virtual and real images corresponding to the object point $P(x_o, y_o, z_o)$ are located at $P(\alpha_V, \beta_V, \gamma_V)$ and $P(\alpha_R, \beta_R, \gamma_R)$, respectively. γ_V and γ_R may be positive or negative. If γ_V is positive, the image is real rather than virtual. If γ_R is negative, the image is virtual. While z_o is always negative, z_r and z_c may be chosen at will within experimental limitations, and either image can be real or virtual.

Viewing distances must be defined in order to calculate angular magnifications. It seems natural to choose z_o as the distance from which the object is seen and γ_V or γ_R as the image viewing distance, whichever is virtual. In other words, the observer's eye is placed in the hologram plane to view both the object and the image. The angular magnification is defined as the ratio of the angle subtended at the eye by the image to the angle subtended by the object. The angular magnification for the virtual image is then

$$M_{ang} = \frac{\partial(\alpha_V/\gamma_V)}{\partial(x_o/z_o)} = \frac{\partial\left(\frac{x_c}{z_c} + \frac{x_o}{z_o} - \frac{x_r}{z_r}\right)}{\partial(x_o/z_o)} = 1 \tag{43}$$

This means that if the observer puts his eyes in the plane of the hologram, he will not be able to obtain any angular magnification by varying geometrical parameters.

The lateral magnification for both the real and virtual images is given by

$$M_{lat} = \frac{\partial \alpha}{\partial x_o} \tag{44}$$

or specifically

$$M_{V\,lat} = (1 + z_o/z_c - z_o/z_r)^{-1} \tag{45}$$

and

$$M_{R\,lat} = (1 - z_o/z_c - z_o/z_r)^{-1} \tag{46}$$

The above formulas are valid for real and virtual images, although practical application is meaningful only for real images. Because the lateral magnification depends on the ratio z_o/z_r, only a certain range of magnifications is possible with one particular hologram. Ranges of magnification for various ratios of z_o/z_r are shown by the curves in Figure 13. For some values of the ratio z_c/z_o a negative magnification results. All this means is that image is no longer real, but virtual.

Normally, the holographic virtual image is observed by looking through the hologram itself. In such a situation, the eyes are not located in the plane of the hologram but a distance ρ in back of it. The angular magnification of the virtual image then becomes

$$M_{ang} = \frac{\dfrac{x_o\ M_{V\,lat}}{\gamma_V + \rho}}{x_o/z_o} = \frac{\dfrac{x_o\ M_{V\,lat}}{z_o\ M_{V\,lat} + \rho}}{x_o/z_o}$$

$$= (1 + \frac{\rho}{z_o\ M_{V\,lat}})^{-1} \tag{47}$$

The angular magnification can at most be unity. This occurs when $\rho = 0$ or $M_{lat} \to \infty$. For all other values of M_{lat}, as determined by the radius of the

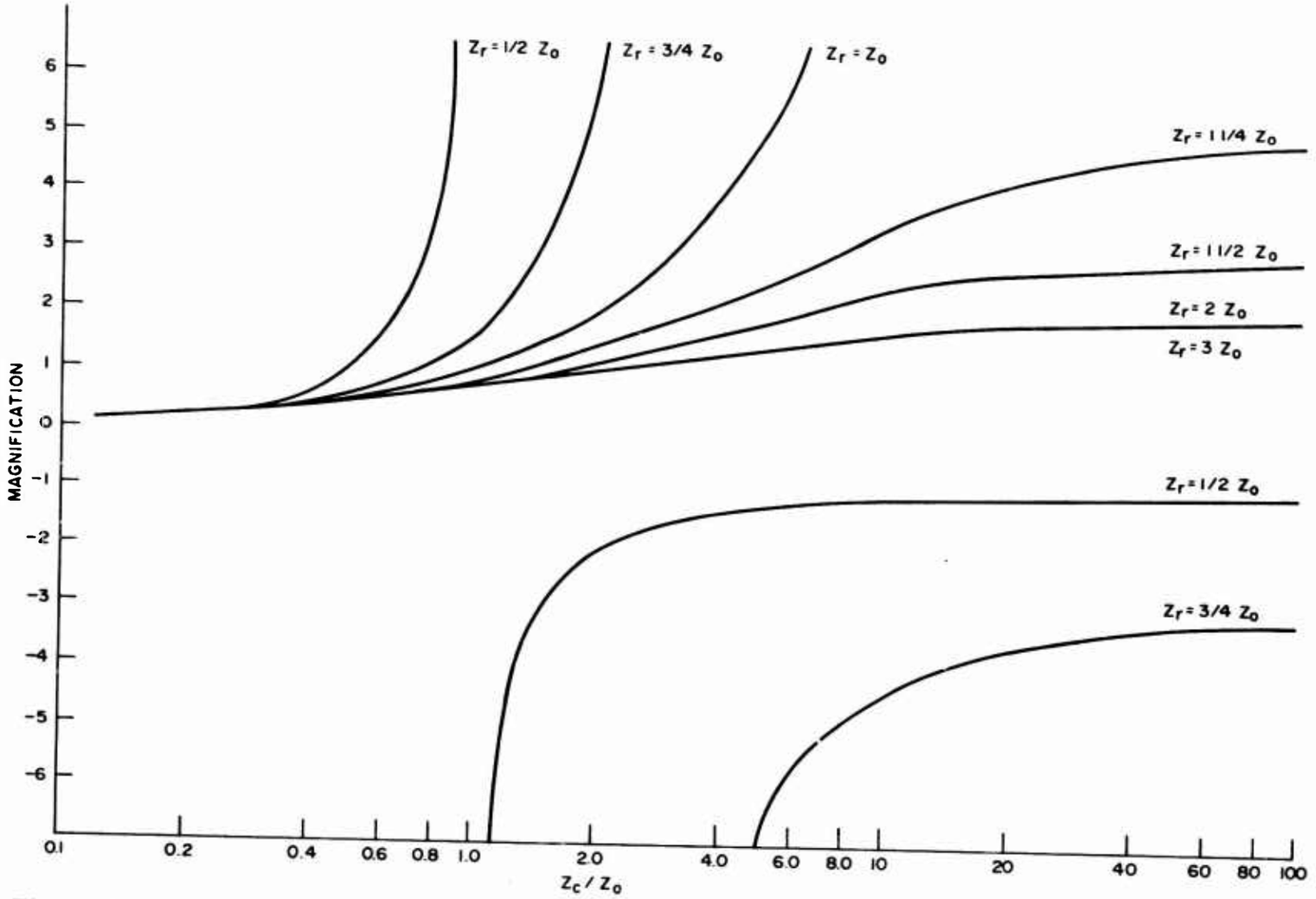

Figure 13. Curves of the Available Lateral Magnification in the Real Image for Various Ratios of the Recording Reference Beam Wavefront Radius, z_r, to the Object Distance, z_o. z_c is the Radius of the Reconstruction Wavefront.

reconstructing wavefront, the magnification is less than unity. If the virtual image is going to be used, it is only meaningful to talk about the angular magnification, rather than the lateral magnification, and this magnification is always unity or less.

Another useful magnification criteria when dealing with 3-D objects and images in holography is the longitudinal magnification. This refers to the magnification along the z-axis and is given by

$$M_{long} = \frac{\partial \gamma_R}{\partial z_o} = -\left(1 - \frac{z_o}{z_c} - \frac{z_o}{z_r}\right)^{-2} = -M_{lat}^2 \qquad (48)$$

The image will appear distorted with an incorrect length-to-width ratio since this magnification is the square of the lateral magnification.

2.4 COHERENCE

Radio waves are usually thought of as an oscillation with a single frequency. Light sources, however, consist of many colors or frequencies. In electronics the source of the wave is generally a well-defined single antenna. On the other hand, conventional light sources consist of a large number of small oscillators or radiators that radiate independently. Consequently, the light illuminating a finite area of surface will not have a wavefront with a constant phase. A light source that emits a wavefront with a constant phase and a narrow band of frequencies is characterized as a coherent source.

The degree of coherence of a light source is quite important in much of modern optics. Holography has made great strides in the last few years primarily because of the availability of highly coherent sources, lasers. A hologram is essentially the recording of the interference pattern resulting from the interaction of two coherent light beams. If these light sources have a poor coherence, the resulting interference pattern will not be well defined. The holographic image will lack contrast and tend to look washed out. In the making of a hologram and generally in its reconstruction, the highest possible coherence is desired.

Perfectly coherent light is monochromatic; i. e., the light consists entirely of one frequency or wavelength. The light is emitted by oscillators, all emitting in phase. No such perfect light source exists; all light is partially coherent. In a rigorous theory, a measure of coherence is a term that ranges from 0 to 1, called the real part of the complex degree of coherence, $|\gamma_{11}(\tau)|$. Perfect coherence corresponds to $|\gamma_{11}(\tau)| = 1$, and no coherence corresponds to $|\gamma_{11}(\tau)| = 0$. In more elementary considerations, the spatial and time coherence of a source are treated separately. The phase across a wavefront does not remain a constant as a function of time because the wavefront consists of light with a finite bandwidth. The time over which good coherence is maintained (coherence time) is approximately $1/\Delta\nu$ where $\Delta\nu$ is the frequency bandwidth of the light beam. The coherence length ℓ_c is defined as the velocity of the light beam times the coherence time, i. e., $c/\Delta\nu$. Light from several different oscillators will have a random phase with respect to each other. The technique used to achieve some degree of coherence in light emitted from conventional sources is to wavelength filter the light through a narrow bandpass filter and then aperture the light through a small opening. The degree of phase coherence across the wavefront is referred to as spatial coherence.

The limitation to the coherence of a laser is the oscillation of more than one longitudinal mode in the laser cavity. The mode spacing in frequency is equal to $c/2L$ where c is the vacuum speed of light and L is the length of the laser cavity. The number of modes that will oscillate is determined by the line width of the active laser media and the net gain in the laser resonator as is shown in Figure 14. Each oscillating mode is a precise frequency, but the sum of all oscillating modes represents a frequency spread that limits the time coherence $1/\Delta\nu$. The coherence length for a He-Ne laser, for example, may be as high as several feet. In making holograms, the path difference between the reference beam and the light reflected from the object whose image is being recorded must be less than the coherence length ℓ_c (see Section 3. 3).

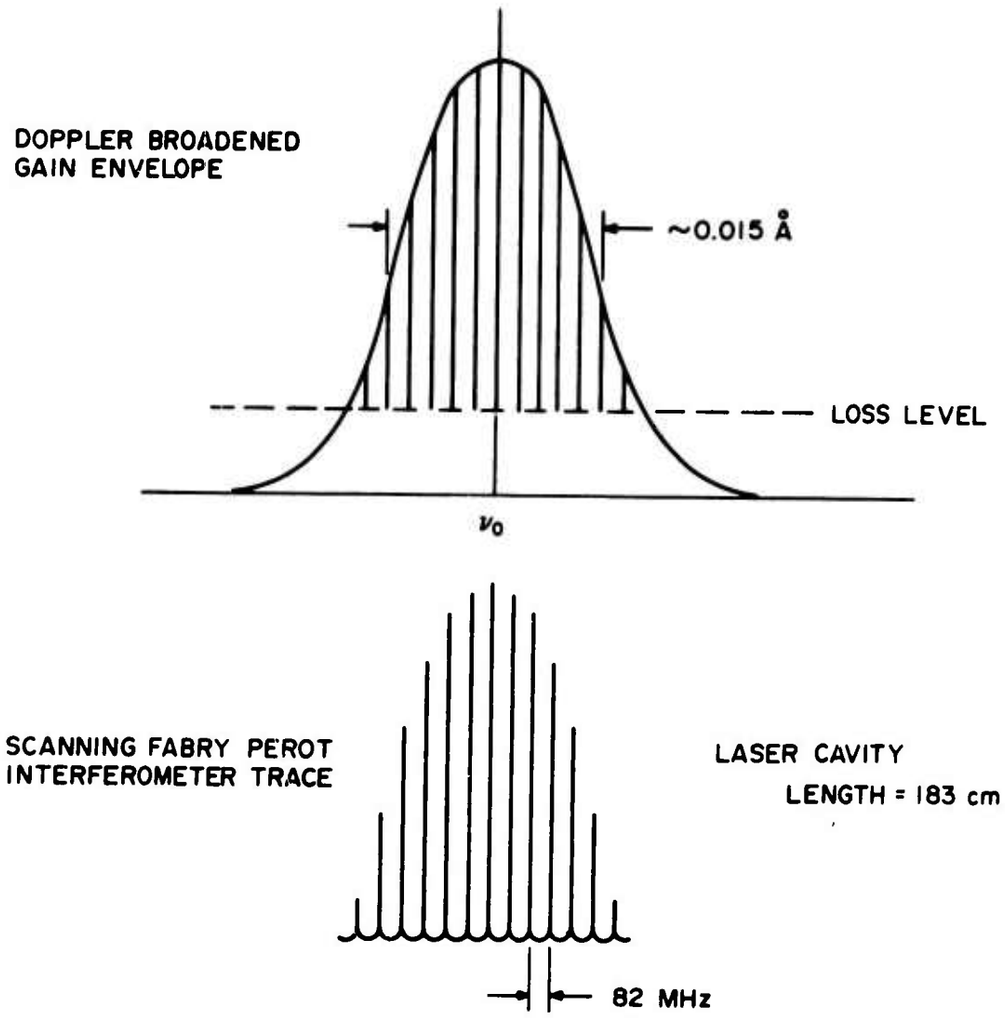

Figure 14. Typical Doppler Line Width of the He-Ne Laser Line and Longitudinal Modes Oscillating in a Laser Cavity.

The number of oscillating longitudinal modes and their relative amplitudes in the He-Ne laser used to record our particular holograms have been determined with a scanning Fabry Perot interferometer.[39] A photograph of the oscilloscope trace showing the output of the interferometer is shown in Figure 15. The coherence function, $|\gamma_{11}(\tau)|$, was calculated after determining the number of oscillating modes and their relative amplitudes. The coherence function can be obtained[40] from the spectral distribution, $G_{11}(\nu)$, of the light source by the following expression.

$$\Gamma_{11}(\tau) = 4 \int_0^\infty G_{11}(\nu)\ e^{-2\pi i \nu \tau}\ d\nu \tag{49}$$

In calculating the integral it was assumed that each oscillating mode represents a delta function in frequency. The calculated real part of the coherence function is

$$|\gamma_{11}(\tau)| = 0.167 + 0.29 \cos \frac{\pi \tau c}{L} + 0.23 \cos \frac{2\pi \tau c}{L} +$$

$$+ 0.166 \cos \frac{3\pi \tau c}{L} + 0.103 \cos \frac{4\pi \tau c}{L} + 0.046 \cos \frac{5\pi \tau c}{L} \tag{50}$$

where L = 183 cm for the He-Ne Spectra-Physics model 125 laser. The cosine terms in higher angle multiples were insignificantly small. This function is plotted in Figure 16. The real part of the function drops to zero at a time difference of approximately 1 nanosecond. The function peaks again at intervals of approximately 12 nanoseconds. The usable coherence length is about 6 inches at path difference intervals of 12 feet.

If the laser beam is broken into two separate beams and these two beams are superimposed at a shallow angle, an interference pattern of parallel straight lines will result with spacing as given by Equation 6. These

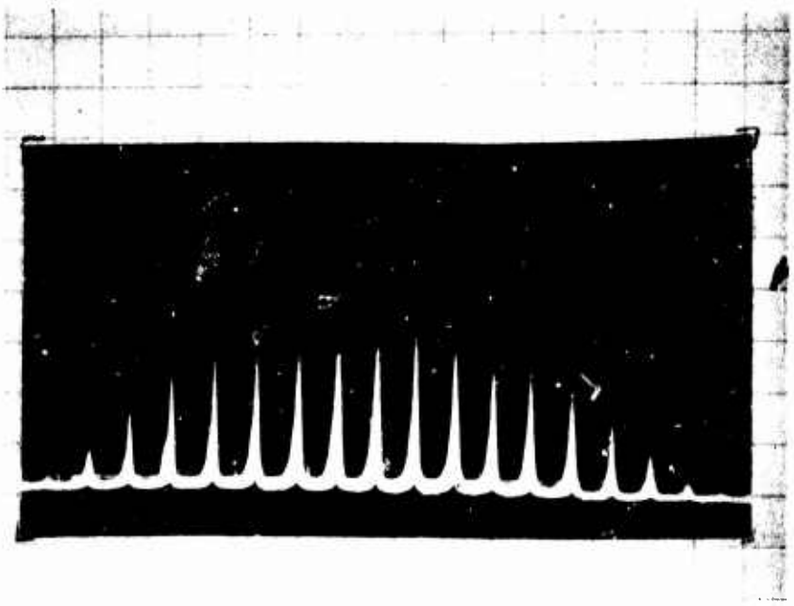

Figure 15. Output Trace of a Scanning Fabry Perot Interferometer Being Illuminated with a Beam from the He-Ne, Model 125, Spectra Physics Laser.

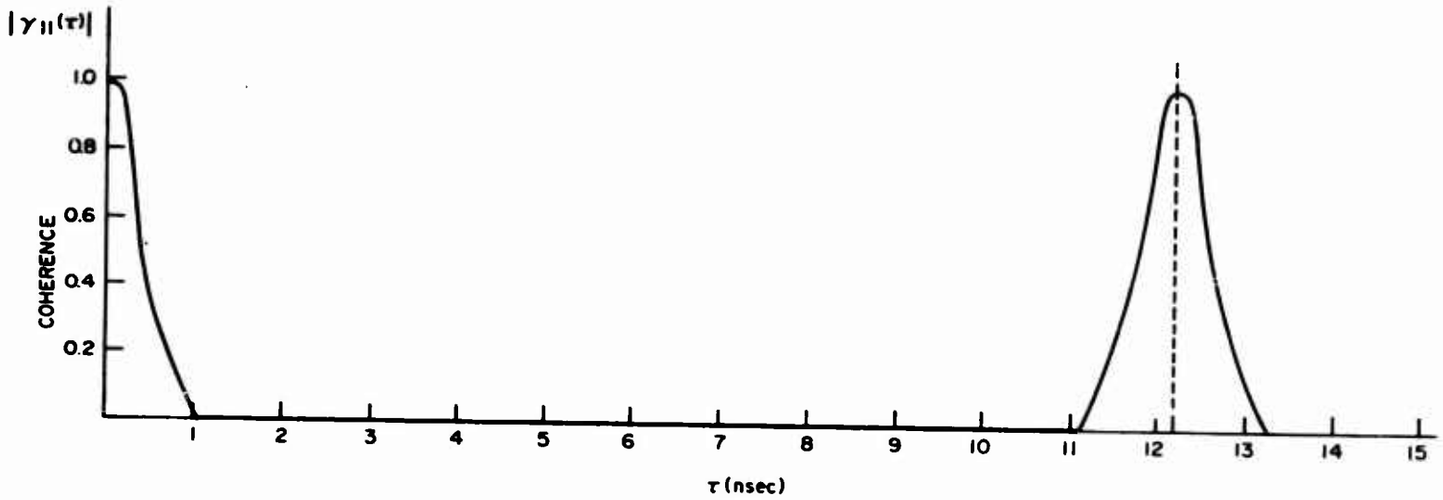

Figure 16. Plot of the Coherence Function, $|\gamma_{11}(\tau)|$ for the Output of the He-Ne, Model 125, Spectra Physics Laser.

straight lines will not be visible if the path difference between the two beams exceeds the coherence length. The visibility of the fringes was defined in Equation 7. This function can be shown to be equivalent to the real part of the complex degree of coherence. Such a fringe pattern was recorded with our laser for various path differences between the two beams. The experimental setup is shown in Figure 17. A density trace with an Ansco microdensitometer was made at right angles to the parallel lines. From these traces the visibility was calculated and plotted as a function of the path or time difference between the two beams. As shown in Figure 18, the determined visibility curve and the real part of the complex degree of coherence do not agree in shape as they should. However, both go to zero at a time difference of approximately 1 nanosecond. The shapes do not agree because of the nonlinearity of the recording media (649F film) and because of the difficulty in maintaining the same beam intensity at one fixed point as the path difference is varied.

Each one of the photographs with the recorded parallel lines (about 240 lines/mm) acts like a grating when inserted into a light beam. The first-order diffracted beam from this grating corresponds to the intensity thrown into the holographic reconstructed image. The amount of light thrown in the first-order diffracted beam was measured and compared with the incident beam for each one of the photographs. It was found, as expected, that a greater percentage of the light was thrown into the first-order (greater efficiency) beam under the conditions of best coherence between the two beams. Again the shape of the curve in Figure 18 does not coincide with either the visibility or the coherence function curves. No significance has been attributed to this lack of agreement since the conditions for exposing the photographs were not uniform. This effort was not refined because of experimental priorities.

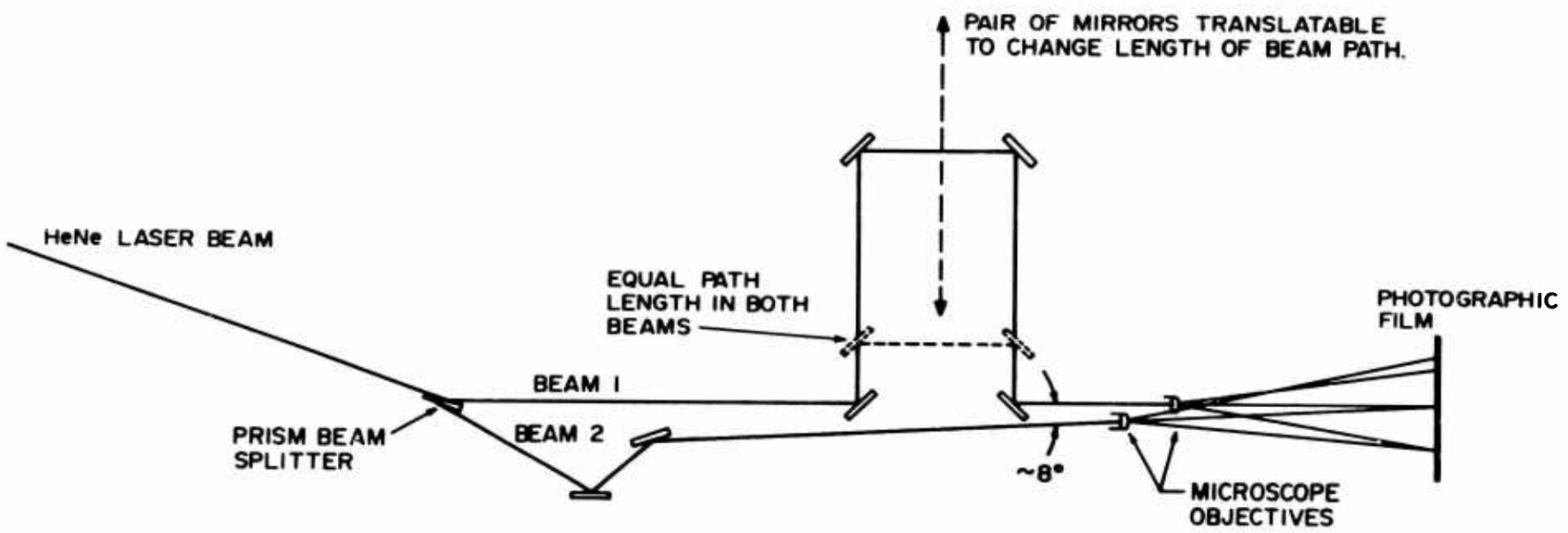

Figure 17. Experimental Apparatus for Determining the Coherence Length of a Laser.

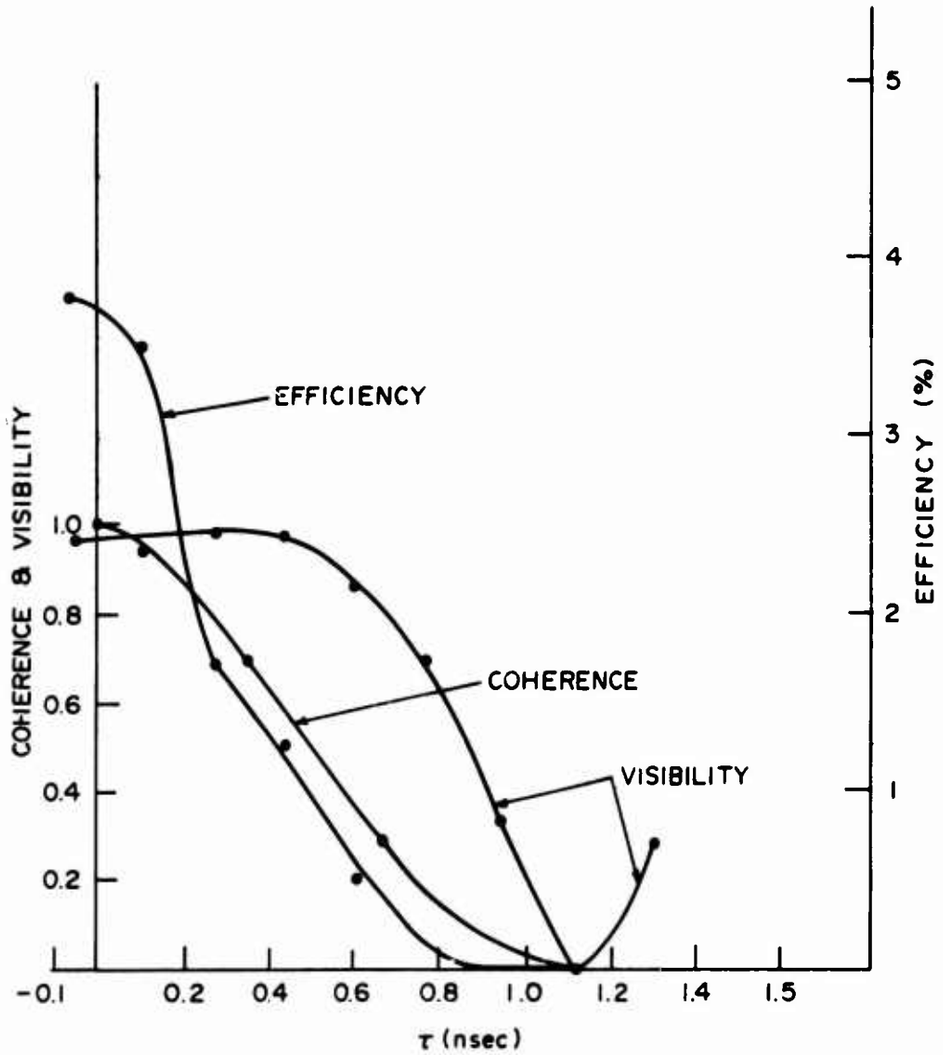

Figure 18. The Fringe Visibility, Holographic Reconstruction Efficiency, and Coherence Plotted as a Function of the Time Difference between Two Interfering Beams.

3. HOLOGRAPHIC RECORDING TECHNIQUES

3.1 INTRODUCTION

The generation of holograms in the laboratory is, for the most part, considerably simpler than the theory would indicate. This is, of course, dependent on the degree to which certain requirements (or constraints) are satisfied. Those of primary concern include the selection of recording parameters, the coherency of the laser, and the vibrational stability of the components. In addition, the selection and control of the development process is important to ensure reproducible results of consistent quality. These items will be considered in more detail in the following sections.

3.2 RECORDING PARAMETERS

In general, the selection of recording parameters involves both theoretical and practical considerations and is usually a compromise between them. The physical positioning of the optical components in the exposure system is, to a large degree, determined by the desired angle between the signal and reference beams. Hence, once the object to be recorded has been selected and the hologram-to-object separation specified, the angular range over which the reference beam may be introduced is fixed. The minimum angle is fixed by the extent of the object so as not to cast a shadow on the recording medium. The maximum angle is usually constrained by the physical size of the bench or table surface. In addition, the minimum angle must be such as to prevent the observer from inadvertently looking at the readout beam.

These requirements must then be weighed against the theoretical considerations concerning the effect of the carrier-wave frequency. As was discussed earlier, these factors involve staying within the frequency response of the film, the angular extent of the object, the nonoverlapping of the sideband and zero-order frequencies, the desired image resolution, and the angular tolerance of the readout beam direction. For the type of objects used for this study and the high-frequency response of the 649F emulsion, it was

found convenient (and acceptable) to introduce the reference beam at an angle of 45° to the film normal.

A decision must then be made as to how many beams of light will be required to illuminate the object. This will be determined by the extent of the angular field over which the object is to be viewed and the extent of the object itself. The first consideration is to illuminate regions of the object(s) that would normally be shadowed by a single beam illumination. The second factor is to ensure that light from all regions of the object will be coherent with the reference beam and, hence, permit interference. (This matter will be taken up in the next section.)

Once the required number of beams has been determined, the means for creating them from a single laser beam may be considered. This may run the gamut from a single beam splitter, prism wedge, or diffraction grating up to a complex arrangement of many of these items together with mirrors. In our particular case, three beams were required (two illuminating and one reference). These were conveniently obtained from the three beams created by a prism wedge. That is, the transmitted beam and the first surface reflection were used to illuminate the object, and the weaker second surface reflection was used for the reference beam. The relative intensities of the beams could be adjusted by rotating the prism wedge to change the reflectivity of the first surface reflection. (Reflectivity of polarized light is a function of the angle of incidence.)

The final exposure system is shown in Figure 19. The optical paths of the three beams are adjusted so that when they strike the photosensitive medium they differ in path length by no more than the coherence length of the laser. The reference beam is diverged with a microscope objective to provide full illumination of the recording film. It is passed through a spatial filter (a 7.5μ pinhole at the focus of the objective) in order to provide a uniform wavefront. The location of this objective and hence the point of origin of the spherical reference wave P (x_r, y_r, z_r) are determined by the size of

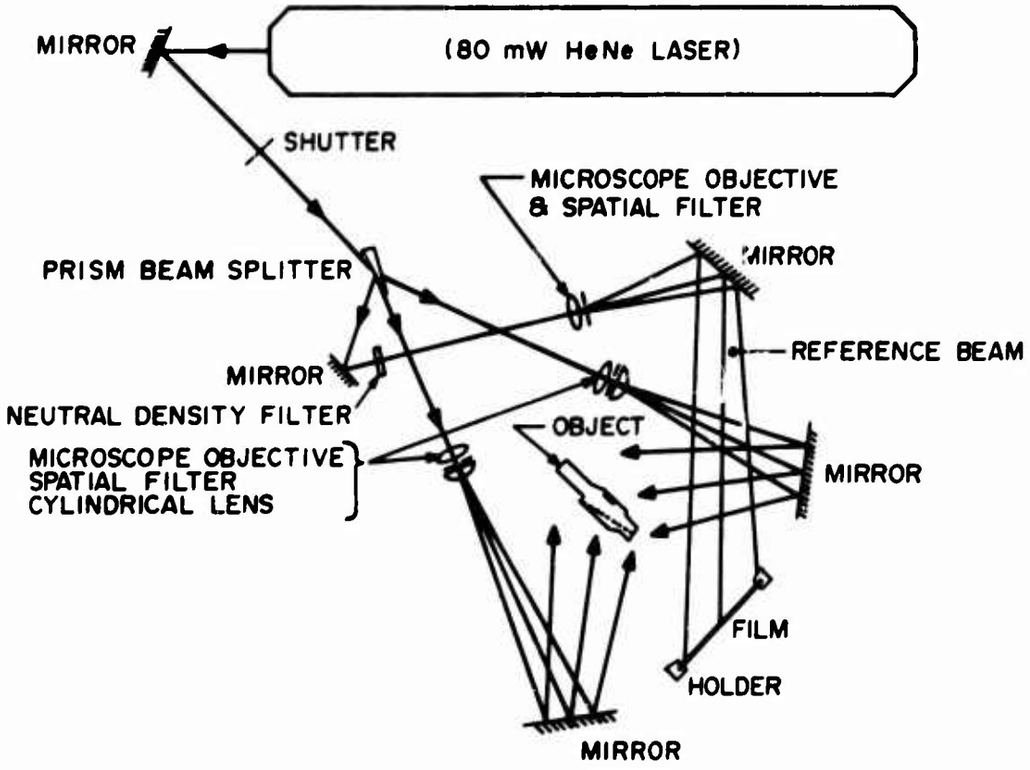

Figure 19. Hologram Exposure System.

the plate to be illuminated and by the requirements on magnification. The illuminating beams are also diverged with microscope objectives and filtered. Due to the shape of the carrier model, the circular cross sections of the illuminating beams were elongated by inserting cylindrical lenses into each beam. The lenses could be rotated to orient the elongated axis along the carrier deck.

The illumination at the recording plane was measured with an EG&G silicon photodiode that had been previously calibrated. The contribution to the total illumination was measured for the object and reference wavefronts independently. By inserting appropriate neutral-density filters into the reference beam, the ratio of reference-to-signal beams was adjusted to 3:1. This value was determined from experience to produce both high efficiency and a distortion free image, although it extends slightly beyond the linear portion of the amplitude transmittance curve.

It has been determined both experimentally and theoretically that the optimum exposure occurs when the resulting amplitude transmittance of the hologram is 50%. With this as the bias point, the exposure time was then determined from the amplitude transmittance versus exposure curves in Figure 10 and the measured illumination. Typical illumination levels (bias) would be in the 0.5$\mu w/cm^2$ to 1.0$\mu w/cm^2$ range, thereby requiring exposures ranging from 30 seconds to 200 seconds depending on the process time. The actual exposure is regulated by a solenoid-actuated shutter controlled with an electronic digital timer.

A photograph of a typical reconstructed image is shown in Figure 20 together with a photograph of the original model.

3.3 COHERENCE REQUIREMENTS

In order to record information about all points in the object space, it is necessary that the light scattered from all object points interact with the reference beam to produce a well-defined interference pattern. This can occur only if the interacting wavefronts are coherent with each other. (For a discussion of the physical nature of coherency, see Section 2.4.)

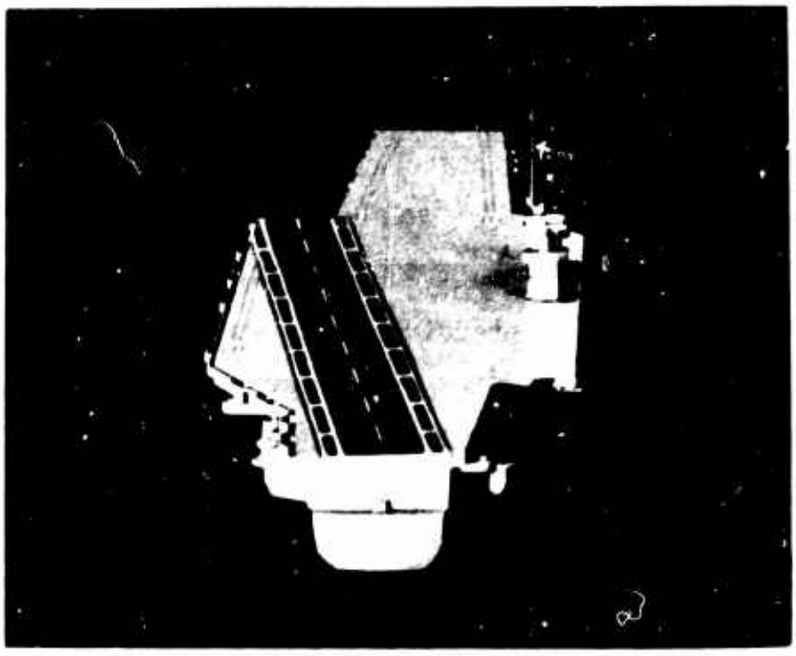

Figure 20a. Actual Model.

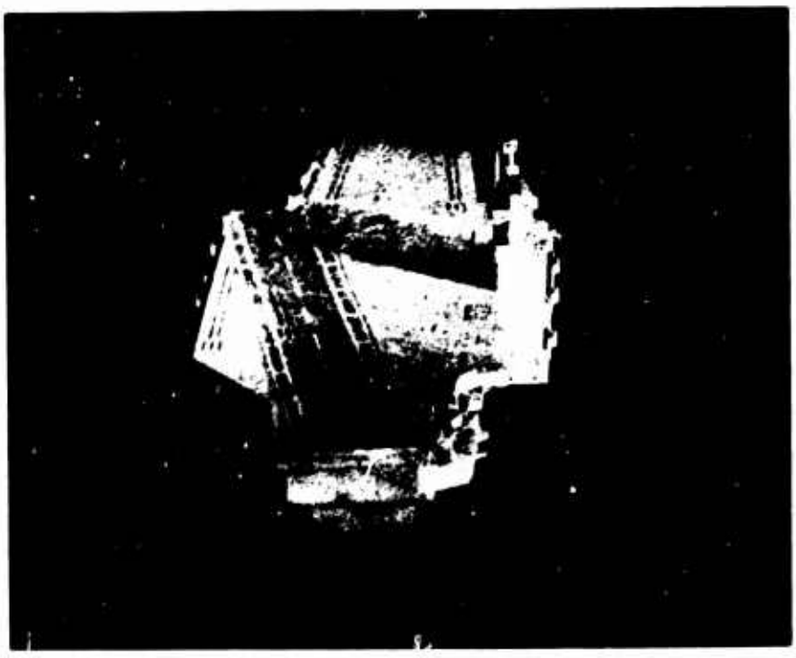

Figure 20b. Reconstructed Virtual Image from a Hologram. Note Image Degradation Caused by Stopping Down Camera to Gain Sufficient Depth of Field.

What this means to the recording process can be described with reference to Figure 21. Let us assume that the optical distance travelled by the central ray of the reference beam in passing from the point of beam splitting, S, to the recording plane, H, has been measured and is represented by the length d_r. In a like manner, let the optical distances travelled by the central ray in each of the illuminating beams in going from the splitting point to the center of the object, O, and then to the recording plane be made equal to each other (i.e., SBO = SCO). If the system is aligned so that the total object ray distance d_o (d_o = SBOH = SCOH) is equal to the reference beam distance d_r, then the wavefronts incident on the recording plane will produce a strong interference pattern. This equality can be created for only one point in the object space (in this case the center). Since the object has a finite extent, ℓ, in a direction perpendicular to the recording plane, all of the object rays will have a different length. It can be shown from Figure 21 that the object ray lengths vary approximately from $d_o + \ell\,(1+\cos\theta)/2$ to $d_o - \ell\,(1+\cos\theta)/2$. For small angles, the difference between the maximum and minimum object

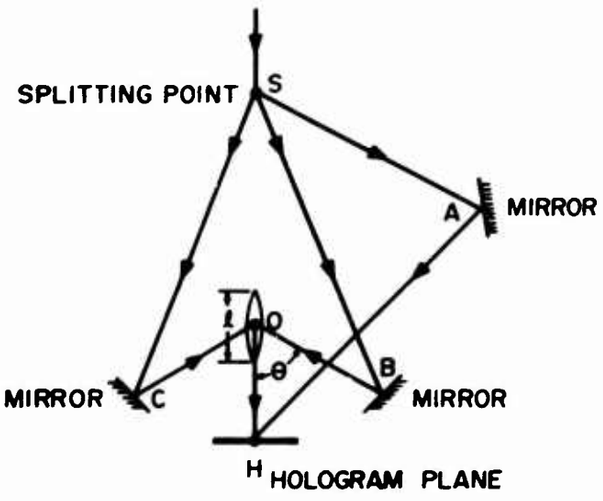

Figure 21. Hologram Recording Technique with Limited Depth of Field.

rays will be approximately 2ℓ. Consequently for an exposure system set up as shown in the figure, the difference between the object beam path and the reference beam path will vary between $\pm \ell$; i. e.,

$$0 \leq |d_r - d_o| \leq \ell$$

Useful interference between these two beams, however, will occur only if their path difference is less than the useful coherence length of the radiation, ℓ_c. The useful coherence length is defined as the half-width of the visibility curve measured between the points at which the visibility is reduced to 50%. We see, therefore, that for the entire object to be recorded, its total length must be less than the useful coherence length of the radiation; i. e., $\ell < \ell_c$.

As indicated in Section 2. 4, the useful coherence length of the Spectra Physics Model 125 He-Ne laser was measured to be 6 inches. The smallest carrier model commercially available, however, was 10 inches long. Consequently, in using this exposure technique, the entire length of the carrier cannot be recorded with equal brightness and fidelity. This was verified experimentally in that the front and rear ends of the deck were not visible in the reconstructed image.

One solution to this problem is to use a smaller model that is shorter than the coherence length. Since none was available, a miniature model was fabricated in the laboratory by scaling down the dimensions of the 10" model. The resulting model was 2. 5" long and made of aluminum. In order to provide diffuse reflection of the illumination, the model was coated with magnesium oxide in a polyvinyl alcohol binder. While this provides an adequate solution, it was not used extensively since there was much less detail in the scaled model.

Consideration must therefore be given to modifications of the exposure system such that the illumination from the object points will always differ from the reference beam by no more than this coherence length. One such solution is shown in Figure 22. In this arrangement the illuminating

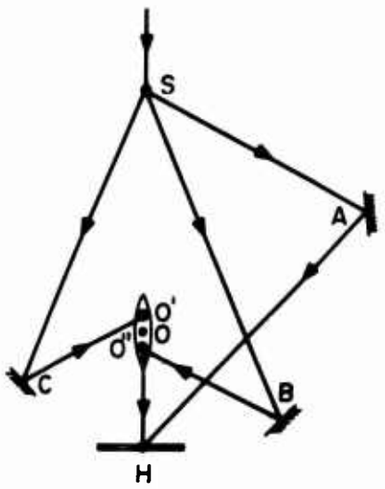

Figure 22. Increasing Depth of Field in Holographic Recording.

beams are changed so that their central rays are directed to different segments of the model. Illuminating beam SBO" illuminates the front half of the deck and SCO' illuminates the rear half. The distances SBO"H and SCO'H are made equal to each other and to reference beam SAH by moving their respective mirrors. As far as each illuminating beam is concerned, it is interacting only with an object of length $\ell/2$. This length is, of course, within the coherence length. In order to provide continuity, the beam diameters are adjusted to allow them to overlap in the central region.

Experimentally, this has provided excellent results and there is no reason why this technique cannot be expanded to allow even larger objects to be recorded.

3.4 STABILITY

If the phase relationship between the signal and reference wavefronts does not remain constant, then the interference pattern between them will also not remain constant. Over the duration of the exposure, any change

in the phase relationship will cause the fringes to shift to a new location on the recording medium. Depending on the degree and rapidity of this shifting, the resulting hologram reconstruction may be seriously degraded or even nonexistent.

Vibration of the optical components in the exposure system is usually the major contributing factor to relative phase changes. If vibrations exist such that one optical path changes by only one-half a wavelength (i. e., 3000 Å) with respect to the other path, then the interference pattern will invert. That is, maxima become minima and vice versa. Depending on the resolution of the film, this would result in complete obliteration of all fringe patterns. In general, however, the phase changes will be random and the subsequent effect on the reconstruction will depend on many factors.[41]

In order to reduce the effects of vibrations, it is best to design a system using highly stable optical components. Such a system should be mounted on a stable working surface such as a granite block or surface plate that is isolated from building vibrations. There are many schemes in the literature on isolation techniques that range from airplane tires to sophisticated, servo controlled, air mounts. Again, the degree of vibration control required will depend strongly on the anticipated exposure (integration) time.

Air currents are also a source of phase variations caused by the vibrations induced by their impinging on the components. They can also affect the refractive index of the air path of each of the beams differently, thereby introducing an optical path difference. This problem is usually eliminated by removing or turning off all sources of air currents (fans, blowers, air conditioning, etc.) and/or constructing an air baffle or screen around the system.

A third cause of phase variations arises from movements of optical components as they come into thermal equilibrium with their environment. A particularly serious violation of this requirement occurs in the removal of the photosensitive medium from its storage container and placement

in the exposing frame. A sufficient delay must be provided to allow the plate to come to equilibrium with its holder and to dissipate any heat picked up from the operator's hands.

3.5 PROCESSING

Since the quality of the reconstructed image(s) is strongly dependent on the nature of the amplitude transmittance curve for a photosensitive medium, anything that affects this curve must be given proper consideration. For a particular medium, the characteristics of this response are primarily controlled by the development process. This process is such that it is capable of an almost infinite number of variations including: type of developer, time of development, temperature, concentrations, etc. A particular example of this is shown in Figure 10, where the amplitude transmittance curve varies in shape and extent as a function of development time.

Because of this complexity, a process developed in our laboratory for use in Lippmann recording[4] was adopted with minor modifications for holography. It consists of:

1.	Pre-soak	Distilled water, 5 min.
2.	Develop	Kodak D-19, 5 min.
3.	Stop	Kodak SB-5, 1 min.
4.	Fix	Kodak non-hardening fixer F-24, 10 min.
5.	Hypo Eliminator	BPI-30, 3 min.
6.	Wash	Distilled water, 10 min.
7.	Soak	Kodak Photo-Flo 200, 1 min.
8.	Dry	Slowly circulating clean air

All processing was done in temperature-controlled one-gallon tanks at 68°F, with agitation provided by peristaltic circulation through spray holes in the bottom of each tank. Drying was done in a dust free atmosphere provided by an Agnew Higgins laminar-flow clean bench. We ensured that the solutions were fresh, in particular the developer, by changing them after 150 square inches of plates had been processed, or within two weeks, whichever came first.

3.6 READOUT

For most display types of holograms, it is not necessary that the hologram be illuminated with a coherent laser beam in order to reconstruct an image. For many applications, a quite satisfactory image is produced when the illumination is with ordinary white light. The only requirement is that the source of light be small (i.e., a point source) so as to produce a degree of spatial coherency across the area that is viewed and that it possess some temporal coherence. This latter requirement is easily obtained by passing the light through a filter before it illuminates the hologram. Although a narrow-band interference filter (5 Å) gives best results, the image is greatly reduced in intensity. Depending on the original object, quite satisfactory results can be obtained from a broader filter of 50-100 Å bandwidth, and even inexpensive dyed acetates are effective.

Figure 23 is a photograph of the reconstructed image using a mercury arc lamp and a 5 Å wide filter as illuminating source. Compare this with the image formed from the same hologram with laser illumination shown in Figure 20.

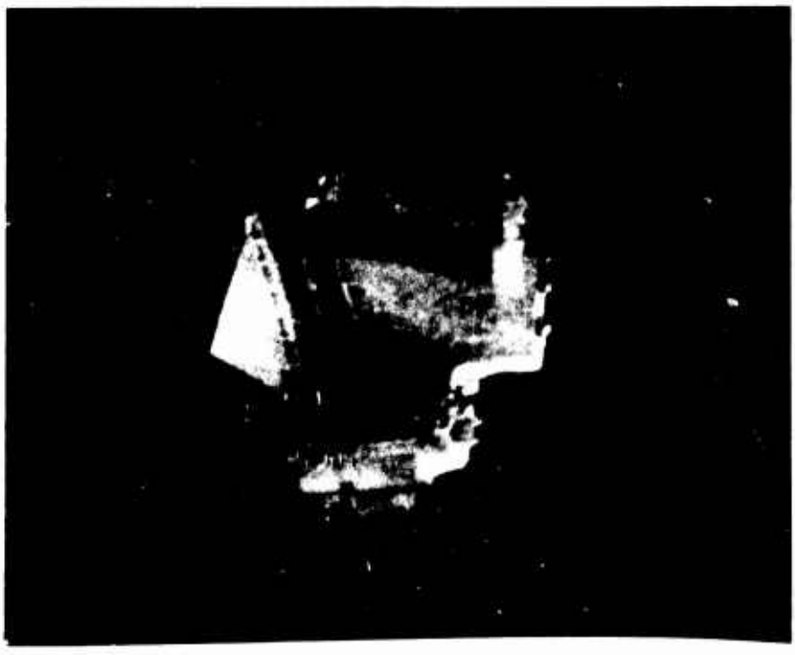

Figure 23. Reconstructed Virtual Image from a Hologram Illuminated with a Mercury Arc Lamp and Filter.

4. HUMAN VISION

The object of the head-up display being considered in this report is to present to the pilot an image of his landing area that is indistinguishable from the view he would actually see if he were looking at the landing site. The image simulation must be done with holographically recorded images or actual models, and therefore the problem is to make the holographic image or actual model appear realistic. There are two factors to be considered in achieving this realism. The first is that the image must contain all of the proper depth cues so that the pilot can estimate his range. Secondly, it is essential that the pilot's eyes be accommodated for vision at a large distance. Therefore, the virtual image seen by the pilot must appear to be located at infinity. Another consideration is that the display must be sufficiently well illuminated so that it can be seen against a bright background such as sunlight reflecting from a cloud bank. On the other hand, at night his eyes must be adapted to darkness and the display must not be bright enough to destroy the desired degree of dark adaptation.

Certain stimuli give rise to space perception.[42] These stimuli have been formalized into a set of rules. Space perception based on the stimuli received by only one eye is termed monocular perception. Binocular perception requires the coordinated activity of both eyes. The binocular or stereoscopic effect arises from the spatial separation of the two eyes. The images on the retinas of the two eyes are different. Objects at different distances will have different relative displacements on each retina. A fusion occurs in the brain so that the two images of an object fuse into a single mental image, and the retinal displacement results in a specific placement in depth. The geometry of the binocular perception is shown in Figure 24. The stereoscopic effect results from the difference in perception angles

$$\alpha_2 - \alpha_1 = \beta_1 - \beta_2 = \gamma$$

In a first approximation it can be shown that

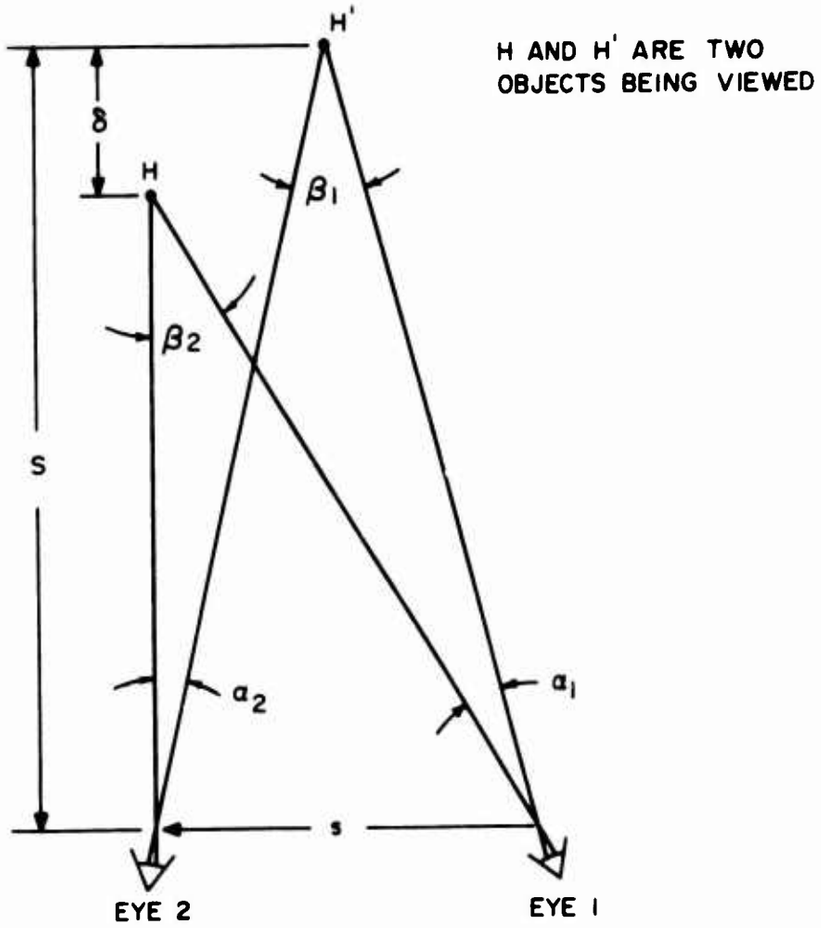

Figure 24. Geometry of Binocular Vision.

$$\gamma = \frac{s\delta}{S^2}$$

A minimum perceptible angle γ_t exists for each individual. The minimum detectable δ is proportional to S^2 and therefore much smaller depths are detectable at short range than at long range. The stereoscopic effect is a very powerful depth cue at short range. The generally useful binocular depth perception is 2000 feet.[43] At this distance one cannot distinguish by the stereopsis cue alone whether objects are at 2000 feet or infinity.

Depth is generally judged by both binocular and monocular cues. At short distances the binocular depth cue is very effective. The monocular cues are also present, but they are overshadowed by the effectiveness of the binocular cue. Within 30 feet the primary source of depth information is the stereopsis cue.[43] A smooth transition occurs from the reliance on the binocular cue for depth information to the monocular cues as the range increases. We are generally unaware of this transition. The everyday event of driving a car provides an example. The stereopsis cue is important in parking, but plays a relatively insignificant role in highway driving.

The important monocular cues are the following:[42]

1. Relative size: Our discrimination of distances is dependent on the size of the retinal image provided by an object and by our past and present experience with objects of the same class. A small retinal image provided by a member of a class of objects called automobiles results in the response "distant automobile."
2. Interposition: The cue of interposition occurs when an overlapping object is said to be nearer than an overlapped object. The overlapping object cuts off a view of part of the overlapped object.
3. Linear perspective: The stimulus condition for this cue is determined by the fact that a constant distance between points subtends a smaller and smaller angle at the eye as the points recede from the subject. A subject reports that lines formed by car tracks, telephone wires, etc., seem to approach each other in the distance.

4. Aerial perspective: When surface details of an object do not provide conditions for requisite visual contrasts, a subject reports that the object seems far off.

5. Monocular movement parallax: When a subject's eyes move with respect to the environment, or when the environment moves with respect to the subject's eyes, a differential angular velocity exists between the line of sight to a fixated object and the line of sight to any other object in the visual field. This condition of differential angular velocity leads to such discriminations as are concerned with the statement that near objects move against the direction of movement and far objects move with the direction of movement (of the head or environment).

The particular display under consideration will be used to simulate distances to the landing site of an eighth of a mile or greater. At these distances the pilot perceives distance primarily through monocular cues. The display must contain the proper monocular cues to simulate this range. A virtual holographic image or actual model is three-dimensional. If such an image is used in the display, the pilot must be prevented from seeing its three-dimensional character. Should the pilot see its three-dimensional character, it would be disconcertingly apparent to him that he is observing an image of a model.

The image presented by the display must be located at a sufficient distance from the pilot so that in viewing it his eyes will be relaxed and he will essentially be accommodated to view distant objects. In the normal eye, variation in lens shape permits a range of accommodation from infinity to 4 to 8 inches. Most of the changes in eye accommodation take place in viewing objects located a few inches to about two feet away. For objects located at 10 feet or beyond, practically no variation in eye focus takes place.[42] The display system should therefore present the image approximately 15 to 20 feet from the pilot in order to preserve the pilot's distance accommodation.

It has been found that at low illumination levels the primary receptors are the rods. It has also been found that the effect of a certain light level on the dark adaptation of rods depends on the wavelength of the light. Red light has the least effect on this dark adaptation. Therefore, where speed of rod adaptation is important, the preadaptation light should be red.[42] For these reasons the display should be in red. However, the red color may be objectionable in distracting from the realism of the image. Further subjective studies will be necessary and may be performed when a breadboard of the holographic head-up display system has been constructed.

5. PROBLEM DEFINITION

The image to be presented to the pilot in his landing approach must be identical in all respects to what he would see if visibility were good. The relative position of the aircraft with respect to the carrier is continually changing. Therefore, the pilot's view of the carrier continually changes and the image presented to him must continually change. The main problem to be solved in the holographic approach is how to make the holographic image dynamically variable.

During the landing, the carrier is moving forward and the sea is causing it to pitch, yaw, and roll. Therefore, a coordinate system fixed in the carrier will be constantly in motion with respect to a fixed inertial coordinate system. The aircraft has its own coordinate system, which moves relative to that of the ship's system. The four coordinate systems -- one fixed inertial, one fixed in the carrier, one in space located at the center of gravity of the aircraft, and one fixed in the aircraft -- are shown in Figure 25.

The coordinate system (x_1, y_1, z_1) has its origin in the center of gravity of the ship, and the relative orientation of the axes in space are fixed. The (x_2, y_2, z_2) system has its origin at the center of gravity of the aircraft and the orientation of the axes in space are again fixed. The orientation is such that the x_1 and x_2 axes are parallel and the plane determined by the x_1 and y_1 axes is parallel to the plane determined by the x_2 and y_2 axes. The coordinate systems (A_1, B_1, C_1) and (A_2, B_2, C_2) are Eulerian systems with the Euler angles belonging to the two systems (θ_1, φ_1, ψ_1) and (θ_2, φ_2, ψ_2) respectively. The (A_1, B_1, C_1) system is fixed in the carrier and the (A_2, B_2, C_2) system is fixed in the aircraft. In the Eulerian system the B and C axes are perpendicular to the A axis. The B axis is determined by the line of intersection of the plane formed by the x and z axes and the plane normal to the A axis. Any variation in θ_1 or θ_2 is known as a pitch of the carrier or aircraft respectively. Nonzero values of φ_1 and φ_2 are known

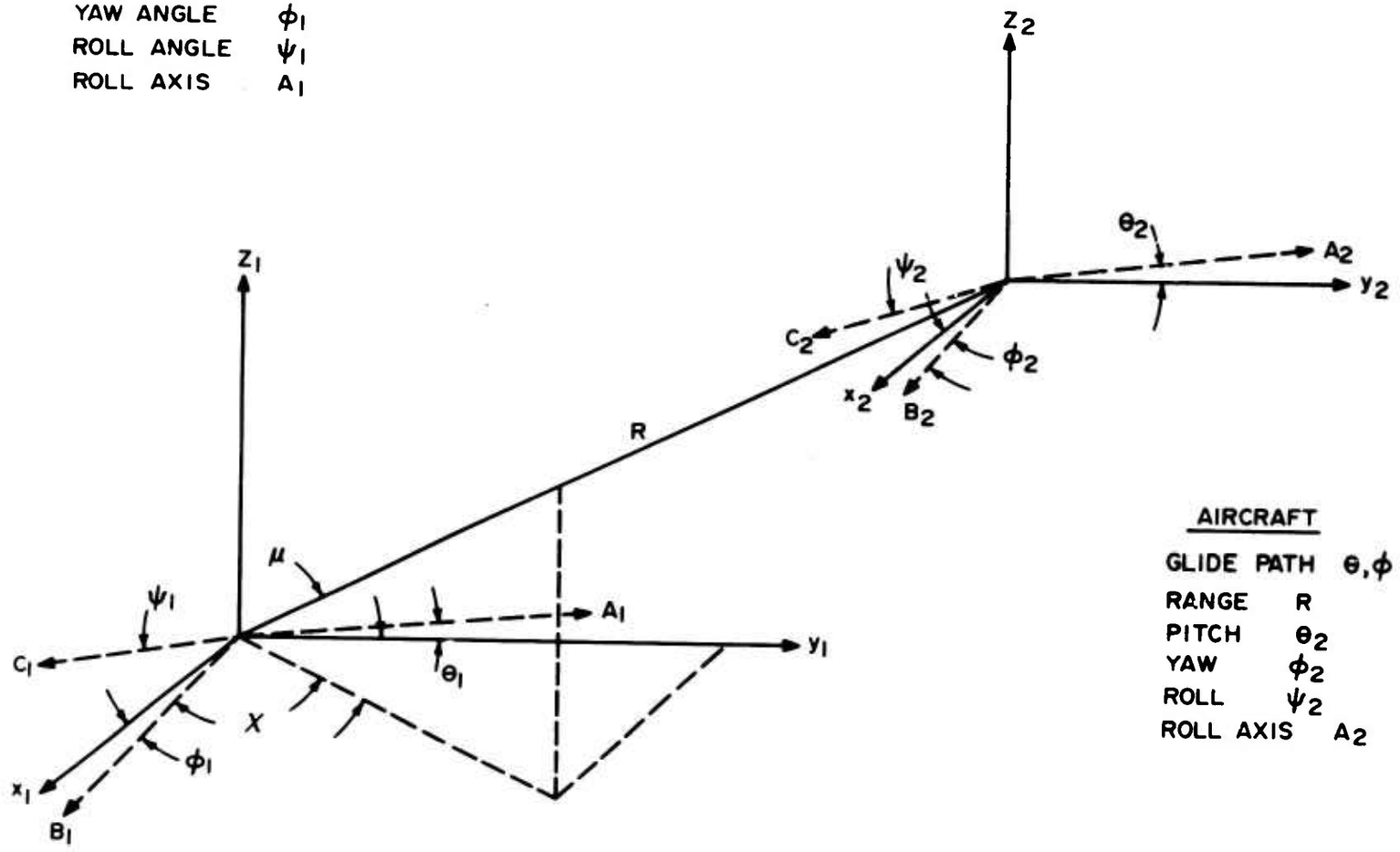

Figure 25. Coordinate Systems for Describing the Movement of an Aircraft with Respect to the Aircraft Carrier.

as a yaw of the carrier and aircraft. Rotation of the carrier about the A_1 axis is a roll with the angular amount measured by ψ_1. The aircraft rolls about the A_2 axis and the corresponding angular measure is ψ_2.

During an approach, the aircraft will pitch, yaw, and roll about its center of gravity. In making a landing approach, the pilot has his eyes fixed on the landing deck of the aircraft carrier. In attempting to simulate his view of the carrier, we must analyze how a range change, pitch, yaw, roll, and glide path change of the aircraft affects his view.

For the present we will assume that the carrier has zero pitch, yaw, and roll. The aircraft is located at a distance R and in the direction of the vector $\vec{R}$ from the carrier. The direction of $\vec{R}$, or what is normally called the aircraft glide path, is defined by the angles μ and χ. With the pilot flying along one glide path with zero pitch, yaw, and roll, he obtains one view of the carrier. If he flies toward the carrier from another direction, he obtains a different view of the carrier. As a gross example, he sees an entirely different area of the carrier when he is flying in toward the side of the ship compared to when he is flying in toward the fantail. When the pilot is coming in for a landing, he can sight down the lines in the center and on either side of the runway. This sighting provides the pilot with a good error discrimination in the angle χ of his glide path. His error discrimination in the angle μ of his glide path is not as good because he does not have such sighting lines. Variations in the angle μ are judged from the apparent longitudinal length of the image. The distance of the aircraft from the carrier along with μ enters into this picture, and therefore the pilot can only sense gross variations in the angle μ. In conclusion, the visual effect of approaching the carrier on a different glide path is a different perspective view of the carrier.

When the aircraft pitches, it rotates about its center of gravity, which is located some distance back from the pilot's windscreen. As can be seen from Figure 26, a pitching motion is visually sensed by the pilot in that area of the windscreen through which he sees the carrier. If his cockpit

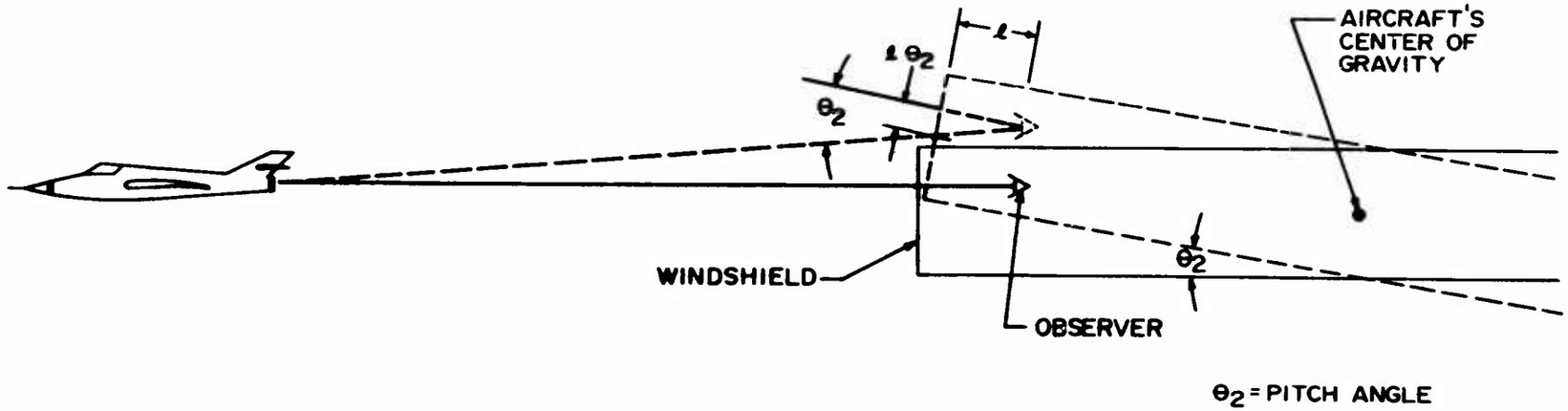

Figure 26. Schematic Showing the Relation between the Pitch Angle and Image Movement in the Windscreen.

pitches up, he will see the carrier through the bottom of the windscreen; if it pitches down, he will see the carrier through the top portion of his windscreen. If the pilot is located a distance ℓ behind the windscreen, the displacement of the image in the windscreen is $\ell\ \theta_2$ for an angular pitch θ_2. Likewise, the yaw motion of the aircraft appears to the pilot as a horizontal displacement of the carrier image in his windscreen. The roll of the aircraft is seen as a rotation of the carrier image about the line of sight.

The pilot starts his approach to the carrier landing from a distance of about 4 miles. At that distance his primary distance cue is monocular. He judges his distance from the size of the carrier image. This is not a very precise range indicator. As he comes closer, the relative size cue remains the primary range cue. At about 2000 feet he may begin to utilize the binocular effect, but the relative size cue remains the dominant range cue down to distances of about 100 feet. Any carrier image simulation is expected to be carried down to a range of 1/8 mile. At this distance and closer, it is expected that the pilot will make actual visual contact. In conclusion, the pilot will sense his range during the entire simulation from the size of the carrier image.

The range in the parameters of pitch, yaw, roll, glide path change, and aircraft range to be simulated will depend on the range in these parameters commonly encountered in a landing approach. For the parameters of pitch and yaw, we are thinking in terms of simulating angles of plus and minus 10 degrees. For roll, the simulation may extend from plus 15 degrees to minus 15 degrees. The glide path selection is centered around the desired landing approach, and the thinking is that plus or minus 15 degrees in both the angles μ and χ may be simulated. The desired range simulation is from 1/8 to 4 miles in a continuous manner.

The question of resolution arises in two ways. First, how much detail should be resolvable in the image? Second, what size steps are permissible in the dynamic variables or what variations are detectable by the

pilot? When the pilot is 4 miles away, he is particularly interested in the carrier outline and in some gross detail. As he comes closer, he is interested in more detail. Because of his speed, his eyes tend to fixate on some aiming point. His interest in detail is mainly centered around his aiming point. The information he is concentrating on is his glide path, pitch, yaw, roll, and range. The image must be of sufficiently good quality to give him the maximum possible information about these parameters. As discussed previously, he is able to quite accurately assess the error in the χ angle of his glide path if the white lines on either side and down the middle of the landing strip are clearly resolved. Without the aid of landing devices such as the "meatball," the μ angle of the glide path is judged from the apparent length-to-width ratio of the carrier. Based on these judgments, it is difficult to determine errors in the μ angle of the glide path. A device that performs the same function as the "meatball" should be incorporated into the simulation display so that the pilot can accurately judge the μ angle of his glide path. Pitch and yaw are seen as a displacement of the image in the windscreen and, because the pilot can use the windscreen as a reference, he can assess his pitch and yaw angles quite accurately. All that is required in the way of optical resolution for determining pitch and yaw is that the outline of the carrier be seen. The pilot can also quite accurately assess his roll if he compares the carrier image orientation with his horizontal reference. The optical resolution need only be adequate so that the pilot can establish either a horizontal or vertical plane in the carrier image. Since the range is judged rather imprecisely from the apparent size of the carrier image, not much accuracy is needed in simulating the carrier image size.

The image simulation must be accomplished so that the pilot can continuously look through his windscreen and view external objects. To do this, a beam splitter must be employed between the pilot and his windscreen. The windscreen must not distort his image of the external world nor cut down his visibility to a great extent. His eyes must continually be accommodated for viewing distant objects. This means that the simulation image must appear as a distant object. Since the simulation device must be compact,

this necessitates that the pilot view an image thrown out in front of the aircraft. The change in accommodation of the eye in viewing an object 10 feet away and one at infinity is negligible. Therefore, to preserve the pilot's distant eye accommodation, the simulation image must be located at least 10 feet in front of him.

6. SUGGESTED SYSTEMS

6. 1 INTRODUCTION

The requirements for the simulation system are that changes in the glide path, pitch, yaw, roll, and range change must be independently simulated. The purpose of this study has been to investigate holographic technologies that will perform this simulation in a relatively simple manner. In the course of the study, it was learned that neither the real nor the virtual holographic image had clear-cut advantages to perform the entire simulation. In fact, it was found that the simulation could also be performed using actual models of the aircraft carrier and conventional optics to process the image. This section describes some of the experimental work that was performed in order to test particular simulation techniques, as well as complete systems using the holographic real and virtual images and two systems using actual models of the aircraft carrier.

6. 2 HOLOGRAPHIC VIRTUAL IMAGE MODE

Holographic recordings of an aircraft carrier model on photographic emulsions backed with glass have been made in sizes of 4" x 5" and 8" x 10". The carrier model used is approximately 10 inches long and its scale is 1:1250. The model is placed approximately 16 inches in front of the hologram. The total angular view of the carrier recorded on the hologram is determined by the hologram's plate size and the distance from the plate to the carrier model. For the 8" x 10" plate the total horizontal angular view is approximately 36^{o}. The vertical angular view is approximately 28^{o}.

After the recording has been made, the holographic plate is inserted into the same holder that was used to record the hologram. The plate is illuminated with the same laser reference beam as was used in the recording. A 3-D image of the same size as the carrier model can be seen by looking through the hologram plate toward the position where the model resided during the recording. This is the virtual image. By moving the head from side to side and up and down, one can see different views corresponding

to the different views the pilot would see along different glide paths. The appropriate view for a particular glide path can be obtained by placing a mask with a small window over the hologram and orienting this window to obtain the desired view. The viewer's head must be moved so that the eyes are always along a line through the center of the window and the center of the fixed image.

The hologram of the virtual image appears to "speckle" and have a granular nature. The reason for this will be discussed further in Section 6. 3. Basically, the reason for observing this granulation is that the eye has a limited aperture. If this aperture is further reduced with a small window, the granulation will increase. In using a window to select the view appropriate to a particular glide path, a compromise must be reached between choosing a small window in order to have good resolution in the selection of different glide path views and keeping the window large enough so that the granulation does not reduce the image quality below an acceptable level.

In looking at the virtual image one can sense that the image is located behind the hologram. In order to maintain the pilot's eye accommodation for distant vision, this image must be projected to a distance of 10 feet or greater. To do this, we have employed a long focal length lens placed between the observer and the hologram. The holographic virtual image must be located just inside the focal length of the lens as shown in Figure 27. Since the virtual image has length along the optical axis, it is best to use a lens with a long focal length compared to the length of the image in order to minimize the length-to-width magnification distortion. This has been tried with a 5" diameter and 20" focal length lens. The image appears to be quite good and one no longer gets the sensation that the image is a few inches behind the hologram. The same thing was tried with a 40" focal length Fresnel lens, but the image quality was not as good.

One can incorporate this lens directly in the recorded hologram, thus eliminating a bulky lens from the viewing system. This is done by

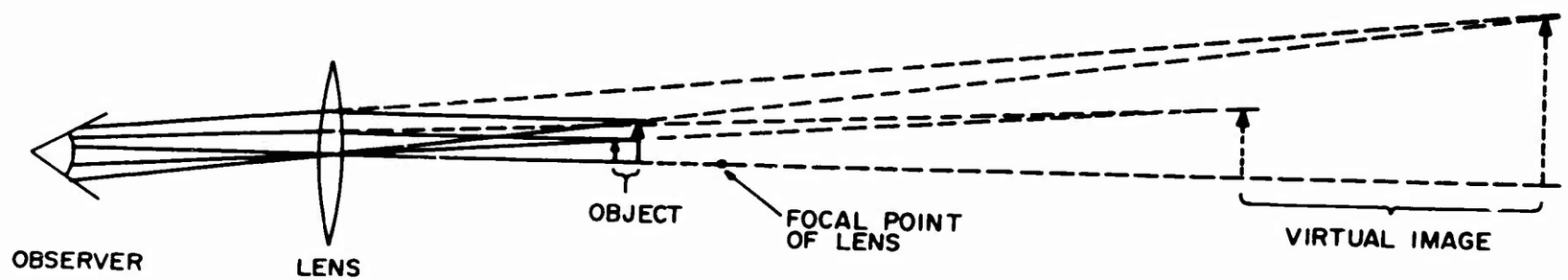

Figure 27. Ray Diagram of a Long Focal Length Lens Projecting a Virtual Image Further from the Observer.

placing the long focal length lens between the hologram and the carrier model so that the light scattered from the model passes through the lens. Some recordings like this have been made. In the total system, however, it is desirable to obtain a variable image magnification directly from the hologram by varying the illumination parameters. This is no longer possible if the lens has been incorporated in the hologram, because now the object is effectively located at infinity ($z_o = \infty$ in Equation 47). The idea of making a hologram through a lens has been dropped because of this reason.

Image magnification must be continuously variable to simulate range. When dealing with the virtual image, it is only meaningful to talk about the angular magnification rather than the lateral magnification. It was shown earlier (see Equation 47) that a variable angular magnification is possible only if the holographic virtual image is viewed from some distance, ρ, in back of the hologram. We have demonstrated in the laboratory that if the observer views the hologram with $\rho = 30$ inches, an angular demagnification of approximately six-fold is possible. In all cases it is a demagnification of the recorded image. A larger range of demagnification should be possible if the holographic plate-to-object distance $P(x_o, y_o, z_o)$ is decreased during the recording. In fact this is desirable since the display must be able to simulate distances up to approximately one-half the carrier's length (1/8 mile). The greatest resolution and the truest proportions in the image are required when the pilot is at this distance, and here the image has not been degraded by the demagnification process.

To vary the demagnification, the radius of the reconstruction wavefront, z_c, needs to be varied (see Equations 45 and 47) over a range from infinity to a few centimeters. A technique to vary the radius of the wavefront by varying the separation of a short focal length lens and a long focal length lens is shown in Figure 28. When the two lenses are separated by a distance equal to the sum of the two focal lengths, the light illuminating the hologram is collimated or the wavefront has a very long radius ($z_c \approx \infty$). As the lenses

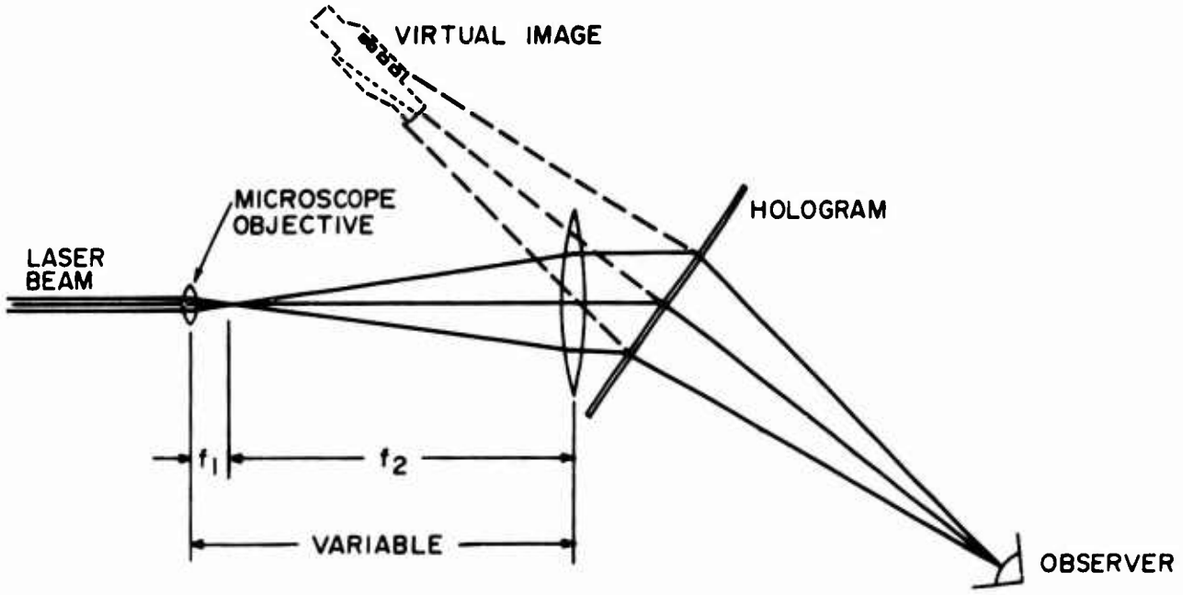

Figure 28a. Variable Spacing of Two Lenses Produces a Variable Magnification of the Holographic Image. A Lens Separation Equal to the Sum of the Focal Lengths Produces an Image of Unity Angular Magnification.

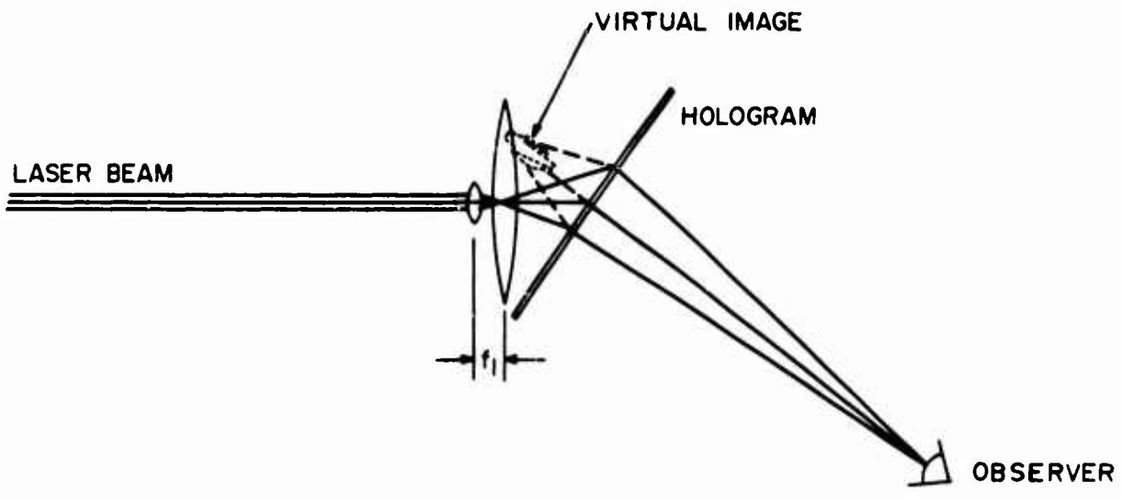

Figure 28b. As the Lens Separation is Reduced, a Demagnified Virtual Image is Produced.

are brought together, the radius of the wavefront shortens. The extreme is reached when the short focal length lens touches the long focal length lens or the beam spread is determined entirely by the short focal length lens. By choosing focal lengths and lens diameters, one attempts to maintain the same illuminated area of the hologram regardless of the radius of the wavefront. A motorized laboratory demonstration model showing the continuous demagnification was built; it is shown in Figure 29. The short focal length lens in this demonstration is a 20X microscope objective; the other lens has a focal length of 8 inches. The microscope objective can be driven along the optical axis by means of the motor and variable-speed gear box.

Pitch and yaw can be simulated by a spatial deflection of the image in two dimensions. This deflection can be accomplished in a purely holographic manner by changing the reconstruction angle, which would require a rotation in space of the reconstruction beam about the intersection of the hologram plane and the reconstruction beam center line. In this rotation, the light intensity in the reconstructed image decreases as $\{[\sin(\theta_i - \theta)]/(\theta_i - \theta)\}^2$. For the particular geometry used, this function goes to zero at $\theta_i - \theta = \pm 5^\circ$. One could then simulate a maximum pitch or yaw angle of approximately $\pm 5^\circ$. In simulating any pitch or yaw angle, the intensity of the image continually decreases as the reconstruction angle changes, and finally at approximately $\theta_i - \theta = \pm 5^\circ$ the image vanishes. This varying image intensity and the small angles that may be simulated indicate that this is not a very fruitful approach to simulating pitch and yaw.

Another technique considered for performing this simulation consists of translating mirrors and rotating a beam splitter. This technique is shown in Figure 30. The image is incident on a beam splitter, which in turn reflects the light toward the pilot's eyes. If this beam is translated parallel to itself and then the beam splitter is rotated a small angle to reflect the light beam back toward the pilot's eyes, the pilot will get the sensation that the light is coming from a position in space that is at an angle with respect to a straight-ahead position. If the distance from the beam splitter to the pilot's

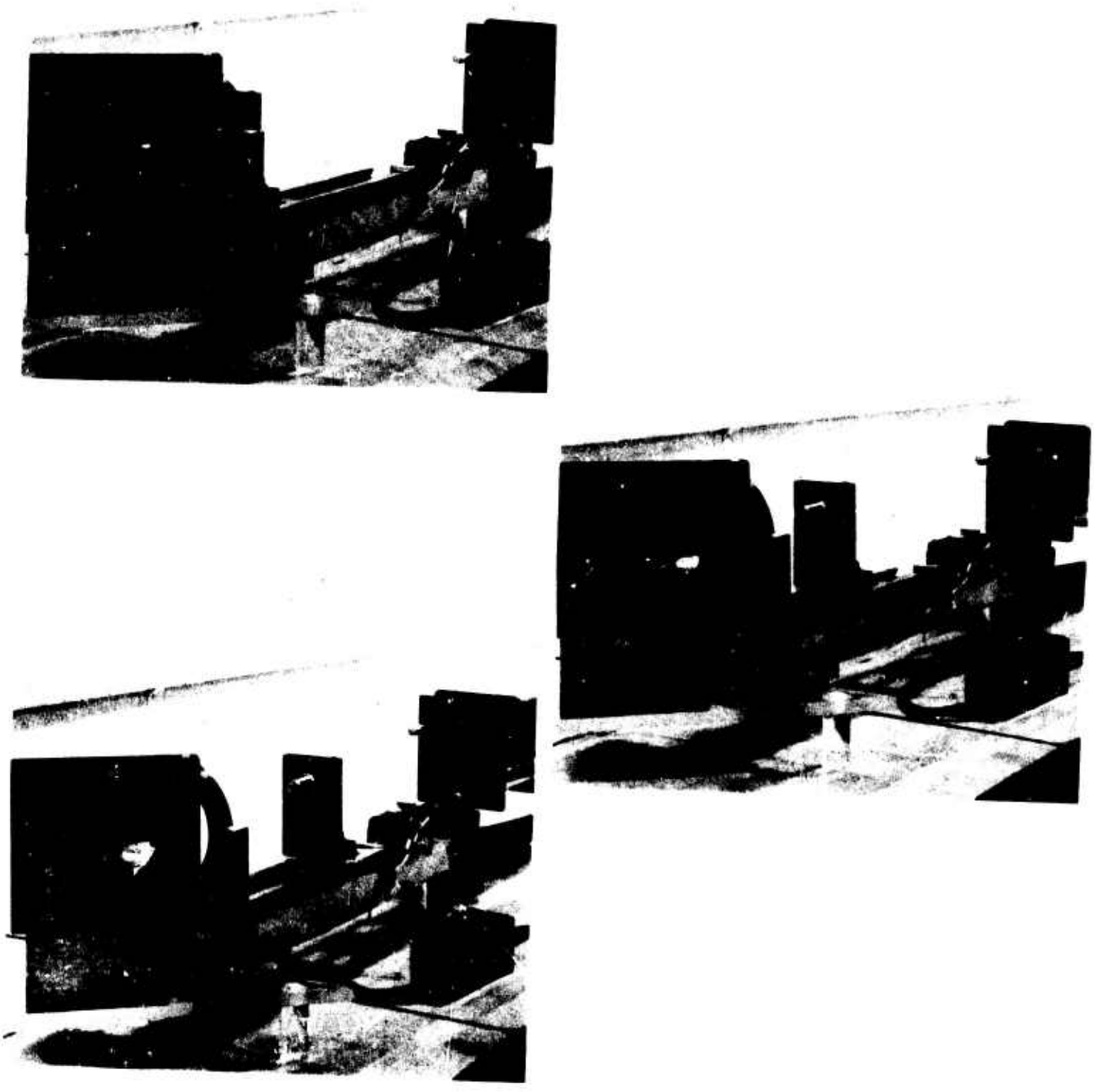

Figure 29. Device for Simulating Range Change in Virtual Image Mode Showing Three Different Image Sizes.

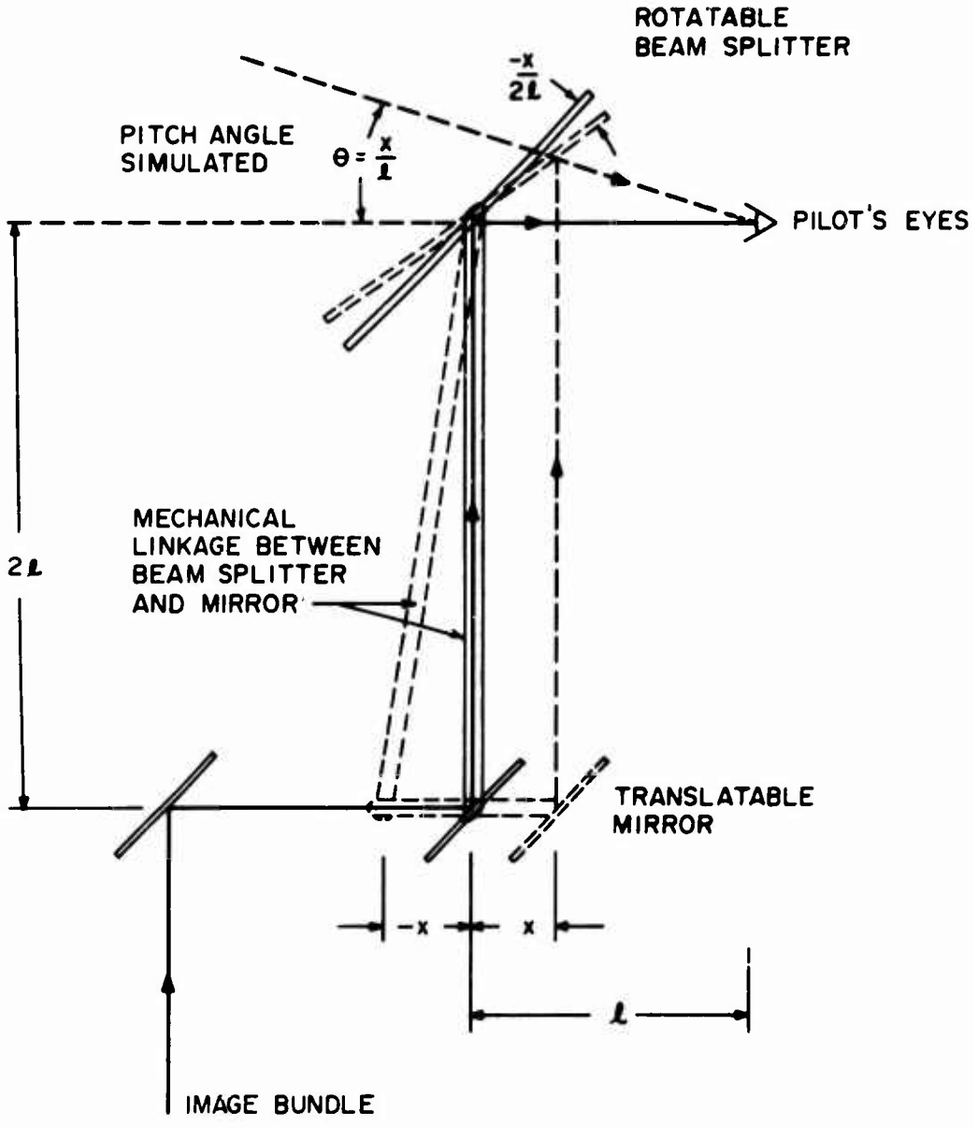

Figure 30. Mechanical Techniques for Simulating Pitch and Yaw.

For instance, rather than pivot the illuminating beam, a small error in the reconstruction angle may be acceptable if the resulting variation in the image intensity is tolerable. Rather than pivot a laser device in space to obtain the angular movement of the illuminating beam, it is possible to use a gimbaled plane mirror and a fixed ellipsoidal mirror. One foci of the ellipsoidal mirror is placed in the plane of the hologram on the optic axis of the system. The other foci is placed at the center of the gimbaled plane mirror. No model of this part of the system has been built and this is an area for future work.

The virtual image is projected to infinity by a long focal length lens following the hologram. The focal length must be sufficiently long so that the holographic virtual image remains inside the focal distance for all magnifications.

Roll simulation is accomplished by rotating the hologram about the optic axis of the system.

The pitch and yaw simulation is accomplished by two pairs of mirrors. The separation of one pair of mirrors controls only yaw. The separation along an orthogonal axis of the other pair controls pitch. The translation of these two mirrors is coupled to the beam splitter by means of the lever arrangement previously described.

6.3 HOLOGRAPHIC REAL IMAGE MODE

In general, the image to be displayed must be removed to infinity to reduce the need for eye accommodation on the part of the pilot. Because of the distances involved, the eye will be unable to determine whether or not the image at infinity is two- or three-dimensional. Consequently, the original image that is subsequently removed to infinity may be either two- or three-dimensional. The previous section dealt with the three-dimensional virtual image from a hologram. In this section we wish to consider the use of the two-dimensional real image and the means by which it can be manipulated to simulate the required degrees of freedom.

It was shown in the theoretical section that a real image, represented by A* (x, y) in Equation 15, is produced when the hologram is illuminated. In general, the term in the reconstruction expression that provides the real image also includes an exponential phase factor that is a function of both reference and illuminating wavefronts. In the case of the plane reference wave and an identical illuminating wavefront, the phase term is exp [i 2 η x]. The effect of this term is to introduce a linear phase shift that is identical to what would occur if a prism were inserted into the wavefront. Consequently, the real image is deviated in position by an angle $\theta = \lambda \eta / 2\pi$ (i. e., it is on a spatial carrier of frequency η). In the case of a more general reference beam such as a spherical wave, the real image term of the amplitude transmittance contains the phase factor exp $[i\pi(x^2+y^2)/\lambda d]$, where d is the distance of the reference point source P (x_r, y_r, z_r) from the hologram. If, in readout, the hologram is illuminated with the same wavefront, the real image term in the reconstructed wavefronts is modulated by the factor exp $[i2\pi(x^2+y^2)/\lambda d]$. This quadratic-phase modulation produces the same effect on the real image as a lens of focal length f = d/2. In this case it is a negative lens. The position and size of the real image will therefore depend upon the original object distance and the effective focal length of the "hologram lens." The conventional lens equations may then be applied. If a different curvature d' is used for readout, the lens will have an effective focal length of $1/f = 1/d + 1/d'$.

Since we are concerned with generating only the real image, these phase factors may be removed by illuminating the hologram with the conjugate of the reference beam rather than an identical wavefront. That is, if a diverging reference beam were used in recording, then a converging beam will eliminate the phase factor on readout. (While this removes the negative lens from the real image, it puts a positive lens into the virtual image wavefront.) Inversion of the illuminating wavefront, however, does not allow simultaneous satisfaction of the Bragg diffraction condition at all points. This is assuming that the recorded spatial frequencies are such as to cause the recording

medium to act as a three-dimensional grating. The result of this mismatch is that only a portion of the image is reconstructed at a time. Satisfaction of the Bragg condition can be re-established if, at the same time the curvature is inverted, the hologram is rotated 180°. When this is done, the illuminating wavefront becomes identical to the original reference beam except that all directions are reversed. This process is shown in Figure 32.

As shown in this figure the reference beam is simply the output of a microscope objective of sufficient power to fully illuminate the recording medium. (Usually a spatial filter is included.) The illuminating wavefront for reconstruction must be the inverse of this and, as shown, must be obtained by using a large diameter lens to image a point source through the hologram back onto the original reference point location. This is not a trivial problem. A well-corrected, large diameter lens must be obtained and incorporated into each display system. While this is certainly feasible, it does add both weight and cost as well as complexity of alignment. To circumvent this requirement we have proposed the use of the technique shown in Figure 33. In this method (Figure 33a), the hologram is made with a converging beam from such a lens. In readout, therefore, only a diverging beam is now required and it is simply obtained (Figure 33b). In this way the requirements are reduced to one large lens that is used only in the recording and not in the reconstruction process. This approach has been tried in the laboratory and appears to work well considering the quality and size of the lens that was available.

An individual subarea of the recording medium will receive information only about a particular view of the object. In the case of the shaded area σ in Figure 33, the recorded view would correspond to what an observer would see in looking through a window of area σ located at an angle θ relative to the deck. There is, therefore, a unique perspective view of the carrier associated with each area element of the hologram. If the illumination is restricted to only a small area in the reconstruction process, the real image formed represents the corresponding view that was recorded in that area. In the case of area σ, the image that would be seen on a screen would have the

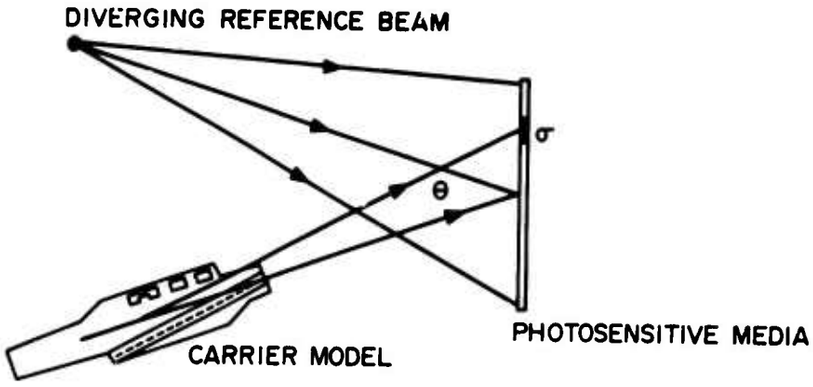

Figure 32a. Conventional Means of Holographic Recording.

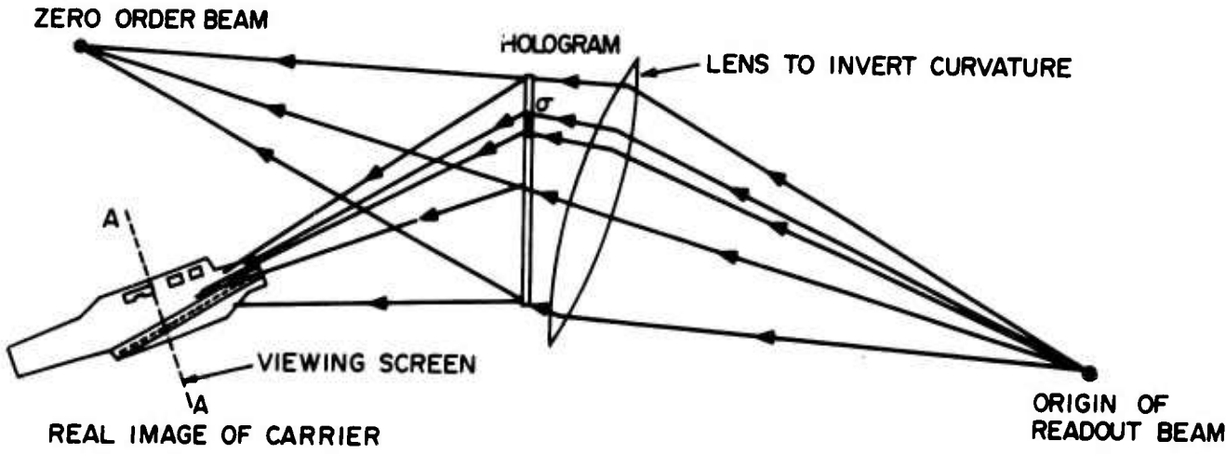

Figure 32b. Conventional Means of Reconstructing Real Image.

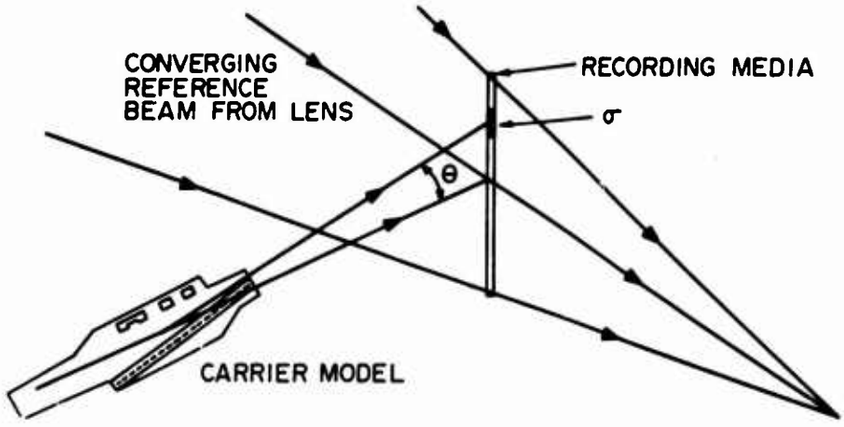

Figure 33a. Modified Means of Holographic Recording.

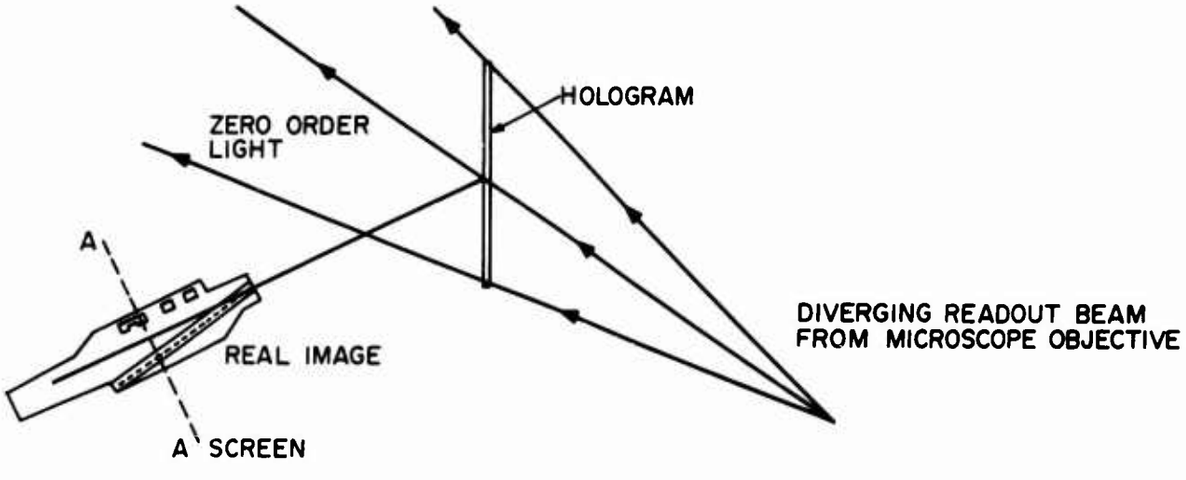

Figure 33b. Modified Means of Reconstructing Real Image.

perspective of the model as seen from the angle θ. As each different area is interrogated, the resulting view would change accordingly. Hence, as the illuminating spot is moved over the surface of the hologram, the reconstructed image will change continually in perspective. The screen on which this image is displayed can be positioned so that there will be no translation of the image associated with the change in perspective. This technique, therefore, allows a means for manipulating the real image so as to display any change in the glide path of the aircraft. The means by which various areas could be addressed is shown in Figure 34. The mirror is pivotable about two axes and would in the final system be controlled by the carrier-to-aircraft telemetry. As a test, this system was set up in the laboratory so that the mirror angle could be controlled through mechanical linkages by a joy stick. The composite photograph in Figure 35 shows five typical images corresponding to different areas of the hologram. (The images were purposely displaced for the photograph.)

The reconstruction of a real image and the subsequent display of this image on a screen introduce a problem unique to the optics of coherent light. This problem arises because we wish to project a three-dimensional real image onto a two-dimensional viewing screen in such a way that the entire image is in focus. This requirement is easily met in conventional optics by reducing the aperture of the optics (as in a camera) so as to increase the depth of focus of the lens. This, too, can be done in holography by reducing the size of the subarea that is interrogated. In both cases the effect is to also reduce the resolution of the "lens." With incoherently illuminated objects, this effect is tolerable over a wide range. With coherent light and, in particular, such light scattered by a diffuse object, the effect of reducing the aperture is to seriously degrade the image. This degradation appears as a speckle pattern that reduces image resolution and eventually destroys all continuity in the image. An example of this effect is shown in Figure 36. The three photographs are of reconstructed real images from the same hologram area with different diameters of the illuminating beam. At large diameters

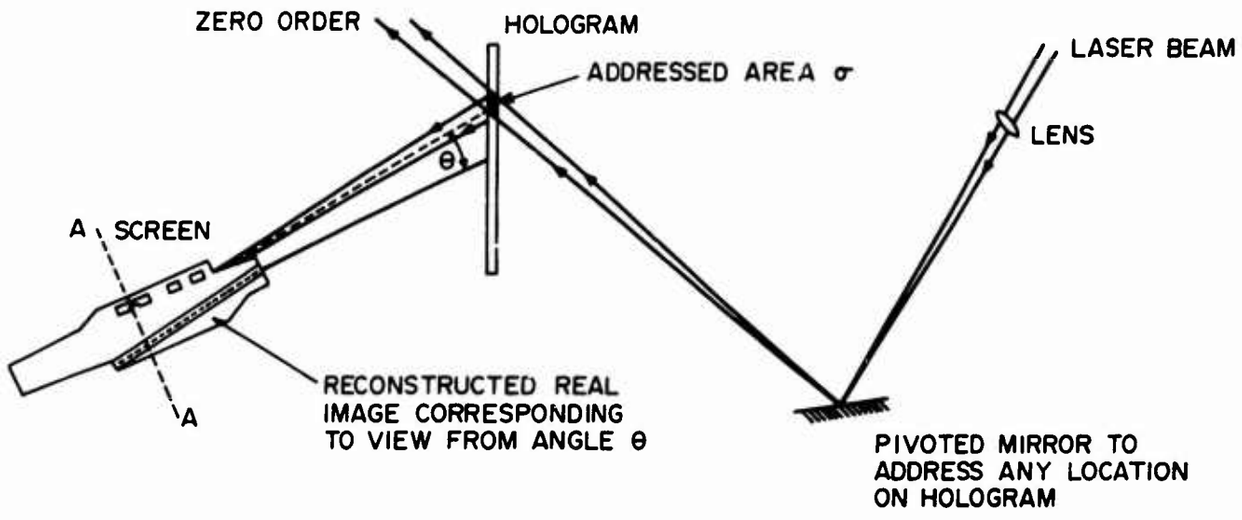

Figure 34. Means of Selecting Glide Path for a Real Image Display.

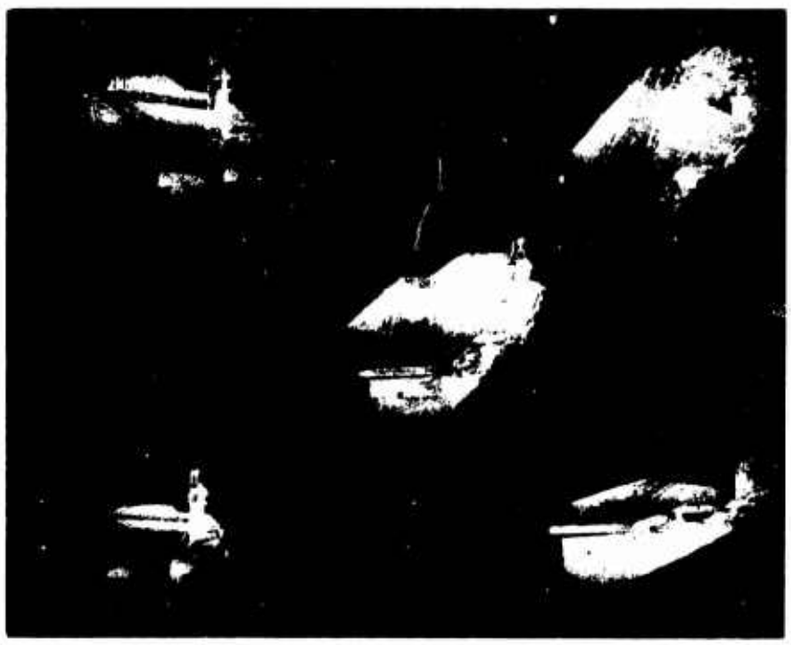

Figure 35. Displayed Real Image Showing Five Typical Glide Paths (Displaced for Clarity).

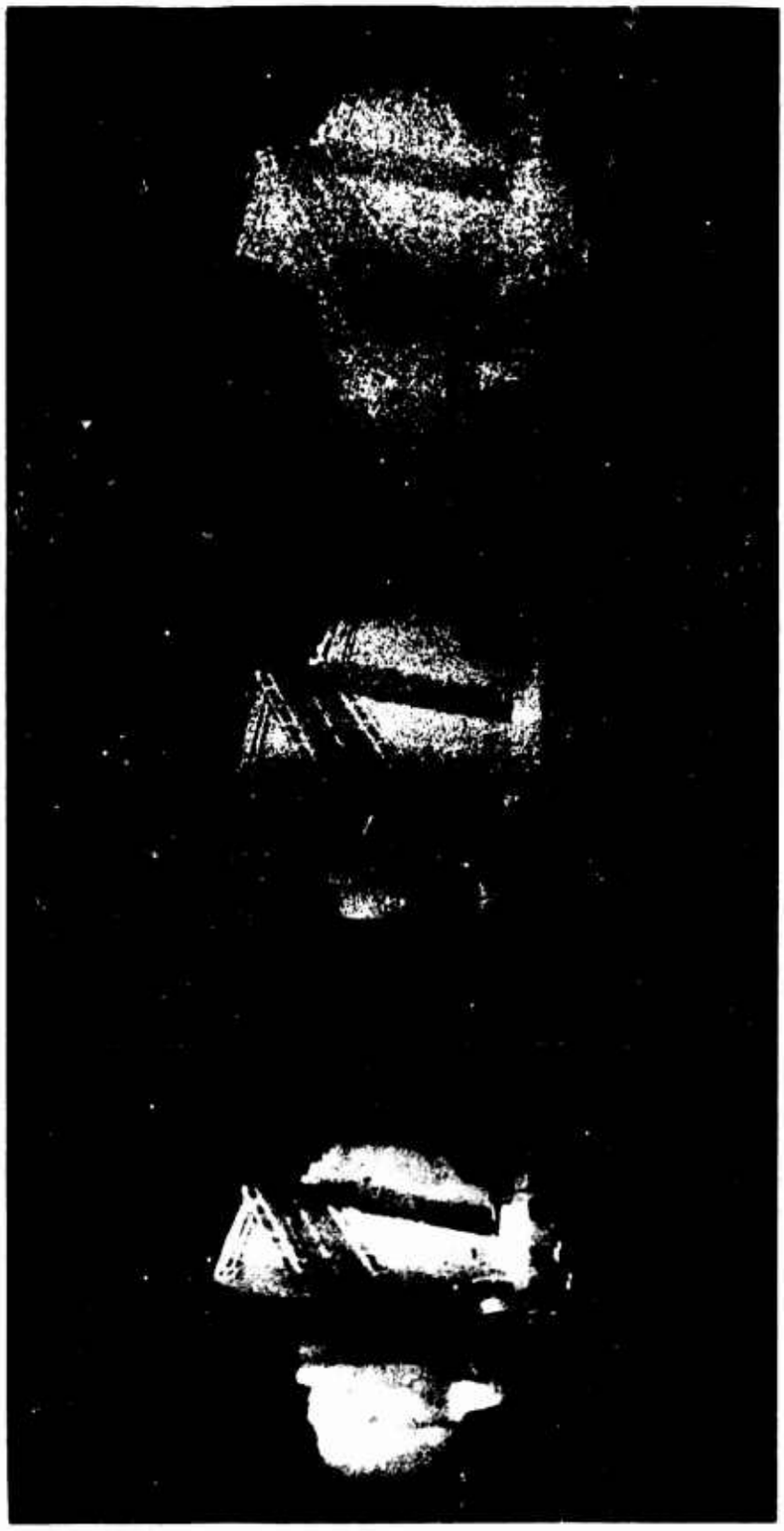

Figure 36. Effect of Changing the Diameter of an Illuminating Beam on Real Image Quality.

the image continuity is good but the depth of focus is very poor. As the aperture is reduced, the depth of focus improves but the image starts to degrade, until finally the image is completely unacceptable. This phenomenon has been treated in the literature[44, 45, 46] and is generally attributed to the roughness of the object surface (roughness with respect to optical dimensions of wavelength). This is such as to introduce many random phase variations within the area corresponding to the diffraction spot that is associated with a particular "lens" aperture. The amplitude of a single image point is, therefore, derived from a large number of independent phase fluctuations and can hence undergo huge statistical fluctuations. These fluctuations in turn give rise to the speckle effect at small apertures (large deflection spot). This problem has, as yet, not been solved except for some two-dimensional objects where depth of focus is not required. Consequently, a compromise must be made between depth of focus and resolution/speckle in the reconstructed real image. The center photograph of Figure 36 represents such a compromise.

It should be noted that the speckle effect is not restricted to the real image only. The virtual image will also produce the same phenomenon, particularly when an attempt is made to photograph the three-dimensional image. Again, in order to get sufficient depth of focus, the camera lens must be stopped down, thus causing a loss in resolution and introduction of speckle. This is readily seen in Figure 20 where the camera was set at f/22 (for both photographs) to obtain enough depth of focus. The difference between coherent and incoherent illumination is evident by the difference in continuity of the two images. In the same manner, speckle is also created during visual observation of the virtual image, since the maximum aperture of the eye (6-8mm) determines a finite diffraction spot.

To represent the continual decrease in range between carrier and aircraft, it will be necessary to magnify the real image. Such magnification can indeed be accomplished by employing a technique analogous to that used for the virtual image, that is, by changing the radius of curvature of the

illuminating light. There is a corresponding change in the image position associated with this magnification. Since we wish to display the real image on a screen, a means must be devised for translating the screen in synchronization with the magnification. It is felt that such a technique would require elaborate mechanical motions and linkages that would be impractical for an airborne system. In addition, motion of the real image plane will not allow the other degrees of freedom to be easily satisfied. Finally, it would be difficult to control the depth of focus/speckle tradeoff since motion of the image plane represents a change in the effective f/number of the hologram "lens." This change in f/number must be compensated for by continually changing the diameter of the illuminating beam in proper synchronization. These considerations make the use of this technique inadvisable for a display system.

Unless some other holographic property for obtaining real-image magnification is discovered, we will have to rely upon more conventional optics. A possible solution is to incorporate a zoom lens into the system. The zoom lens will be used to magnify the real image (now on a fixed screen) and at the same time relay it to a second, fixed, screen. The zoom lens is capable of providing continuous magnification over a range determined by the screen separation and the choice of lens. It has yet to be determined if a lens is available that will provide the desired magnification range without requiring too large a separation of the screens. In addition, the effect of the aperture of the zoom lens on image brightness, speckle, and quality will have to be investigated.

Provisions for supplying the image motion required to simulate the pitch and yaw motion of the aircraft must now be considered. In general these degrees of freedom manifest themselves as a translation of the image in two dimensions on the windscreen. A means for accomplishing this was introduced in the theoretical discussion, where it was shown that the hologram acts much like a grating and consequently must satisfy the grating equation (Equation 22). The result is that the reconstructed image can be

moved by changing the angle at which the readout illumination is incident on the hologram. An optical system that allows this variation in illumination angle is shown in Figure 37, which shows the glide path select mechanism. It can be seen that the two motions are relatively independent. This motion is restricted, however, by the decrease in image intensity as the angle of incidence changes. Since the image motion is angular, the amount of translation resulting on the screen will be determined by the lever arm or the screen-to-hologram separation. A proper choice of exposing parameters (angles, hologram-to-model separation, and thickness of recording medium) will have to be made to permit sufficient latitude to the resulting motion and to keep the image brightness from dropping below a predetermined level. Use of this technique will depend strongly on the limits of pitch and yaw motion required of the simulation. If this motion is excessive, it may not be possible to maintain image brightness at the extremes. In addition, the motion may exceed the linear field of the zoom lens used for magnification. If either of these should occur, we may have to resort to more conventional optics to provide image translation. This can be simply done by inserting a mirror in the path of the light from the zoom lens. With the viewing screen properly repositioned, this mirror could be pivoted about two independent axes so as to translate the magnified image on the screen. Because of the simplicity of the latter technique and because it may be so readily implemented, discontinuing consideration of the grating effect may be advisable. A mirror may be required in the system anyway to fold the optical path and to reduce the overall system size.

The final degree of freedom (aircraft roll) can, in theory, be achieved by using the properties of a hologram. A single, simple motion, such as rotating the hologram in its own plane, can be used if certain conditions are met. The rotation axis must be normal to the hologram plane and pass through the reconstructed image. In addition, the illuminating (readout) beam must rotate at the same time so as to be always incident on the same addressed area. Otherwise the perspective view will change. The

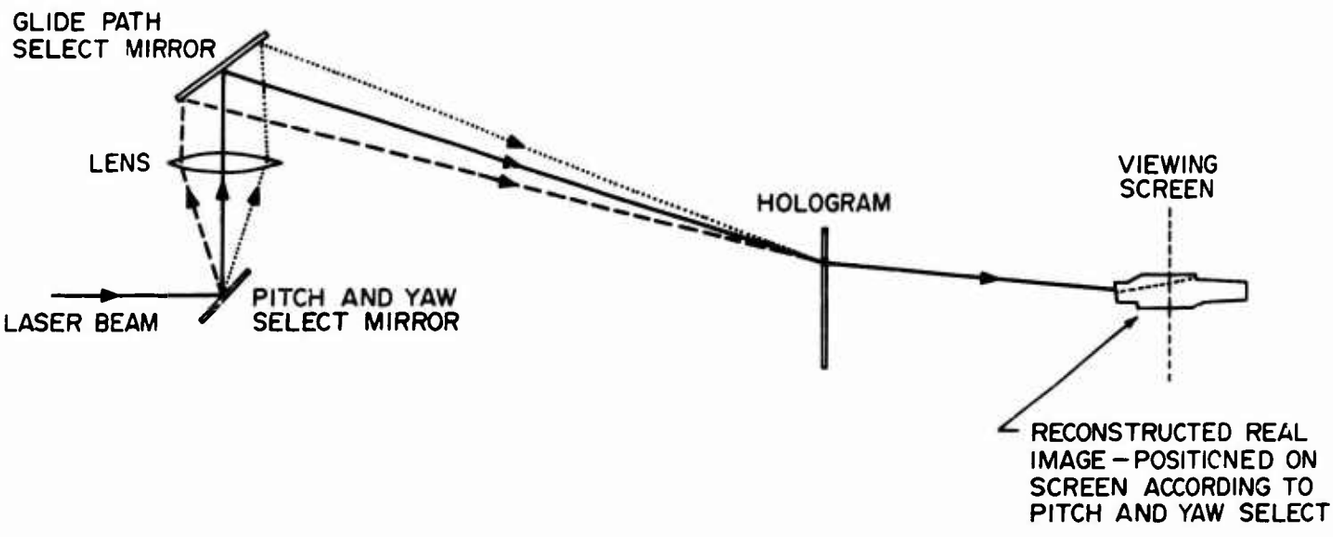

Figure 37. Combining Glide Path Select with Pitch and Yaw Select.

angle that the readout beam makes with the addressed area's normal must also not change unless commanded to do so by the pitch and yaw controls. These conditions can be met; they are accomplished by using the system shown in Figure 37 and rotating it about an axis oriented as indicated in Figure 38. Since the pitch and yaw controls cause the image to translate, the axis of rotation will not always pass through the image. This will cause the image to process about the axial position as roll is introduced. Depending on the degree of roll, this may or may not be serious. An alternate approach is to use conventional optics and insert an inverting or rotating device in the path of the light coming from the zoom lens. Such a device would be similar to a Dove prism in operation, but would have to be fabricated from mirrors to provide a large enough aperture for imaging. One possible arrangement is shown in Figure 39 and consists of two mirror sets. The mirrors in each set are at right angles to each other. The bottom set, M_1 and M_2, is fixed. The upper set, M_3 and M_4, is mounted so that it can rotate about a vertical axis through the center of the intersection of the bottom mirrors. A rotation of the upper set by an angle ω causes the observed image to rotate by an angle 2ω as shown by the ray diagram in the figure.

The choice between these two techniques will depend on their relative ease of implementation and the degree of roll to be simulated.

The resulting image displayed on the viewing screen can now be removed to infinity by placing a lens so that this image is in its focal plane. This is analogous to the method used for the virtual image except that we are here using a two-dimensional image. A composite system is shown in Figure 40.

6.4 NONHOLOGRAPHIC MODES

6.4.1 Television Link

A carrier model and a TV camera on board the aircraft carrier offer another method of performing the simulation without the use of holography. The TV camera is focused on the carrier model. The model and

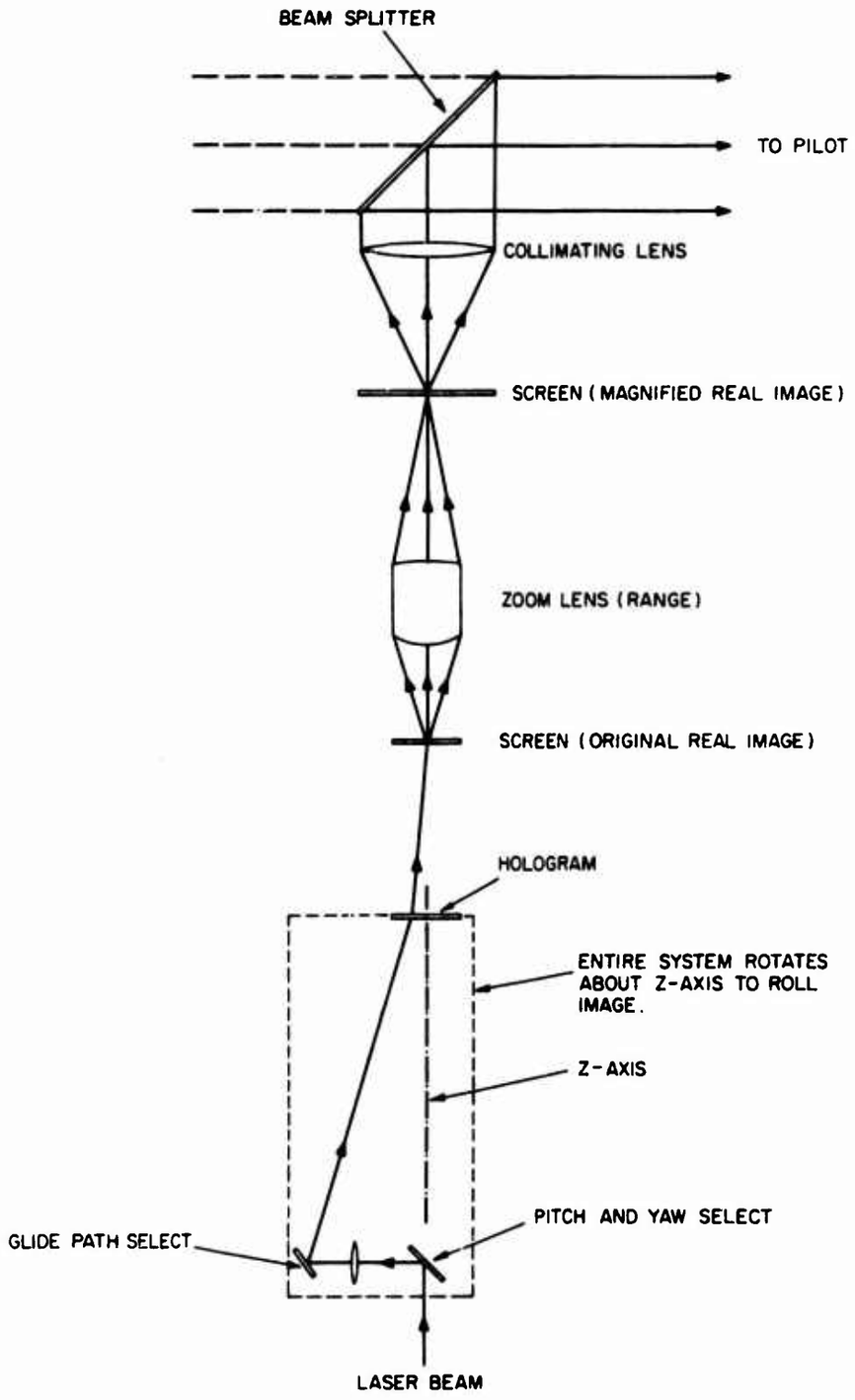

Figure 38. Real Image Display System Using Primarily Holographic Properties.

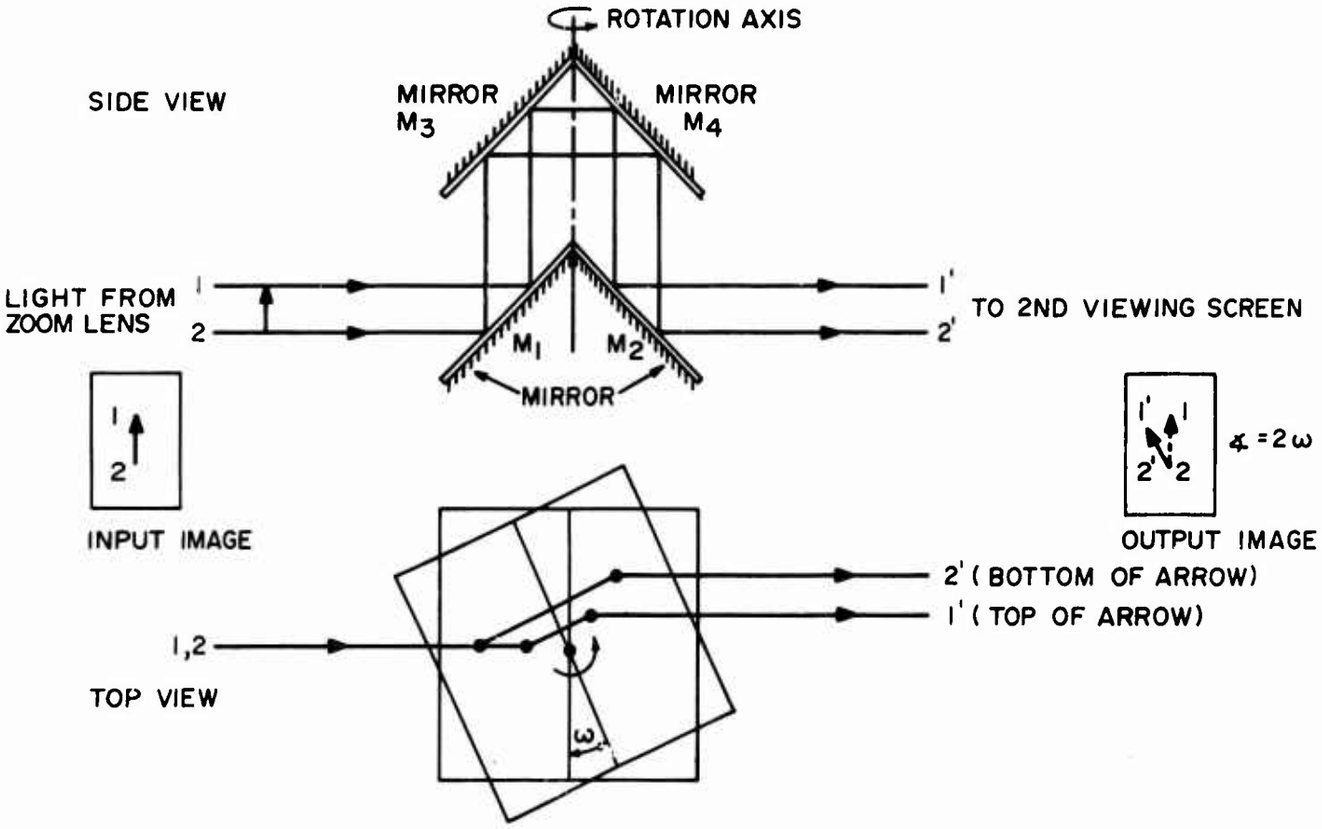

Figure 39. Mechanism for Introducing Roll into Image.

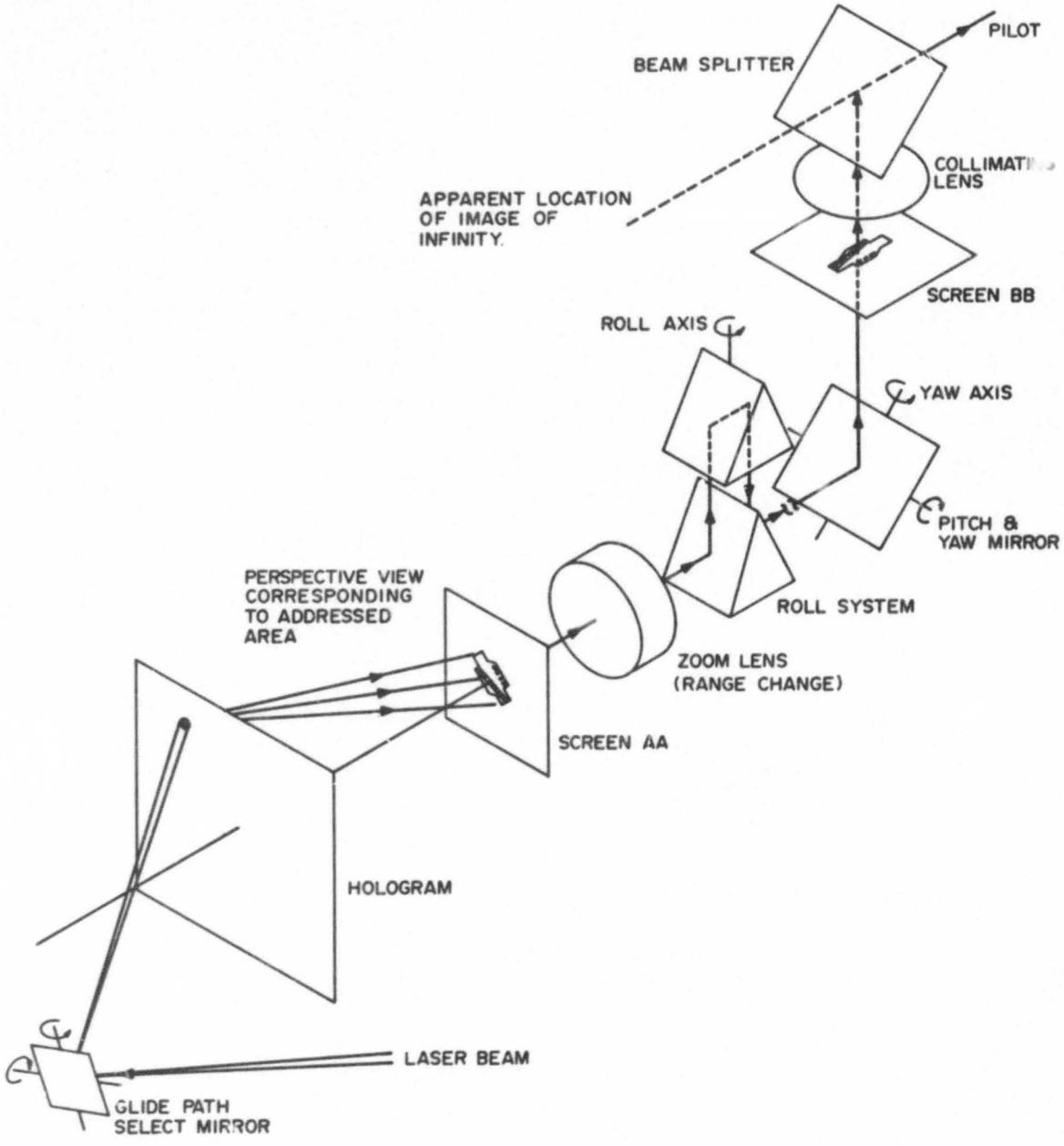

Figure 40. Real Image Display System Using Primarily Conventional Optics.

camera are manipulated so that the camera receives an image identical to the image that the pilot sees during his approach to the carrier. The appropriate image of the carrier is transmitted to the landing aircraft via a television link. The television picture in the aircraft is presented on the same head-up display the pilot already has for presenting symbolic information.

The roll, pitch, yaw, range, and glide path of the aircraft are known on the ship by means of radar and communication links between aircraft and ship. All this information is fed to a TV camera, which is focused on a model of the carrier as shown in Figure 41. The camera mount permits the camera to be moved to the right or left and up or down about a pivot point located in the center of the carrier model. This motion permits the selection of the glide path of the aircraft. To simulate the pitch and yaw of the aircraft, the camera is mounted in a gimbal arrangement that permits the camera to pitch and yaw exactly as the aircraft is doing. The pitching and yawing of the camera moves the image up or down and to the right or left on the pilot's CRT or beam splitter. Roll is simulated by rotating the camera about its optical axis. Range change or image size is controlled by a zoom lens mounted on the front of the camera.

To add additional realism to the simulation, the carrier model could also be mounted in a gimbal arrangement. The model could then be made to pitch, yaw, and roll with respect to the camera exactly as the real ship is doing with respect to some fixed frame of reference.

6. 4. 2 Model

The hologram used in the previously described holographic real image display system has the primary function of generating a real image of an aircraft carrier. This image is then operated on, for the most part, by conventional optics so as to simulate the view that would be seen from an aircraft. The real image, however, may be replaced with an actual model; if it is properly manipulated, the same degrees of freedom may be satisfied and displayed. This can be accomplished by using the mechanisms shown in

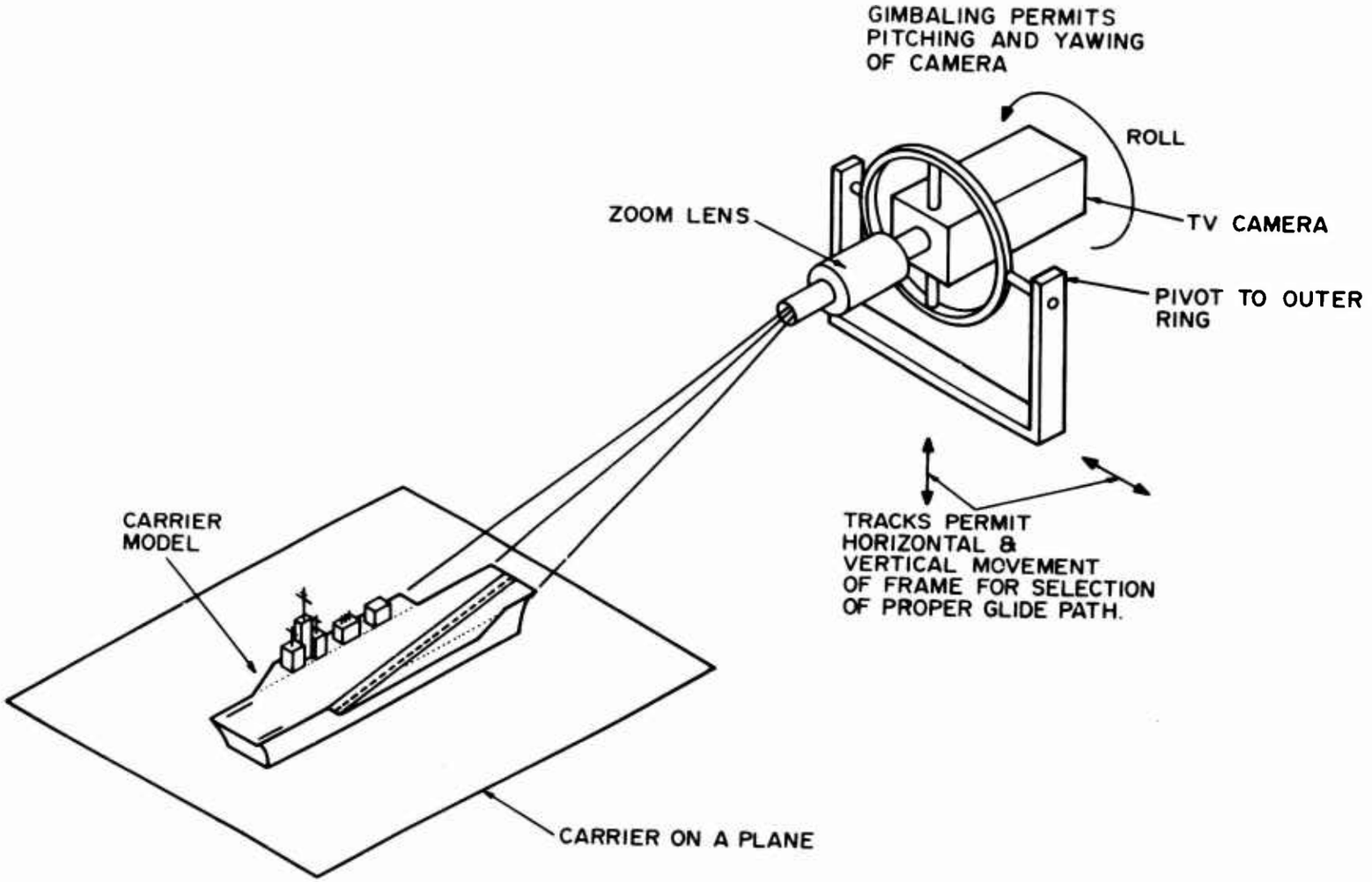

Figure 41. TV Link Head-Up Display System.

Figures 42 and 43. As before, the effect of range change is accomplished by imaging the model onto a viewing screen by means of a zoom lens and producing magnification.

The change in perspective view (glide path) is accomplished by mounting the model on a gimbal system that allows the model to be rotated about two axes. One axis is vertical and the other is horizontal. Both axes are through the flight deck, and both axes are perpendicular to the optic axes of the system. Rotation about these axes provides a different perspective view to the zoom lens. This view is relayed to the screen.

The effect of aircraft pitch and yaw appears, as discussed previously, as a translation of the image in the field of the windscreen. Figures 42 and 43 show a means for accomplishing this. The zoom lens and carrier model with gimbal are an integral unit such that, when this system is pivoted about the center of the lens, the carrier remains on the optic axis of the lens. The entire optic axis, however, moves and thereby changes the location of the projected image on the screen. The axes of rotation are shown in Figure 42. In general, as long as the carrier model is constrained to the optic axis of the lens, the entire system may be pivoted about any point to provide translation of the image. It is also possible to keep the above system fixed and translate the image by reflecting it from a pivoted mirror as described previously.

The last degree of freedom, roll, is seen by the pilot as an angular tilt of the carrier and true horizon with respect to an arbitrary reference on his windscreen. This can be accomplished in this system by including an additional gimbal on the carrier model support. This gimbal is such as to allow the model to be rotated about the optic axis so that the perspective view is not altered. This is shown in Figure 42, where both the model and glide path gimbals are mounted on a rocker-type gimbal whose center of curvature is on the optic axis.

The remainder of the system consists of a viewing screen, a collimating lens, and a beam splitter (Figure 43), which are used in the same manner as for the real image display system.

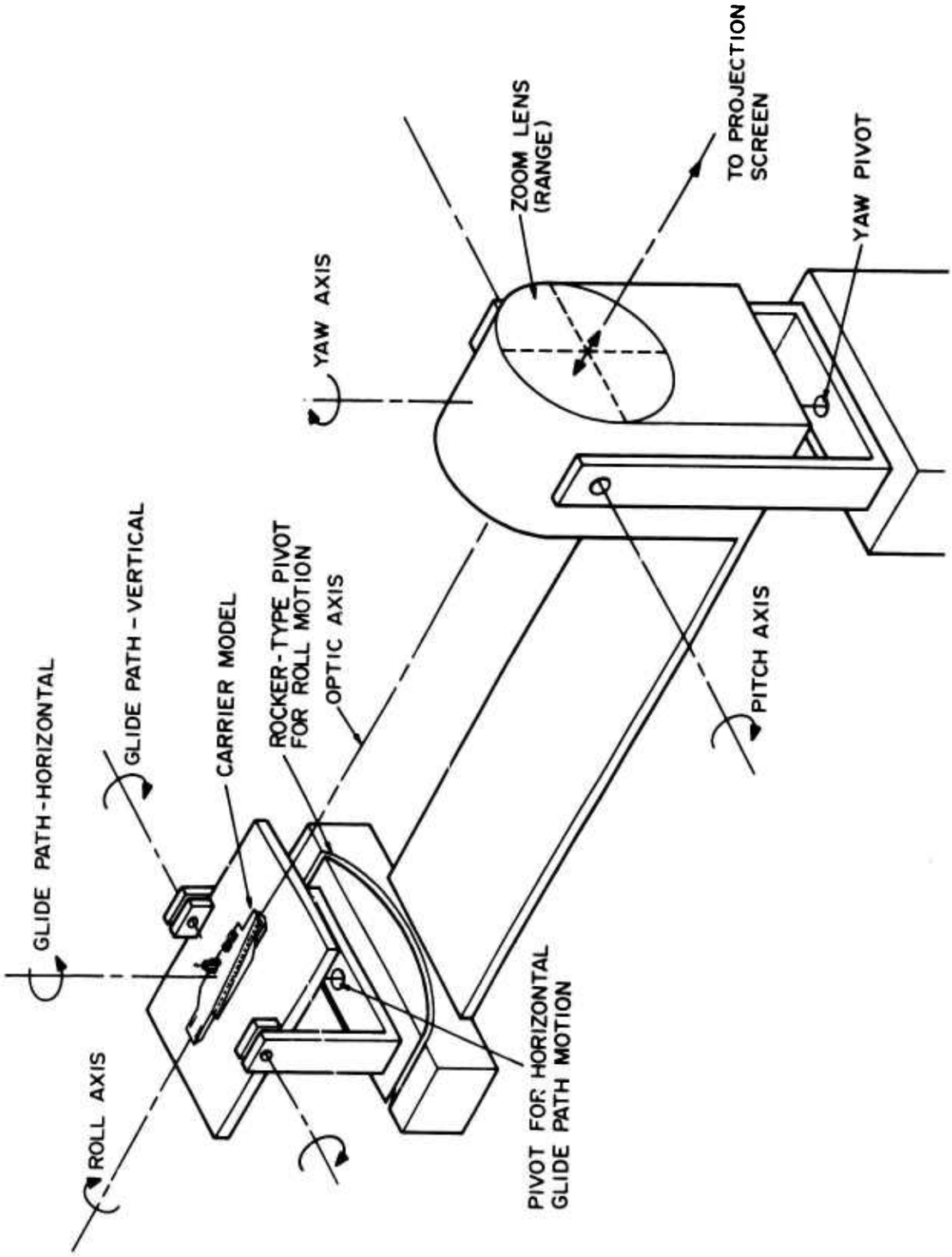

Figure 42. Means for Simulating Six Degrees of Freedom with a Model.

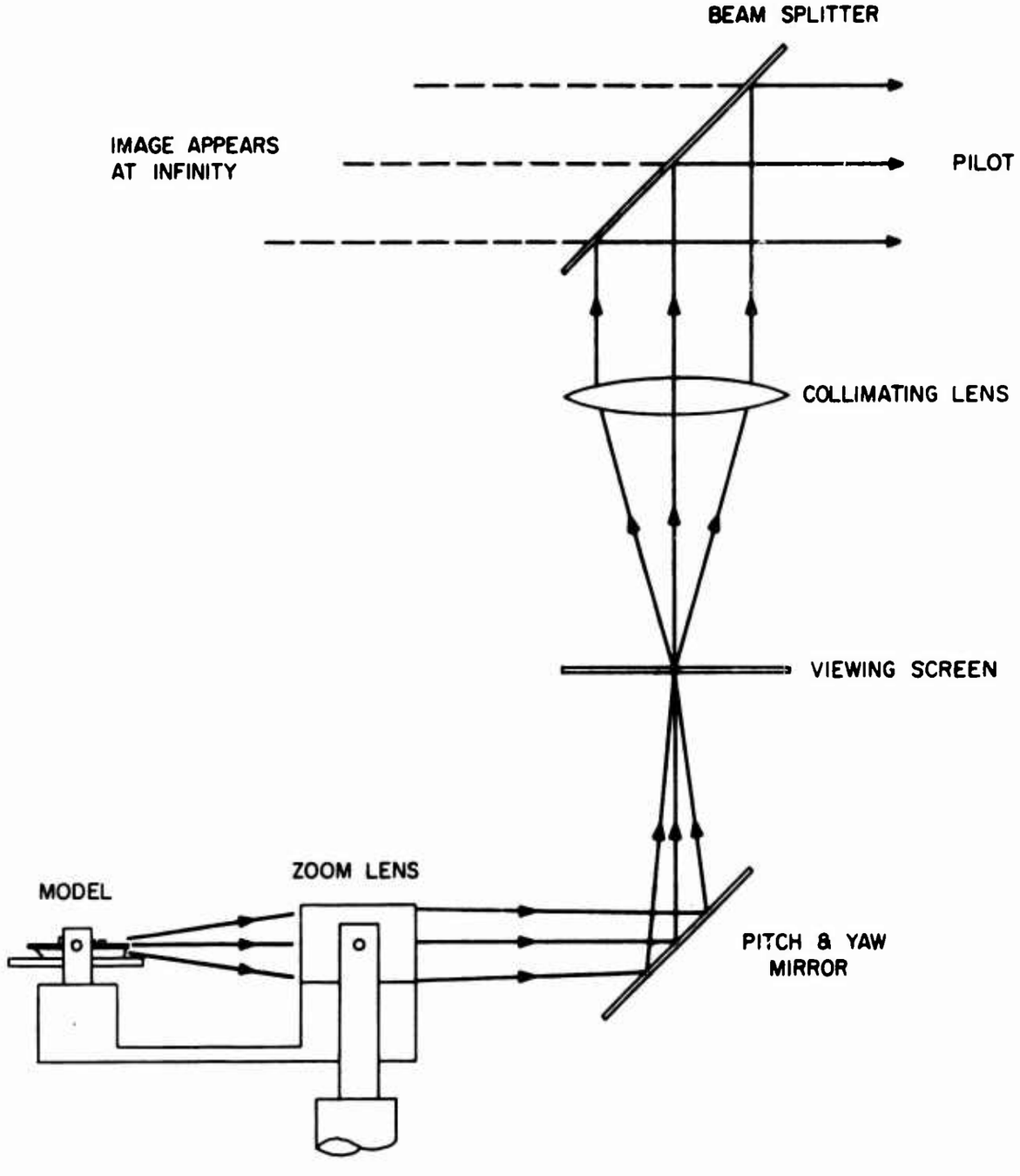

Figure 43. Display System Using a Model.

An additional feature of this system is that the display can be generated in full color by using the proper model and illumination. Laser illumination is no longer needed.

7. SYSTEMS INTERFACING

7.1 INTRODUCTION

Any true holographic image, real or virtual, is capable of six apparent degrees of freedom--three translational and three rotational. The three translational degrees of freedom are X- and Y-translation (orthogonal to the viewer's line of sight) and Z-translation (or, correspondingly, magnification). The three rotational degrees of image freedom will be referred to as pitch, yaw, and roll. (Image pitch, yaw, and roll should not be confused with the aircraft angular degrees of freedom. Image pitch and yaw are completely unrelated to aircraft attitude in the landing situation described here.) In a holographic cockpit display, the image must be manipulated in response to changes in the real-world situation in order to provide a realistic representation of the real world. Section 6 describes the methods used to manipulate the holographic image in the six degrees of freedom. This section will describe methods for deriving command signals, for each of the degrees of freedom, to drive a holographic cockpit display used to depict a carrier-deck landing situation.

Table I lists the six degrees of freedom and their corresponding real-world stimuli in the carrier-deck landing situation. (Figure 44 shows a block diagram of the system.) Also listed is the source of the command signals needed to drive the holographic display in response to changes in the real-world situation.

7.2 X AND Y IMAGE TRANSLATION

During a visual landing approach to an aircraft carrier, the position of the touch-down point will vary somewhat in the pilot's field of view. If the aircraft's roll axis were aimed directly at the touch-down point, this point would appear centered in the pilot's field of view through the windscreen. However, since the aircraft is normally approaching with a considerable angle-of-attack, the touch-down point (as well as the entire carrier) appears depressed from the center of his field of view through the

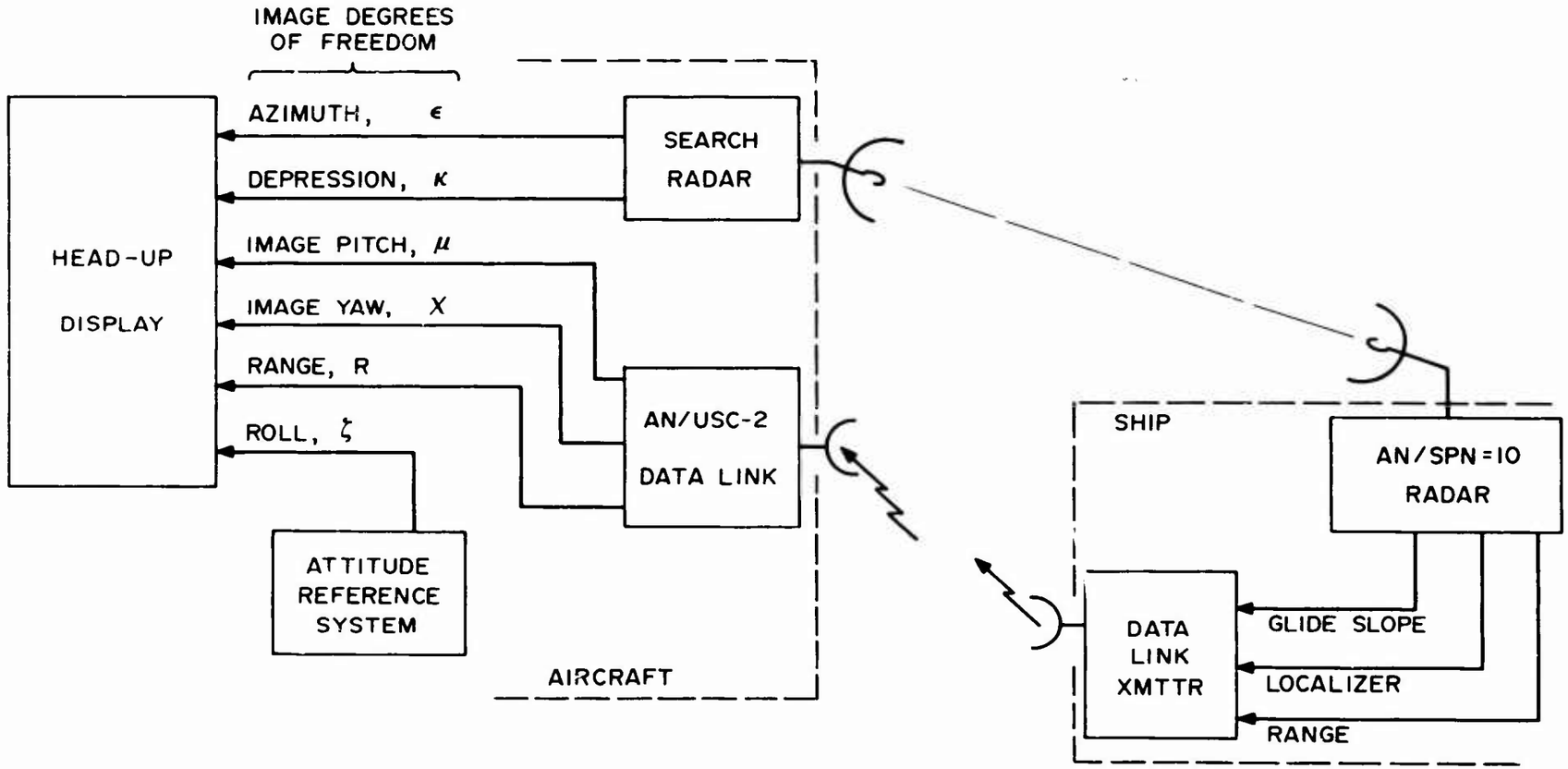

Figure 44. Head-Up Holographic Display Signal Interfacing.

TABLE I.

Image Degree of Freedom	Real-World Representation	Symbol	Signal Source
Pitch[1]	Vertical Glide Path Deviation (Glide Slope)	μ	AN/SPN-10 via existing Data Link AN/USC-2
Yaw[1]	Horizontal Glide Path Deviation (Localizer)	χ	AN/SPN-10 via existing Data Link AN/USC-2
Roll[1]	Aircraft Roll	ζ	Aircraft's Attitude Reference System
X-Translation	Azimuth Angle (from A/C roll axis)	ϵ	Aircraft's Search Radar Azimuth Gimbal Drive[2]
Y-Translation	Depression Angle (from A/C roll axis)	κ	Aircraft's Search Radar Elevation Gimbal Drive[2]
Magnification (Simulated Z-Translation)	Slant Range	R	AN/SPN-10 via Data Link

Notes:

1. The center of rotation of the image is the touch-down point.

2. Search radar pointing angles are referenced to the A/C boresight axis.

windscreen. In addition, if there happened to be a crosswind component relative to the deck, the pilot would fly his approach with some "crab" angle to compensate for drift. This crab angle would slew the touch-down point either left or right in the pilot's field of view through the windscreen, even though the plane might be following the glide path precisely. Normally, during aircraft recovery operations, the carrier cruises into the wind to put the relative wind vector straight down the canted landing deck's centerline. This minimizes the aircraft's closing speed and negates the crosswind component.

It can be said, then, that the position of the touch-down point in the pilot's field of view through the windscreen depends only on the angle between the aircraft's roll axis and an imaginary line from the airplane to the touch-down point. This angle may be resolved into a horizontal and a vertical component, which will be referred to, respectively, as azimuth angle (ϵ) and depression angle (κ). See Figure 45. It should be stressed that depression angle, as used here, is measured from the aircraft's roll axis, not from the horizontal. It therefore includes the aircraft's pitch attitude. For convenience, a depression angle (below the aircraft's centerline) will be considered positive; an elevation angle will be considered a negative depression angle. (It is difficult to imagine a situation, during a landing approach, in which the pilot sees the touch-down point elevated above the aircraft roll axis.) Also, an azimuth angle to the left of the aircraft centerline will be considered a positive angle; to the right, a negative angle.

In any head-up display that aspires to present the pilot's view of an aircraft carrier, the image of the carrier must translate in X and Y in response to changes in the aforementioned azimuth and depression angles. Presumably, the range of these angles will be small enough that the linear translation of the image may be in direct proportion to the angles themselves, rather than to the sines of the angles.

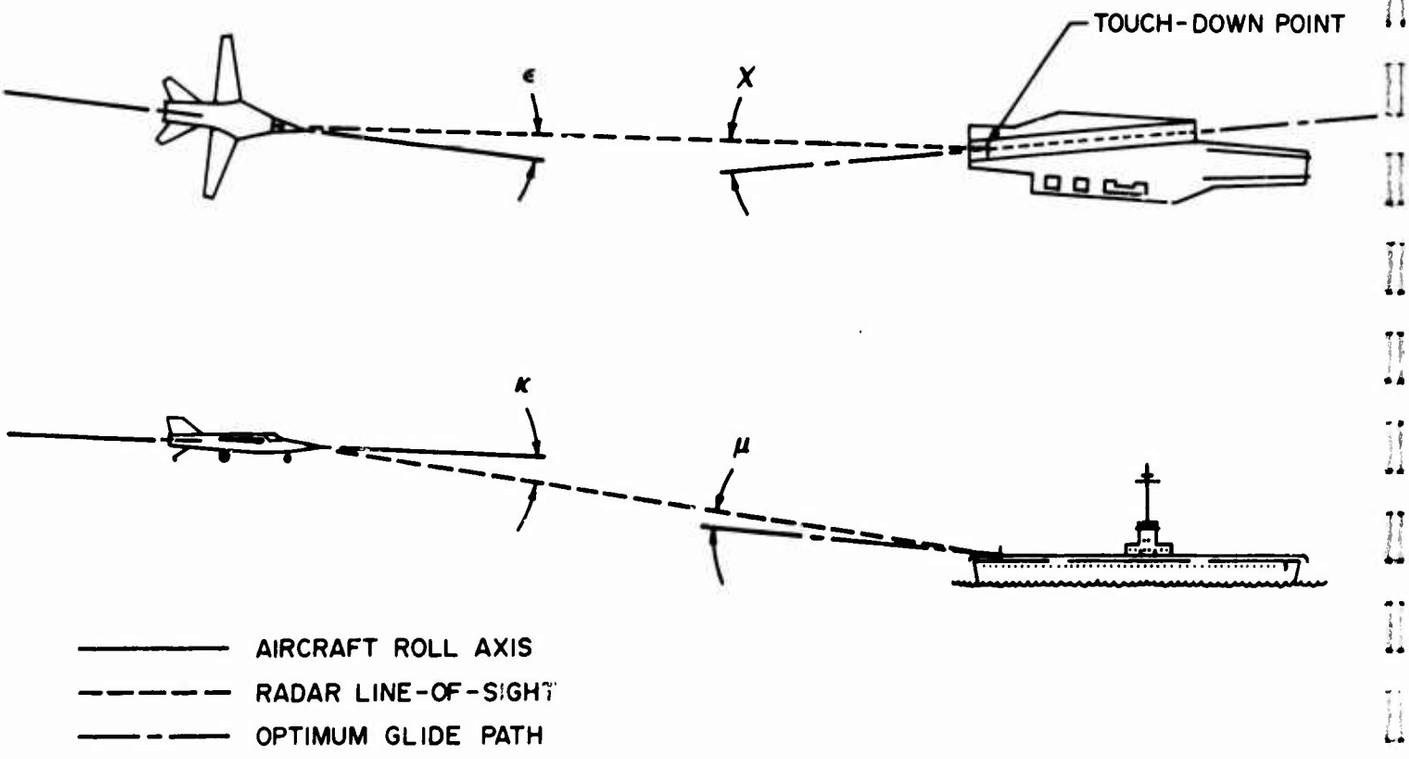

Figure 45. Angular Relations of Carrier Deck and Aircraft.

Probably the best source of azimuth and depression angle signals is the aircraft's search radar. With the radar boresight-referenced (rather than horizon-referenced) and tracking the carrier, the azimuth and depression angle signals may be read directly from the appropriate pointing gimbal drives and used to drive the display.

It may be that the carrier would present too expansive a radar cross-section to prevent "hunting" of the tracking radar (and a corresponding jitter in the display image) at closer range. Or, it could be that other ships or aircraft in the vicinity might constitute ambiguous targets that would preclude automatic acquisition of the carrier. (Automatic radar acquisition of the mother ship is a necessity, since the pilot's work load is too great during his landing approach for him to identify, acquire, and lock-on the target.) Both of these potential problems might be prevented by using a retrodirective radar target on the rear of the ship immediately below the flight deck and by operating the search radar at reduced receiver sensitivity. Also, automatic acquisition of the carrier might be accomplished by the use of an IFF-type radar transponder aboard ship.

7.3 IMAGE ROTATION, PITCH, AND YAW

If an aircraft is approaching a carrier precisely on the glide path, the pilot's perspective view of the carrier will not change substantially, although, of course, the carrier will loom larger and larger in his field of view. On the other hand, if the aircraft deviates from the glide slope, the pilot's perspective of the ship will change accordingly. If he drops below the glide slope, the pilot will see the deck foreshortened. If he deviates to the right of the glide path, he will see more of the starboard side of the ship, and the superstructure will obscure a different area of the deck. (The pilot's perspective view of the carrier actually will change somewhat with range because his view is not a true parallel projection, but rather is a convergent projection. The convergence effect will not be evident except at very close range.)

Thus, the pilot's perspective view of the carrier depends only on the aircraft's position with respect to the glide path, and this perspective view is completely independent of the aircraft's attitude.

The aircraft's position with respect to the glide path may be taken as an angle between the glide path and a line joining the aircraft and the touch-down point. This angle may be resolved into a vertical and a horizontal component, which will be referred to, respectively, as glide slope deviation (μ) and localizer deviation (χ). See Figure 45. "Localizer" and "glide slope" are terms associated with ILS (Instrument Landing System), used in commercial aviation. A different terminology may be used with SPN-10; the meaning, however, is the same.

To continue the sign convention, a glide slope deviation above the nominal glide path will be considered positive; below, negative. The nominal glide slope will be, perhaps, 3 1/2 degrees above the horizontal. Similarly, a localizer deviation to the port side of the landing deck's centerline will be considered positive; to the starboard, negative.

In order to change the perspective of an aircraft carrier in a holographic display, the image of the carrier must pitch and yaw in response to aircraft deviations above and below the glide path and to left and right of the deck's centerline. If the aircraft moves two degrees above the glide path, the carrier image must pitch downward two degrees from its nominal (on-glide path) aspect. If the aircraft drifts three degrees left of the localizer centerline, the ship's image must yaw three degrees counter-clockwise from its nominal (on-glide path) aspect.

The glide slope and localizer deviation signals that would command the display image in pitch and yaw are available from the shipborne AN/SPN-10 Landing System tracking radar. These signals are normally transmitted to the aircraft by means of the AN/USC-2 data link and are used to drive a cross-pointer indicator on the instrument panel. These same signals could easily be used to drive the holographic display image in pitch and yaw.

7.4 IMAGE ROLL

As the aircraft approaches the carrier, it will roll somewhat to the left and right in response to control inputs. Correspondingly, the pilot's view of the carrier and the horizon will roll relative to the aircraft, but in the opposite sense. In order to present a realistic presentation, the holographic image must be made to roll in response to aircraft roll. (The ship's roll might also be portrayed, but it is doubtful that this would convey any useful information to the pilot.) Aircraft roll will be designated as θ, and a roll angle to the left of horizontal will be considered positive.

The signal to command the display in roll is readily available from the aircraft's Attitude Reference System. This unit normally provides signals to the Attitude Director Indicator.

7.5 IMAGE MODIFICATION

The visual angle subtended by the aircraft carrier is inversely related to the range from the carrier ( ). In a holographic display, apparent range of the image would be altered by changing the magnification of the image. Range signals may be derived from the shipborne AN/SPN-10 and transmitted to the aircraft via one channel of the data link.

8. SUMMARY

Developments in holographic displays during this contract indicate the possibility of advancements in the evolution of head-up display systems. Holographic images are true three-dimensional images, exhibiting all the depth and parallax of their real-world counterparts with a realism and detail that are not limited by a computer's storage capacity. Being truly three-dimensional, holographic images may be manipulated in six degrees of freedom, to simulate the relative motion of the scenes that they represent. This manipulation may be done directly, without going through a coordinate transform computation for each point in the image, as is required with contact analog imagery.

The object of an ideal head-up display is to present an image to a pilot that is identical to the view he would see if the landing area were not obscured by foul weather or darkness. The initial efforts of the Phase I contract involved analysis of exactly what happens to the real image of a carrier perceived by a pilot on a carrier landing approach when the plane yaws, pitches, rolls, changes glide path, and changes range. According to this analysis, a change in glide path is perceived as a different view of the carrier. The relative distance from the carrier (range) is perceived as a variation in the image size of the carrier. Yaws and pitches of the plane are perceived as translations of the carrier image right or left and up or down in the windscreen. As the plane rolls, the image appears to rotate about an axis, which is the line of sight. A holographically generated image system to simulate the real view of the carrier must, therefore, use image manipulation techniques that reproduce the effects of yaw, pitch, roll, glide path changes, and range changes of the real carrier image. One outstanding problem is to achieve manipulation of each degree of freedom entirely independent of manipulations of all other degrees of freedom.

The experimental investigations of Phase I indicate that there appears to be little difficulty in producing quality holograms of an extended,

three-dimensional object. The only restrictions encountered were those imposed by geometry and space, which tend to limit the minimum angle between signal and reference beams, the physical separation of the reference point from the recording plate, and model illumination techniques. These limitations are not serious. The effort was restricted to conventional holography of the sideband Fresnel class and did not include Fourier, Fraunhoffer, or Lippmann type configurations.

The type of hologram considered is capable of creating either a real or virtual image, according to the manner in which it is illuminated. This fact coupled with the understanding of the general problem derived from the analysis indicated that it would be possible to structure the display system using either a holographically generated real or virtual image. Each approach provides convenient solutions to a different subset of problems associated with the required degrees of freedom; that is, the real image allows ease in manipulating the change in glide path (perspective) and pitch and yaw motions, while in a virtual image mode it is more convenient to simulate range change in addition to providing better image quality.

Both systems were considered during this contract period, but at the end of the contract there was not sufficient information to rule out either approach. One type of image will eventually be ruled out on the basis that the other type is less complicated and mechanically easier to implement. In addition, the implementation simulating each degree of freedom is hopefully more independent of every other degree of freedom with one type of image as compared to the other type.

Some mechanisms to simulate various independent degrees of freedom were constructed. It had been anticipated that range change would be the most difficult to simulate with purely holographic techniques. Range change was successfully simulated without the use of multiple holograms. The single hologram approach eliminates flicker problems. In particular, it has been shown that it is impossible to achieve a holographic angular

magnification greater than unity and that this may limit the total range of range simulation. Further study of the problem is necessary to determine if the range simulation presently achieved is adequate.

Designs of head-up display systems using holographic real and virtual images have been made. In addition, two systems, which use a carrier model rather than a holographic image, have also been considered. The experiments and investigations that have been performed have convinced us that holography offers the best approach to the simulation of an aircraft landing. In fact, it is the only approach, besides actual models, that permits the continuous selection of views of the landing area.

It is recommended that further work on a holographic head-up display system combine the simulation of all degrees of freedom for the real and virtual image systems. After this investigation the most promising approach should be selected, and a feasibility model constructed.

This model should not be the ultimate in compactness or design simplicity, but should show independence in the simulation of each degree of freedom.

This model will be of great assistance in determining what system approximations are permissible for future designs. The permissibility of an approximation will be based on maintaining a display that is psychologically acceptable to the pilot and that will significantly assist him in his landing approach.

9. APPENDIX -- SIGNIFICANCE OF CONJUGATE WAVEFRONT

In the equation representing the wavefronts reconstructed from a hologram (Equation 15), a term appears that is the complex conjugate of the original object wavefront. It will be shown here that this function represents the formation of a real image of the original object.

If we consider an object point O situated with respect to the hologram as shown in Figure 46, then an individual ray from O, passing through the hologram at point P, can be characterized by the expression:

$$U = a\, e^{i\vec{k} \cdot \vec{r}}$$

where a is the amplitude of the ray and $\vec{k}$ is the propagation vector with magnitude $|k| = 2\pi/\lambda$. The vector $\vec{r}$ represents the position of point P with respect to an origin in the hologram plane.

If we take the complex conjugate of U, we obtain a new function:

$$U^* = a\, e^{-i\vec{k} \cdot \vec{r}}$$

Since the scalar product $\vec{k} \cdot \vec{r}$ represents the projection of the vector $\vec{k}$ into the direction of the vector $\vec{r}$, we see that these projections are in the opposite directions for U and U^*. The only way this can happen is for the vector $\vec{k}$ to become rotated by an angle 2θ to a new symmetric position on the other side of the plane normal at point P. This means that the new vector $\vec{k}'$ now propagates toward a point O' that is the mirror image of point O with respect to the recording plane.

If all other rays $\vec{k}_i$ are drawn, it will be seen that they are all directed toward point O'. From this we can generalize that the light emanating from point O will produce a wavefront that, when conjugated, will be redirected so as to form an image of O at O'. The entire assemblage of points representing a three-dimensional object will likewise be imaged into a region of space symmetric with the plane of the hologram. Consequently,

the complex conjugate, $A^*(x, y)$, of an arbitrary wavefront, $A(x, y)$, will produce a real image of the object that originally created the wavefront.

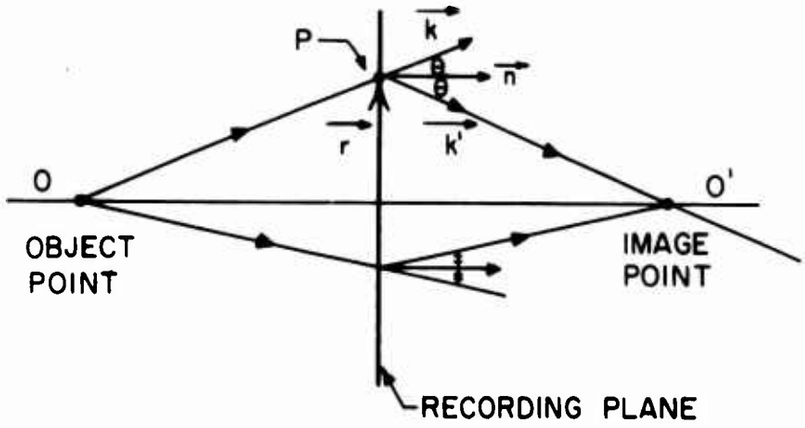

Figure 46. Real Image Formation from a Hologram.

10. REFERENCES

1. G. Lippmann, J. De Physique 3 (1894) 97.
2. H. Fleisher, et al., "Optically Accessed Memory," Final Technical Documentary Report, Contract No. AF33-657-11589, 1 Sept. 1963 to 28 June 1965, Appendix II.
3. Ibid., Appendix III.
4. H. Fleisher, et al., "A Block Transfer, Optically Accessed Memory," Final Technical Report No. AFAL-TR-66-307, November 1966.
5. A. A. Friesem, A. Kozma, G. F. Adams, Appl. Opt. 6, 851 (1967).
6. E. N. Leith, et al., Appl. Opt. 5 1303 (1966).
7. E. N. Leith and J. Upatnieks, "Wavefront Reconstruction with Diffused Illumination and Three Dimensional Objects," J. Opt. Soc. Am. 54, pp. 1295-1301, (1964).
8. K. S. Pennington and L. H. Lin, "Multicolor Wavefront Reconstruction," Appl. Physics Letters 7, pp. 56-57, 1965.
9. B. P. Hildebrand and K. A. Haines, "Contour Generation by Wavefront Reconstruction," Program, Opt. Soc. Am., March 1966.
10. H. Fleisher, et al., "An Optically Accessed Memory Using the Lippmann Process for Information Storage," Optical and Electro-Optical Information Processing, MIT Press, 1965.
11. "AF Checks on Holographic Image Storage," Laser Focus 12, March 15, 1966.
12. D. Gabor, "Character Recognition by Holography," Nature 208; pp. 422-423, 1965.
13. A. W. Lohmann and D. P. Paris, "Synthesis of Binary Holograms," Advance Program, 1966 Quantum Electronics Conference, Phoenix, Arizona, p. 44.
14. A. W. Lohmann and D. P. Paris, "Binary Image Hologram," Program, Opt. Soc. Am., March 1966 Meeting, p. 7.
15. M. P. Givens and W. J. Sieniens-Wapniarki, "The Experimental Production of Synthetic Holograms," Program Opt. Soc. Am. Mtg., March 1966, p. 7.

16. C. Cochran, "New Method of Making Fresnel Transform with Incoherent Light," J. Opt. Soc. Am. 65, p. 457, 1965.

17. A. W. Lohmann, "Wavefront Reconstruction for Incoherent Objects," J. Opt. Soc. Am. 55, pp. 1555-1556, 1965.

18. G. W. Stoke and R. C. Restrick, "Holography with Spatially Non-Coherent Light," Appl. Physics Letters 7, pp. 229-231, 1965.

19. F. S. Harris, Q. C. Sherman, and B. H. Billings, "Copying Holograms," Appl. Optics 5, pp. 665-666, 1966.

20. "Kodak Materials for Practical Holograms," Eastman Kodak Brochure, August 1965.

21. E. N. Leith, J. Upatnieks, B. P. Hilebsand, and K. Haines, "Requirements for a Wavefront Reconstruction Television Facsimile System," Journal SMPTE 74, pp. 893-896, 1965.

22. E. N. Leith, "Holography's Practical Dimension," Electronics, pp. 88-94, 1966.

23. "First Holographic Movies Produced by Stanford," IEEE Stud. Jour. 3, p. 41, 1965.

24. J. M. Burch, "The Application of Lasers in Production Engineering," Production Eng., Vol. 44; pp. 431-442, Sept. 1965.

25. R. J. Collier, E. T. Doherty, and K. S. Pennington, "Application of Moire Techniques to Holography," Applied Phys. Letters, 7, pp. 223-225, 1965.

26. R. E. Brooks, L. O. Heflinger, and R. E. Wuerker, "Interferometry with a Holographically Reconstructed Comparison Beam," App. Physics Letters, 7, pp. 248-249, 1965.

27. K. A. Stetson and R. L. Powell, "Interferometric Hologram Evaluation and Real-Time Vibration Analysis of Diffuse Objects," J. Opt. Soc. Am. 55, pp. 987-992, Aug. 1965.

28. B. P. Hildebrand and K. A. Haines, "Interferometric Measurements Using the Wavefront Reconstruction Technique," Appl. Optics, 5, pp. 172-173, 1966.

29. M. H. Horman, "An Application Wavefront Reconstruction to Interferometry," Appl. Optics 4, pp. 333-336, 1965.

30. R. Hioki, and T. Suzuki, "Reconstruction of Wavefronts in all Directions," Japan J. Appl. Phys. 4, p. 816, 1965.

31. H. Kogelink, "Holographic Image Projection Through Inhomogeneous Media," B. S. T. J. 44, pp. 2451-2455, 1965.

32. E. N. Leith and J. Upatnieks, "Holography Imagery through Diffusing Media," J. Opt. Soc. Am. 56, p. 523, 1966.

33. B. J. Thompson, J. Ward, and W. Zinky, "A Readout Technique for the Laser Fog Disdrometer," Conference American Meteorological Society, April 1965.

34. "Lasers and Holograms," Photo Methods Ind. 10, 12, 14, Nov. 1965.

35. H. M. A. El-Sum and A. V. Baez, "Preliminary Experiments on X-ray Microscopy by Reconstructed Wavefronts," Phy. Rev. 99, p. 624, 1955.

36. M. E. Haine and T. Mulvey, "Diffraction Microscopy with X-rays," Nature 170, pp. 202-203, 1952.

37. A. V. Baer, "Resolving Power in Diffraction Microscopy with Special Reference to X-rays," Nature 169, pp. 963-964, 1952.

38. R. W. Meier, J. Opt. Soc. Am. 55, 987 (1965).

39. C. F. Mooney, "The Application of Resonant Scanning Interferometers to Laser Problems," Laser Focus, p. 25, October 1967.

40. M. Born and E. Wolf, "Principles of Optics," The MacMillan Co., New York (1964).

41. E. N. Leith et al., Proc. Spring Joint Computer Conference, 1966.

42. Vision and Visual Perception, C. H. Graham, Editor, John Wiley & Sons, (1965).

43. P. Vlahos, "Information Display," Nov/Dec. 1965, p. 10.

44. P. S. Considine, J. Optical Soc. Am. 56, 1001 (1966).

45. J. Devilis, J. L. Reynolds, "Theory and Applications of Holography," Addison-Wesley, p. 56 (1967).

46. L. H. Enloe, Bell Syst. Tech. Journal, 1479 (1967).

Unclassified

Security Classification

DOCUMENT CONTROL DATA - R&D

(Security classification of title, body of abstract and indexing annotation must be entered when the overall report is classified)

1 ORIGINATING ACTIVITY (Corporate author) International Business Machines Corporation Systems Development Division Poughkeepsie, N. Y.	2a REPORT SECURITY CLASSIFICATION Unclassified 2b GROUP not applicable

3 REPORT TITLE

Holographic Head-Up Display -- Phase I

4 DESCRIPTIVE NOTES (Type of report and inclusive dates)

Technical Report (5-15-67 to 11-14-67)

5 AUTHOR(S) (Last name, first name, initial)

Harris, Thomas J.
Habegger, Millard A.
Sincerbox, Glenn T.
Hanna, David W.

6 REPORT DATE	7a TOTAL NO OF PAGES	7b NO OF REFS
December 15, 1967	123	46

8a CONTRACT OR GRANT NO	9a ORIGINATOR'S REPORT NUMBER(S)
N 00014-67-C-0453	None
b PROJECT NO	
c	9b OTHER REPORT NO(S) (Any other numbers that may be assigned this report)
d	None

10 AVAILABILITY LIMITATION NOTICES This document is subject to special export controls and each transmittal to foreign governments or foreign nationals may be made only with prior approval of ONR ,(code 461), Washington, D.C. 20360.

11 SUPPLEMENTARY NOTES	12 SPONSORING MILITARY ACTIVITY
	Office of Naval Research Air Systems Program (Code 461) Washington, D.C.

13 ABSTRACT

Numerous applications of display systems require the presentation of visual information that can be continuously altered with time. In particular, a head-up display system as used by an aircraft commander must provide a simulation of the real-world exterior to his vehicle, and, at the same time, represent any change in his attitude with respect to a predetermined segment of this real world. (U)

In the particular case of an aircraft landing approach, one can characterize the pilot's view of the aircraft carrier and its subsequent variations into six degrees of freedom. The display must provide the view corresponding to the instantaneous values of these parameters and change as any one or more of the parameters change. (U)

This report describes the development work on displays of this type using sideband or carrier-frequency Fresnel holographic recorded images. An important feature of the holographic approach is that a true 3-D image of an object can be recorded. It is, therefore, possible with a single hologram to present an infinite number of different views of an object to an observer. Continuous control of the pertinent parameters is required to make a dynamic real-time display. (U)

High quality holograms of aircraft carrier models have been made in sizes up to 8 by 10 inches. Techniques and systems for manipulating the holographic real and virtual images from these holograms have been tested and are described. (U)

This work was performed by the IBM Systems Development Division, Product Development Laboratory, at Poughkeepsie, N. Y. with assistance from IBM's Federal Systems Division, Electronics Systems Center, at Owego, N. Y. (U)

DD FORM 1 JAN 64 1473

Unclassified

Security Classification

Unclassified

Security Classification

14 KEY WORDS	LINK A		LINK B		LINK C	
	ROLE	WT	ROLE	WT	ROLE	WT
Displays **Head-Up Display** **Holography**						

INSTRUCTIONS

1. ORIGINATING ACTIVITY: Enter the name and address of the contractor, subcontractor, grantee, Department of Defense activity or other organization *(corporate author)* issuing the report.

2a. REPORT SECURITY CLASSIFICATION: Enter the overall security classification of the report. Indicate whether "Restricted Data" is included. Marking is to be in accordance with appropriate security regulations.

2b. GROUP: Automatic downgrading is specified in DoD Directive 5200.10 and Armed Forces Industrial Manual. Enter the group number. Also, when applicable, show that optional markings have been used for Group 3 and Group 4 as authorized.

3. REPORT TITLE: Enter the complete report title in all capital letters. Titles in all cases should be unclassified. If a meaningful title cannot be selected without classification, show title classification in all capitals in parenthesis immediately following the title.

4. DESCRIPTIVE NOTES: If appropriate, enter the type of report, e.g., interim, progress, summary, annual, or final. Give the inclusive dates when a specific reporting period is covered.

5. AUTHOR(S): Enter the name(s) of author(s) as shown on or in the report. Enter last name, first name, middle initial. If military, show rank and branch of service. The name of the principal author is an absolute minimum requirement.

6. REPORT DATE: Enter the date of the report as day, month, year; or month, year. If more than one date appears on the report, use date of publication.

7a. TOTAL NUMBER OF PAGES: The total page count should follow normal pagination procedures, i.e., enter the number of pages containing information.

7b. NUMBER OF REFERENCES: Enter the total number of references cited in the report.

8a. CONTRACT OR GRANT NUMBER: If appropriate, enter the applicable number of the contract or grant under which the report was written.

8b, 8c, & 8d. PROJECT NUMBER: Enter the appropriate military department identification, such as project number, subproject number, system numbers, task number, etc.

9a. ORIGINATOR'S REPORT NUMBER(S): Enter the official report number by which the document will be identified and controlled by the originating activity. This number must be unique to this report.

9b. OTHER REPORT NUMBER(S): If the report has been assigned any other report numbers *(either by the originator or by the sponsor)*, also enter this number(s).

10. AVAILABILITY/LIMITATION NOTICES: Enter any limitations on further dissemination of the report, other than those imposed by security classification, using standard statements such as:

(1) "Qualified requesters may obtain copies of this report from DDC."

(2) "Foreign announcement and dissemination of this report by DDC is not authorized."

(3) "U. S. Government agencies may obtain copies of this report directly from DDC. Other qualified DDC users shall request through

_____."

(4) "U. S. military agencies may obtain copies of this report directly from DDC. Other qualified users shall request through

_____."

(5) "All distribution of this report is controlled. Qualified DDC users shall request through

_____."

If the report has been furnished to the Office of Technical Services, Department of Commerce, for sale to the public, indicate this fact and enter the price, if known.

11. SUPPLEMENTARY NOTES: Use for additional explanatory notes.

12. SPONSORING MILITARY ACTIVITY: Enter the name of the departmental project office or laboratory sponsoring *(paying for)* the research and development. Include address.

13 ABSTRACT Enter an abstract giving a brief and factual summary of the document indicative of the report, even though it may also appear elsewhere in the body of the technical report. If additional space is required, a continuation sheet shall be attached.

It is highly desirable that the abstract of classified reports be unclassified. Each paragraph of the abstract shall end with an indication of the military security classification of the information in the paragraph, represented as *(TS)*, *(S)*, *(C)*, or *(U)*.

There is no limitation on the length of the abstract. However, the suggested length is from 150 to 225 words.

14. KEY WORDS: Key words are technically meaningful terms or short phrases that characterize a report and may be used as index entries for cataloging the report. Key words must be selected so that no security classification is required. Identifiers, such as equipment model designation, trade name, military project code name, geographic location, may be used as key words but will be followed by an indication of technical context. The assignment of links, rules, and weights is optional.

Unclassified

Security Classification